TECHNICAL UNIVERSITY OF LIBEREC
Faculty of Science, Humanities and Education

Department of Physics

_____

Studentská 1402/2, 461 17 Liberec 1, Czech Republic

Study of the Magnetically Induced QED Birefringence of the Vacuum in experiment OSQAR

Dissertation

Ing. Štěpán Kunc

Liberec 2017

TECHNICAL UNIVERSITY OF LIBEREC
Faculty of Science, Humanities and Education

Department of Physics

_____

Studentská 1402/2, 461 17 Liberec 1, Czech Republic

Study of the Magnetically Induced QED Birefringence of the Vacuum in experiment OSQAR

Disertační práce
k získání akademického titulu Doktor (Ph.D.)

Autor:	Ing. Štěpán Kunc
Školitel:	Doc. RNDr. Miroslav Šulc, Ph.D.
Školící pracoviště:	Katedra fyziky, Fakulta přírodovědně-humanitní a pedagogická
	Technická univerzita v Liberci
	Studentská 1402/2, 461 17 Liberec 1
Studijní program:	P3901 / Aplikované vědy v inženýrství
Studijní obor:	3901V012 / Fyzikální inženýrství
Rozsah disertační práce:	104 stran
	34 obrázků
	3 tabulek
	80 vzorců
Místo a rok obhajoby:	Liberec 2017

....

V Liberci dne   Ing. Štěpán Kunc

Prohlášení

Byl jsem seznámen s tím, že na mou disertační práci se plně vztahuje zákon č. 121/2000 Sb. o právu autorském, zejména § 60 – školní dílo.

Beru na vědomí, že Technická univerzita v Liberci (TUL) nezasahuje do mých autorských práv užitím mé disertační práce pro vnitřní potřebu TUL.

Užiji-li disertační práci nebo poskytnu-li licenci k jejímu užití, jsem si vědom povinnosti informovat o této skutečnosti TUL; v tomto případě má TUL právo ode mne požadovat úhradu nákladů, které vynaložila na vytvoření díla, až do její skutečné výše.

Disertační práci jsem vypracoval samostatně s použitím uvedené literatury a na základě konzultací se školitelem disertační práce.

Současně čestně prohlašuji, že tištěná verze práce se shoduje s elektronickou verzí, vloženou do IS STAG

………………………….   …………………………….

V Liberci dne   Ing. Štěpán Kunc

Poděkování

Rád bych poděkoval všem, kteří mi pomáhali a byli oporou při vzniku této disertační práce. V prvé řadě školiteli Doc. RNDr. Miroslavu Šulcovi, Ph.D. za vedení disertační práce a pomoc při řešení vědeckých problémů. Velké podělkování patří mojí ženě Pavle, která vždy trpělivě podorovala moje vědecké počínání. V neposlední řadě patří poděkování mým rodičům a kolegům.

Abstrakt

Klasická elektrodynamika vakua je lineární teorií a nepředpokládá foton-fotonový rozptyl ani jiné nelineární vazby mezi elektromagnetickými poli. V roce 1936 učinili Euler, Heisenberg a Weisskopf v raném vývoji kvantové elektrodynamiky (QED) předpoklad, že samotné vakuum se může chovat jako anizotropní médium za přítomnosti vnějšího magnetického pole. Tento jev je známý pod anglickým označením Vacuum Magnetic Birefringence (VMB) a od jeho prvních kvantitativních výpočtů v roce 1970 je stále velkou výzvou pro optickou metrologii. Když se lineárně polarizované světlo pohybuje silným příčným magnetickým polem ve vakuu, polarizační stav světla se změní na eliptický podobně jako v anizotropním krystalu. Rozdíl v indexech lomu řádného a mimořádného paprsku je přímo spojen se základními konstantami, jako je konstanta jemné struktury nebo Comptonova vlnová délka. Dvojlom vakua (VMB) by mohl vznikat také z existence lehkých skalárních nebo pseudoskalárních částic, jako jsou axiony nebo axionům podobné částic. Axion se rozpadá na dva fotony a to by se projevilo jako odchylka od počáteční předpovědi QED.

Tato práce zkoumá možnosti měření VMB pomocí supravodivých magnetů z Large Hadron Collider (LHC). Vysoce citlivé měření dvojlomu za použití elektro-optického modulátoru je analyticky vypočítáváno a experimentálně ověřeno na Cotton-Moutonově (CME) jevu v dusíku. Měření probíhalo v rámci experimentu OSQAR v Evropské organizaci pro jaderný výzkum (CERN). V práci jsou diskutovány různé zdroje šumu a výsledná citlivost měření dvojlomu. Disertace se také zabývá využitím optického rezonátoru pro měření VMB. Na konci textu je představeno nové originální řešení pro měření VMB pomocí supravodivých magnetů se statickým magnetickým polem.

Klíčová slova:

Polarimetrie, ellipsometr, magnetický dvojlom vakua, OSQAR, Axion, Cotton-Moutonův jev v dusíku

Abstract

Classical electrodynamics in a vacuum is a linear theory and does not foresee photon-photon scattering or other nonlinear effects between electromagnetic fields. In 1936 Euler, Heisenberg and Weisskopf put framework, in the earliest development of quantum electrodynamics (QED), that vacuum can behave as a birefringent medium in the presence of the external transverse magnetic field. This phenomenon is known as Vacuum Magnetic Birefringence (VMB) and it is still challenging for optical metrology since the first calculations in 1970. When linearly polarized light travels through the strong transverse magnetic field in vacuum, the polarization state of the light would change to elliptical. The difference in the refraction indexes of the ordinary and extraordinary ray is directly related to fundamental constants, such as fine structure constant or Compton wavelength. Contributions to VMB could also arise from the existence of light scalar or pseudoscalar particles, such as axions or axions like particles. Axions couple to two photons and this would manifest itself as a sizeable deviation from the initial QED prediction.

This thesis investigates the possibility of the VMB measurement with Large Hadron Collider (LHC) or other superconducting magnets. High sensitive birefringence measurement based on the electro-optic modulator is analytically calculated and experimentally tested on Cotton-Mouton effect (CME) in nitrogen gas. Measurements were made in experiment OSQAR at European Organization for Nuclear Research (CERN). Various sources of noise are discussed, and a sensitivity of the setup is presented. Optical cavities and their implementation are proposed and calculated. At the end of the thesis, the new solution for VMB measurement with superconducting magnets is presented.

Keywords:

Contents

List of symbols

Symbol	Unit	Meaning
A	[1]	Complex envelope vector
A_{1x}, A_{1y}	[1]	Complex envelope parameters
T_{11}, T_{12}	[1]	Parameters of Jones matrix
$a_{y,x}$	[1]	Magnitude of polarization ellipse
B	[T]	Magnetic induction vector
c	[m s^{-1}]	Speed of light
d	[m]	Length of the resonator
$E(r,t)$	[Vm^{-1}]	Electric field vector
e	[C]	Elementary charge
F	[1]	Optical cavity finesse
FSR	[Hz]	Free spectral range
f	[Hz]	Frequency
f_m	[Hz]	Modulation frequency of EOM
g	[GeV^{-1}]	Coupling constant
G	[Ω]	Impedance of the photodiode
$\hbar$	[eV s rad^{-1}]	Reduced plank constant/ Dirac constant
I	[W]	Light Intensity
I_0	[W]	Light intensity reaching analyzer
i_{tot}	[A]	Overall noise current
i_{shot}	[A]	Shot noise current
$i_{johnson}$	[A]	Johnson noise current
i_{dark}	[A]	Dark noise current
i_{RIN}	[A]	Residual intensity noise current
i	[1]	Complex unit
J	[1]	Jones vector
J_n	[1]	Bessel function coefficients of the n-th order
k_B	[J K^{-1}]	Boltzmann constant
L	[m]	Length of the magnetic field

M_a	[GeV]	Inverse coupling constant
m	[eV]	Mass of the particle
m_e	[eV]	Electron mass
N	[1]	Number of pass through magnetic field region
N_{RIN}	[1]	Relative intensity noise parameter
$n_\parallel$	[1]	Index of refraction for light polarized parallel to $\boldsymbol{B}$
$n_\perp$	[1]	Index of refraction for light polarized perpendicular to $\boldsymbol{B}$
n_e	[1]	Extraordinary refraction index
n_o	[1]	Ordinary refraction index
$n + ik$	[1]	Complex index of refraction
Δn	[1]	Difference between $n_\parallel$ and $n_\perp$
Δn_u	[$T^{-2}\ atm^{-1}$]	Normalized Cotton-Mouton birefringence of gases
Δn_{uv}	[T^{-2}]	Normalized Cotton-Mouton birefringence of Vacuum
$\boldsymbol{P, A}$	[1]	Jones matrix of lineal polarizer
P	[atm]	Pressure
q	[A/W]	Responsivity/quantum efficiency of the photodiode
R_0	[m]	Radius of mirror
$\boldsymbol{R}$	[1]	Rotation Jones matrix
R	[1]	Amplitude reflection coefficient (reflexivity)
ROC	[m]	Radius of curvature
$\boldsymbol{S}$	[1]	Jones matrix of spurious birefringence
$\boldsymbol{T}$	[1]	Jones matrix
$\boldsymbol{T'}$	[1]	Transformed Jones matrix
T_0	[rad]	Depth of modulation
T	[K]	Thermodynamic temperature
T_m	[rad]	Phase change of modulator
T	[rad]	Phase change
t	[s]	Measurement time
Δt	[s]	Time frame

T_r	[1]	Amplitude transient coefficients (transmissivity)
V_m	[V]	Modulation voltage of EOM
V_π	[V]	Half wave voltage of EOM
V_{DC}	[V]	DC component of photodiode voltage
V_{1f}	[V]	Rms AC output voltage of DSP Lock –in amplifier
ΔV_{Bias}	[V]	Bias voltage difference
w	[m]	Waist of Gaussian beam
x, y, z	[1]	Cartesian system coordinates
α	[1]	Fine structure constant
Δ	[rad]	Phase difference of EOM
Δv_f	[Hz]	Resonance bandwidth
ζ	[1]	Ellipticity of EOM modulator
λ	[m]	Wavelength
λ_e	[m]	Compton wave length of the electron
η	[Ω]	Impendence of the medium
μ_0	[Hm^{-1}]	Permeability of the vacuum
ς	[rad]	Phase change induced by spurious signal
σ^2	[1]	Extension ratio of polarizers
$\varphi_{x,y}$	[rad]	Initial phase state of x, y electric filed component
φ	[rad]	Phase difference (retardation) between components of electric field vector
τ	[s]	Optical cavity decay time
ψ	[1]	Ellipticity
$\emptyset$	[1]	Scalar and pseudoscalar field
Ω	[eV]	Photon energy
ω	[Hz]	Frequency of the light
Ω	[Hz]	Radial frequency of laser
ϑ	[Hz]	Radial frequency of modulator

List of abbreviations

Shortcut	Meaning
ALPS	Any Light Particles Search
CAST	The CERN Solar Telescope
CME	Cotton-Mouton effect
DAQ	Data acquisition system
DC	Direct current
DESY	Deutsches Elektronen-Synchrotron
DSP	Dual phase
EOM	Electro-Optic modulator
FE	Ferrara
FFT	Fast Fourier Transform
FSR	Free spectral range
FWHM	Full width half maximum
LHC	Large Hadron Collider
LIGO	Laser Interferometer Gravitational-Wave Observatory
LNL	Legrano National Laboratory
LSW	Light Shining through the Wall experiment
MOKE	Magneto-optical Kerr effect
NPBS	Nonpolarizing beam splitter
OSQAR	The Optical Search for QED Vacuum Birefringence, Axions and Photon Regeneration
PEM	Photo-Elastic modulator
PID	Proportion, Integration, Derivation
PVLAS	Polarizzazione del Vuoto con LASer, "polarization of the vacuum with laser"
QED	Quantum Electrodynamics
QCD	Quantum Chromodynamics
RAM	Residual amplitude noise
ROC	Radius of curvature
SBC	Solei Babinet compensator

S/N	Signal to noise ratio
TEM	Transverse Electromagnetic Waves
TEM	Transversal mode
VMB	Vacuum Magnetic Birefringence
VIRGO	VIRGO experiment (named by Virgo cluster)

1 Introduction

The aim of this dissertation is to study the possibility of QED Vacuum Magnetic Birefringence (VMB) measurement with superconducting LHC dipole magnets in experiment OSQAR at CERN. The primary goal of the thesis is to developed and to test the ellipsometry modulation technique suitable for the slowly varying and static magnetic fields. The dissertation could serve as the technical design of VMB measurement in the next generation of experiment OSQAR.

In the first two chapters, the reader will find an introduction to the theory of Vacuum Magnetic Birefringence, the polarization, the optical anisotropy and Cotton-Mouton effect. The review of past and existing experiments in the field of VMB is presented and discussed.

In chapter three the high sensitive ellipsometer based on ellipsometry modulation techniques similar to other VMB experiments is described. However, presented setup, developed at the Technical University of Liberec, uses novel solution to measure the birefringence in slowly varying magnetic fields with spurious birefringence signals. This innovative solution was implemented at CERN in experiment OSQAR and was successfully tested on Cotton-Muotton effect measurement in nitrogen gas.

In chapter four we discuss the further improvements of presented setup. Chapter four also describes the implementation of the optical resonant cavity to experiment OSQAR and its first tests and prototypes.

The last chapter five is about heterodyne ellipsometry solution suitable for static magnetic fields. In the beginning, we present the solution described by the collaboration PVLAS and in the second half, we present the entirely new solution of heterodyne ellipsometry for VMB measurements.

Development, calculations and all the tests of the presented ellipsometer, were made by the author of the thesis only, as well as Cotton-Mouton measurement in nitrogen gas and design of new heterodyne ellipsometry technique for static magnetic fields. Development and testing of the optical resonant cavity were made in cooperation with colleagues from experiment OSQAR.

1.1 Vacuum Magnetic Birefringence

From the beginning of the 20th century, we know that any medium shows a linear birefringence in the presence of an external transverse magnetic field $\boldsymbol{B}$.[1] This phenomenon was firstly studied in detail by Cotton and Mouton in 1905 and therefore is known as the Cotton-Mouton effect (CME) [2].

In 1935 and 1936 Euler, Kochel, Weisskopf and Heisenberg, in the earliest development of quantum electrodynamics (QED) [3]–[5], put the framework for the existence of such effect also in vacuum. The Cotton-Mouton effect in vacuum known as Vacuum Magnetic Birefringence (VMB) was calculated in 1970 as one of the nonlinear optical effects described by the Euler-Heisenberg-Weiskopf effective Lagrangian [6], [7]. It can be seen as the result of the interaction of external magnetic field with quantum vacuum fluctuation.

In a vacuum, therefore, index of refraction $n_\parallel$ for light polarized parallel to $\boldsymbol{B}$ is expected to be different from the index of refraction $n_\perp$ for light polarized perpendicular to $\boldsymbol{B}$.

$$\Delta n = (n_\parallel - n_\perp) \tag{1}$$

For symmetry reasons, the difference Δn is proportional to B^2,

$$\Delta n = \Delta n_u\, B^2 P \tag{2a}$$
$$\Delta n = \Delta n_{uv}\, B^2 \tag{2b}$$

where $\Delta n_{u,uv}$ is normalized Cotton-Mouton birefringence of medium (gasses Δn_u, vacuum Δn_{uv}) and P is the pressure.

When linearly polarized light passes through the region of the transverse magnetic field with difference Δn, it acquires an ellipticity ψ. The ellipticity to be measured can be written as,

$$\psi = \pi \frac{L}{\lambda} \Delta n \sin 2\theta \tag{3}$$

where L is length of the magnetic field region, λ the light wavelength, and θ the angle between light polarization and the magnetic field direction.

In a dilute matter like gas, the Cotton-Mouton effect is very weak, and it needs very sensitive ellipsometers to be measured. For example difference Δn in refraction indexes of parallel and perpendicular polarization with respect to $\boldsymbol{B}$ in Helium, in the field of 1 T and under pressure of 1 atm is $\Delta n \approx 2.4 \times 10^{-16}$ [8], [9]. In a vacuum, quantum electrodynamics (QED) predicts that a field of 1 T should induce anisotropy of the index of refraction of about $\Delta n \approx 4 \times 10^{-24}$ [6], [7].

Cotton-Mouton effect dependence on the pressure in gas makes it an ideal candidate for ellipsometry setup sensitivity testing. If we reach the absolute level of vacuum in a perfect case, we should end up only with contributions from VMB. Since the vacuum is never absolute, Cotton-Mouton effect in gas is one of the possible sources of the false signal [10], [11].

It is evident from weak anisotropy induced by magnetic field in vacuum and equation (3) that for successful measurement of VMB effect one needs very sensitive ellipsometer and a high magnetic field in a region, which should we make as long as possible.

From the first prediction of Vacuum Magnetic Birefringence this very primary effect has not yet been experimentally verified.

In 1986 Maiani, Petronzio, and Zavattini showed that a neutral, spinless boson both scalar and pseudoscalar, that couples with two photons, could induce an ellipticity similar to the one predicted by QED [12]. Moreover, an apparent rotation of the photons into real boson results in a vacuum magnetic dichroism, which is absent in the framework of standard QED [6]. The measurement of ellipticity and dichroism including their signs can in principle thoroughly characterize the hypothetical boson, its mass m_a, the inverse coupling constant M_a, and the pseudoscalar or scalar nature of the particle. Maiani, Petronzio, Zavattini´s paper was essentially motivated by the search for Peccei and Quinn's axions [13]. Axions are pseudoscalar, neutral, spinless bosons introduced to solve what is called the *strong CP problem*. Axion are also one of the main candidates for *dark matter*.

1.2 Review of Vacuum Magnetic Birefringence experiments

Some of the first experiments to measure the VMB were based on the use of an interferometer of the Michelson type. One of the two arms passed through a region where a transverse magnetic field was present inducing a difference in the light velocity what should be observed as a phase shift.

In 1979 Iacopini and Zavattini [14] proposed the first sensitive ellipsometer to measure the ellipticity induced on linearly polarized laser beam by the presence of a transverse magnetic field. An optical cavity was part of the setup to increase the optical path in the magnetic field region [15]. The effect to be measured in proposed configuration was modulated in a view to use a *heterodyne* technique to increase the signal to noise ratio.

Iacopiny and Zavattiny performed experimental measurements with electromagnets in CERN, and they tested proposed sensitive heterodyne ellipsometer on Cotton-Mouton effect (CME) in different gases [16], [17]. Modulation of the CME effect was realized via rotation of the electromagnet itself, and an optical cavity to increase the optical length in the magnetic field was optical delay cavity with $N \sim 100$ passes. The sensitivity of tested ellipsometer was not sufficient to reach the VMB level.

Following Zavattini´s proposal and first tests, a similar apparatus has been set up at the Brookhaven National Laboratory, USA. The Project is known as BRFT [18], [19] also used the multipass optical cavity $N \sim 500$ in order to increase the optical path in the magnetic field region. BRFT collaboration used two Brookhaven electromagnets as the source of external magnetic field and the modulation of the field was realized by the current modulation in the coil. No evidence for dichroism induced by the magnetic field nor ellipticity was found. The sensitivity was not enough to neither detect QED effect nor for quantum Chromodynamics QCD effect. Limits on the axion parameters and Cotton-Mouton effect of helium has been published in 1993 for the first time [19].

In 1991, a new attempt to measure the vacuum magnetic birefringence has been started at the Legrano National Laboratory, Italy, by the PVLAS (LNL)

collaboration [20]–[22]. This experiment was based on Zavattini´s proposal from 1979. A Fabry-Perot resonant cavity was used for the first time to increase the effect to be measured ($N \sim 50\,000$), while the superconducting $5\,T$ magnet rotates around its own axis to provide the heterodyne signal. The PVLAS collaboration has published the observation of a magnetically induced dichroism in vacuum [23]. This result has triggered a lot of interest, because of the possible existence of the axion. This measurement was in contradiction with other experiments looking for axions as CAST, OSQAR or ALPS. Very recently PVLAS collaboration has posted a preprint disclaiming their previous observations of magnetically induced dichroism in a vacuum on the internet. In later papers, PVLAS did not confirm any results for ellipticity or dichroism measurements in vacuum [24].

In 1996 Q&A experiment was established in Taiwan [25] and again this research was based on Zavattini´s proposal from 1979. Similarly to PVLAS experiment Q&A collaboration has used Fabry-Perot resonant cavity to increase optical path in magnetic field $N \sim 30\,000$. As a source of magnetic field, Q&A collaborators used rotating permanent magnet instead of superconducting one. The First test of ellipsometer was made in 2003 and final results were published in 2009, 2010 as Cotton-Mouton effect measurement in different gases as a function of pressure and the limit for axion search [26], [27]. Similarly to BRFT and PVLAS (LNL), Q&A experiment was not enough sensitive to reach the level of QED Vacuum Magnetic Birefringence.

In the 2000 year, different setup from Iacopini and Zavattini scheme was proposed. BMV experiment is based in Toulouse, France and is run by National Laboratory of High magnetic fields [28]. Research setup relies on resonant Fabry-Perot cavity ($N \sim 10^5$) which is similar to PVLAS but for the magnetic field modulation, the magnetic pulse is used instead of rotating magnet or modulated current. The measurement is made as homodyne type. This novel technique is similar to ringdown spectroscopy and since the Zavattini proposal from 1979, it is the first realized different setup and ellipsometry principle used for VMB measurement [11].

In 1998 PVLAS (FE) was established in University of Ferrara. Ellipsometer is based on the same principle as previous one in PVLAS (LNL), but this time

experimenters used rotating permanent magnet in Halbach configuration. It is much easier to reach higher modulation frequencies instead of rotating with a large superconducting magnet or modulate current in the coil. To rotate with the magnet on higher rates improve the signal to noise ratio, since all VMB experiments are influenced by $1/f$ noise. PVLAS (FE) have also introduced a new principle of zero measurement which is very important to study and eliminate all spurious signals and noises. Because of relatively small dimensions of PVLAS (FE), it is possible to place the whole setup on one granite table, therefore experimenters are able to control resonant optical cavity with the extremely high finesse of $F = 5 \times 10^5$, which is giving them extremely long optical path NL in magnetic field region ($N \sim 3 \times 10^5$). Nowadays PVLAS (FE) setup is the most advanced VMB ellipsometer ever build [29]–[31].

In 2006 experiment OSQAR in CERN, Switzerland / France was established. OSQAR experiment is one of the three tests still running with the aim to measure VMB. First tests with ellipticity measurements on experiment OSQAR were made by Miroslav Král [32] as Cotton-Mouton effect measurement in air. This doctoral thesis is second experimental approach at experiment OSQAR in the field of VMB measurements and is based on the principle similar to PVLAS, but with the aim to conduct useful setup for further measurements on static magnetic fields produced by superconducting LHC or Hera dipole magnets.

At the end of this section, we have to announce that there was also proposed other different setup compared to Zavattini proposal. It was experiment Fermi Lab 877 [33], [34] and this experimental scheme is based on frequency measurement instead of amplitude measurement. Unfortunately, after the first tests in the laboratory, the experiment was stopped due to lack of funding and has never been started again.

In the field of vacuum magnetic measurements, we have to mention also experiment CAST [35], [36], ALPS [37], [38] an OSQAR LSW [39]–[41] but these experiments look for Axion and axion-like particles in different ways.

Experiment	PVLAS	BMV	**OSQAR**
Laser wavelength [nm]	1064	1064	**632.8**
Magnet type	pernament	puls EM	**static EM**
B^2L [T^2m]	10	5.8	**1159**
B max [T]	2,5	6.5	**9**
Cavity finesse	7×10^5	4.45×10^5	**NA**
QED ellipticity [rad]	5×10^{-11}	9×10^{-11}	**2.3×10^{-14}**
Detection scheme	heterodyne	homodyne	**homodyne**
Magnet modulation frequency [Hz]	10	500	**NA**
Duty cycle	1	3×10^{-6}	**NA**
Ellipsometer sensitivity [rad/$\sqrt{\text{Hz}}$]	5×10^{-7}	5×10^{-8}	**1.25×10^{-4}**
Measurable change of Δn	15×10^{-23}	8.1×10^{-21}	**1.8×10^{-14}**

Tab I. Parameters of experiments. PVLAS [31], BMV [11], OSQAR [42] (this study).

2   Theoretical Background

2.1   The polarization of light

One of the primary task in VMB measurement is to develop an ellipsometer, which should be as precise as possible [43]. We will need a theoretical background in light polarization. The ellipticity, which we want to measure, is the polarization state of the light after passing through the area of interest. It is also crucial to understand that birefringence is introduced almost in all media and therefore we put the general view to optical anisotropy which is the origin of birefringence. We will also introduce Jones formalism (light polarization matrix calculations) [44] for the practical reasons of easy calculation of expected signal coming to our detector.

2.1.1 Polarization

The polarization of light is determined by the direction of the electric field vector, which varies through time and space $E(r, t)$. For monochromatic light, all components of vector $E(r, t)$ vary sinusoidally and the end point of the vector $E(r, t)$ moves in the plane and traces an ellipse Fig 1. (left). In paraxial optics, when the light propagates in direction of the z axis, the waves are transverse electromagnetic waves (TEM) and the electric field vector lies in the in the $x - y$ plane Fig 1. (right). If the wave propagates in isotropic medium, the polarization ellipse stays unchanged during the propagation, and we can say, that light is *elliptically polarized*.
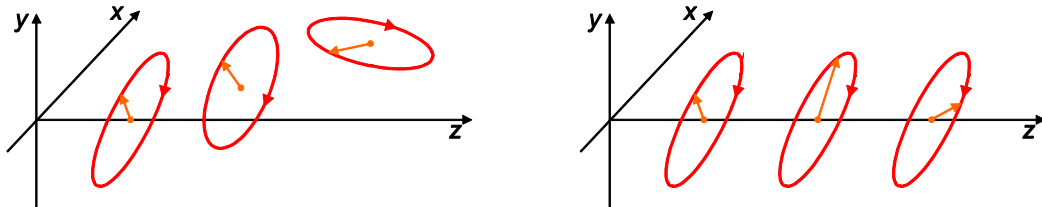

Fig 1. Electric field vector at different position: (left) arbitrary wave; (right) paraxial wave or plane wave propagating in the z direction in isotropic media. [45]

The orientation and ellipticity of the ellipse determine the state of polarization of the optical wave, the size of the ellipse is determined by the optical intensity. When the ellipse became a straight line or a circle, we speak about *linearly polarized* or *circularly polarized* light respectively [45].

Monochromatic plane wave of frequency ω propagating in the z direction with velocity c can be described as

$$E(z,t) = Re\left\{A exp\left[j2\pi\omega(t - \frac{z}{c})\right]\right\} \tag{4}$$

Where A is the complex envelope

$$A = A_x\hat{x} + A_y\hat{y}, \tag{5}$$

to describe the polarization of this wave we need to find the position of the endpoint of vector $E(z,t)$ for all z positions as a function of time. Expressing A_x and A_y in terms of their magnitudes and phases $A_x = a_x\exp(j\varphi_x)$ and $A_y = a_y\exp(j\varphi_y)$ and combining them into (4) and (5) we get

$$E(z,t) = E_x\hat{x} + E_y\hat{y}, \tag{6}$$

where

$$E_x = a_x \cos\left[2\pi\omega\left(t - \frac{z}{c}\right) + \varphi_x\right] \tag{7a}$$

$$E_y = a_y \cos\left[2\pi\omega\left(t - \frac{z}{c}\right) + \varphi_y\right] \tag{7b}$$

are the x and y components of the electric field vector $E(z,t)$. The components E_x and E_y are periodic functions of $t - z/c$ oscillating at frequency ω. Equations (7 a, b) are the parametric equations of the ellipse.

$$\frac{E_x{}^2}{a_x{}^2} + \frac{E_y{}^2}{a_y{}^2} - 2\cos\varphi \frac{E_x E_y}{a_x a_y} = \sin^2\varphi, \tag{8}$$

where $\varphi = \varphi_x - \varphi_y$ is the phase difference between E_x and E_y.

At a fixed value of z, the end of the electric vector rotates in the $x - y$ plane, tracing out the ellipse. In the time frame Δt, the end point of electric-field vector trace out the surface of an elliptical cylinder (see Fig 2.). The electric field repeats its motion periodically with wavelength λ.
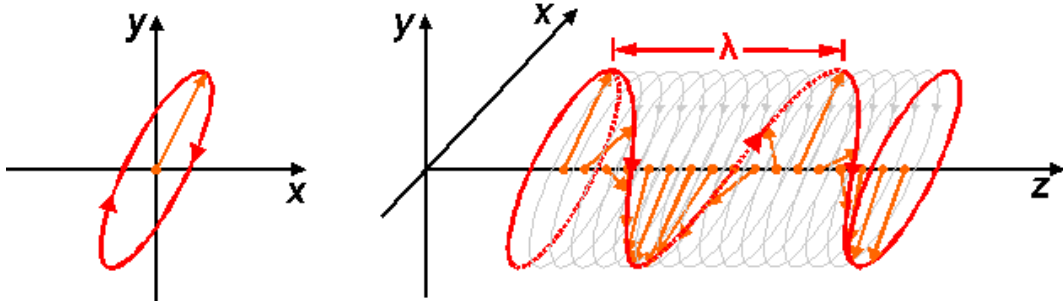
Fig 2. (Left) Rotation of the electric field endpoint at fixed position z; (right) Trajectory of the endpoint of electric field vectored fixed time frame Δt. [45]

The state of polarization depends on the shape of the ellipse which corresponds to the ratio of the magnitudes a_y/a_x and the phase difference φ of x and y component of the electric field. The size of the ellipse determines the intensity of the electromagnetic wave

$$I_m = \frac{a_x{}^2 + a_y{}^2}{2\eta}, \tag{9}$$

where η is the impedance of the medium.

The elliptically polarized light is the general case of the polarization states. In theory, we can find two special situations of polarization state as we have mentioned above. First is *linear polarization*, it occurs when one of the components a_x or a_y vanishes or when phase difference $\varphi = 0$ or π. The second important state of the polarization is *circular polarization*, it occurs when $\varphi = \mp\pi/2$ and $a_x = a_y = a_0$.

23

Corresponding to $+$ or $-$ we speak about *the right circularly polarized* or *the left circularly polarized* light.
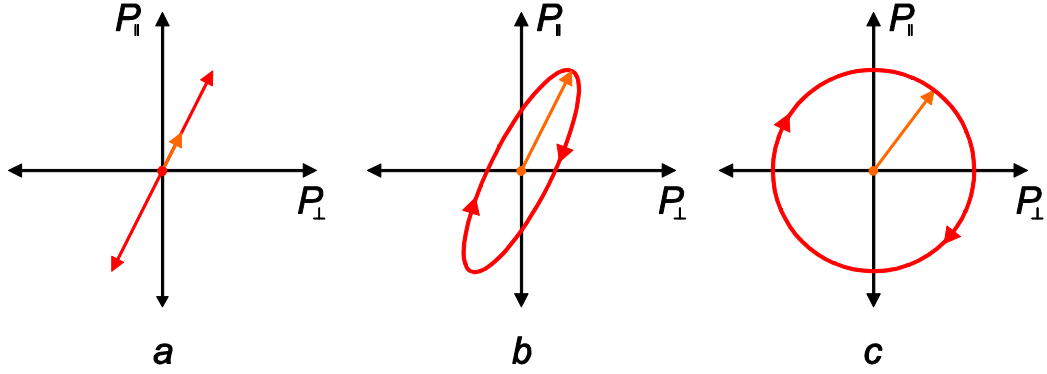

Fig 3. (a) Linear polarization; (b) elliptical polarization; (c) right circular polarization. [45]

2.1.2 Matrix Representation – Jones formalism

A monochromatic plane wave of frequency ω propagating in the z direction is completely characterized by the complex envelopes,

$$A_x = a_x \exp(j\varphi_x) \tag{10a}$$
$$A_y = a_y \exp(j\varphi_y) \tag{10b}$$

of the x and y components of the electric field. It is suitable to write these envelopes in the form of the vector

$$\boldsymbol{J} = \begin{bmatrix} A_x \\ A_y \end{bmatrix} \tag{11}$$

known as the *Jones vector*.[44]

When we would like to describe how the plane wave of arbitrary polarization propagates through an optical system that maintains the wave plane and changes only its polarization. We assume the optical system to be linear and the principle of

superposition is valid. The input A_{1x}, A_{1y} and output complex envelopes A_{2x}, A_{2y} are in general related by the weighted superposition's [43], [45]

$$A_{2x} = T_{11} A_{1x} + T_{12} A_{1y} \tag{12a}$$

$$A_{2y} = T_{21} A_{1x} + T_{22} A_{1y} \tag{12b}$$

where T_{11}, T_{12}, T_{21} and T_{22} are constants describing the polarization system. Equations (12) are general for all linear optical polarization devices. It is more often to write relations (12) in matrix notation.

$$\begin{bmatrix} A_{2x} \\ A_{2y} \end{bmatrix} = \begin{bmatrix} T_{11} & T_{12} \\ T_{21} & T_{22} \end{bmatrix} \begin{bmatrix} A_{1x} \\ A_{1y} \end{bmatrix} \tag{13}$$

Where 2x2 matrix $\boldsymbol{T}$ with elements T_{11}, T_{12}, T_{21} and T_{22} is called *Jones matrix* We can simplify relation (13) by using Jones vectors $\boldsymbol{J_1}, \boldsymbol{J_2}$ and Jones matrix $\boldsymbol{T}$ as

$$\boldsymbol{J_2 = TJ_1} \tag{14}$$

Jones matrix determines the effect of the optical system of the polarization state and intensity of the incident wave.

To calculate more complex optical setups, we can use a cascade of Jones matrices since $\boldsymbol{T_1}$ followed by another $\boldsymbol{T_2}$ is equivalent to a single system characterized by the matrix $\boldsymbol{T = T_2 T_1}$. We need to keep in mind that matrix multiplication is not commutative so the Jones matrices of the different devices should be in order which light is transmitted through them. First should appear to the right in the matrix product since it applies to the input Jones vector first.

The elements of the Jones vector and Jones matrices depend on the choice of the coordinate system. If these items are known in one coordinate system, they can be determined in another coordinate system by using rotation matrix $\boldsymbol{R}$.

$$\boldsymbol{R(\theta)} = \begin{bmatrix} \cos\theta & \sin\theta \\ -\sin\theta & \cos\theta \end{bmatrix} \tag{15}$$

If we transform Jones vector $\boldsymbol{J}$ from one coordinate system in a new coordinate system rotated by an angle θ, then the new Jones vector $\boldsymbol{J}'$ is given by

$$\boldsymbol{J}' = \boldsymbol{R}(\boldsymbol{\theta})\boldsymbol{J} \qquad\qquad (16)$$

Similarly, when we would like to transform Jones matrix $\boldsymbol{T}$ into new coordinate system with $\boldsymbol{T}'$ we get

$$\boldsymbol{T}' = \boldsymbol{R}(\boldsymbol{\theta})\boldsymbol{T}\,\boldsymbol{R}(-\boldsymbol{\theta}) \qquad\qquad (17)$$

Jones matrixes and vectors used for following calculation of optical setups are in Table II.

Jones vector of linear light polarization with rotation angle α respect to zero axis determination	$\boldsymbol{J}(\boldsymbol{\alpha}) = \begin{bmatrix} \cos\alpha \\ \sin\alpha \end{bmatrix}$
Jones matrix of rotation. Rotation of the angle θ respect to zero axis	$\boldsymbol{R}(\boldsymbol{\theta}) = \begin{bmatrix} \cos\theta & \sin\theta \\ -\sin\theta & \cos\theta \end{bmatrix}$
Jones matrix of phase retarder with fast axis along y direction, φ represents the delay (change) in y on phase	$\boldsymbol{T}(\boldsymbol{\varphi}) = \begin{bmatrix} \exp(-\mathrm{i}\varphi) & 0 \\ 0 & 1 \end{bmatrix}$
Jones matrix of ideal linear polarizer along x direction	$\boldsymbol{P}_i = \begin{bmatrix} 1 & 0 \\ 0 & 0 \end{bmatrix}$
Jones matrix of the real linear polarizer with the fast axis along the x direction, σ represents a polarization factor of the polarizer.	$\boldsymbol{P} = \begin{bmatrix} 1 & 0 \\ 0 & \sigma \end{bmatrix}$

Tab II. Examples of Jones matrixes and vectors used in this dissertation

2.2 Birefringence of light in an anisotropic medium

Birefringence is indirectly observed for many centuries. First knowledge of birefringence is known from Vikings. They used Icelandic limestone for precise detection of sun position in cloudy days to navigate their Drakars [46].

The physical effect of birefringence was described for the first time by Rasmussen Bartholy in 1669. Birefringence was first observed and studied by Bartholy on the crystal of Icelandic limestone (*CaCO₃*).

Birefringence, or double refraction, is the separation of a ray light into two beams called *ordinary* and *extraordinary* when it passes through the birefringent medium such as crystal. The origin of birefringence in the matter was fully understood in the framework of electromagnetic theory by James Clark Maxwell [47]. A series of his works showed that light propagates in the optical media at different speed depending on their permittivity and permeability. Basically in an optically anisotropic material permittivity and permeability values are different for different polarization of light and the light just spreads at different speeds in different directions.

Birefringence is quantified by:

$$\Delta n = n_e - n_o \tag{18}$$

Where n_o is the refractive index for the *ordinary* beam and n_e is the refractive index of the *extraordinary* beam.
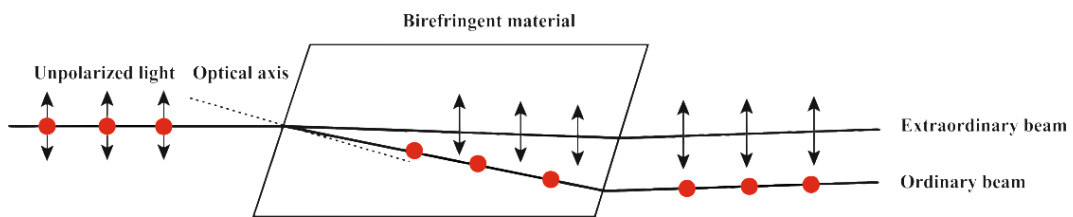

Fig 4. Light propagating through the birefringence media

Birefringence of light can be further observed under a different condition in gasses, liquids, colloids, solids, plasma and according to QED and QCD also in vacuum.

Birefringence is in many cases induced by external fields or forces, by an electric field *Kerr effect* [48], by magnetic field *Cotton-Mouton effect* [2], *Voigt effect*, by the stress in solids and by the flow of liquids. There are also other effects which can change the polarization state of light, such as *Faraday effect*, *Magneto-optical Kerr effect* (*MOKE*). Diffraction and refraction on surfaces also cause polarization change of the light.

All these polarization effects are in the sense of VMB measurement parasitic effects, but they contribute to a general view of VMB problem. We can say that some change in polarization state of light is connected to all media and surfaces which the light is passing through. So one has to use proper solution to distinguish measured signal from all parasitic ones, and this is, in my opinion, the biggest challenge in VMB optical metrology.

2.3 Cotton-Mouton effect

Because the VMB effect is from a measurement point of view exactly same as Cotton-Mouton effect in gas, we will put a few words about it. Also until now, all experiments were calibrated through the Cotton-Mouton effect in gas [8], [9], [26], [32]. In the final stage of VMB experiment, one is lowering the pressure in the apparatus to the level where the contribution from CME effect is negligible since the CME shows up the linear dependency to pressure P.

It is known since the beginning of the 20th century that any medium shows a linear birefringence in the presence of an external transverse magnetic field B. This phenomenon was firstly observed in a colloidal suspension by the Italian physicist, Majorana in 1902 and later in liquids by Cotton and Mouton in 1905 [2]. This effect observed in gasses is called Voigt effect but all community of experimentalist looking for VBM and axion-like particles are using only Cotton-Mouton effect name. Cotton-Mouton effect is analogue of the Kerr electro-optic effect [48], so one can also use Kerr effect to calibrate his ellipsometer [49].

For the symmetry reasons, the CME effect is proportional to the square of magnetic field B and the ordinary and extraordinary polarization direction are corresponding to parallel and perpendicular polarization direction to transverse magnetic field

$$\Delta n = n_e - n_o = n_\parallel - n_\perp = \Delta n_u \, PB^2 \qquad (19)$$

The phase retardation φ of light between these two polarization directions after passing through the transversal magnetic field $\boldsymbol{B}$ of the length L is:

$$\varphi = \frac{2\pi}{\lambda} \Delta n_u \, PB^2 L, \qquad (20)$$

where λ is the wavelength of the light, Δn_u is the normalized Cotton-Mouton birefringence, P pressure, B magnetic induction and L is the length of the magnetic field.

If the incident light polarization making an angle θ with respect to the transverse magnetic field $\boldsymbol{B}$ passes through the field of length L, the corresponding ellipticity to be measured is given as

$$\psi = \frac{\varphi}{2} \sin 2\theta = \frac{\pi}{\lambda} \Delta n_u \, PB^2 L \sin 2\theta \qquad (21)$$

The normalized Cotton-Mouton birefringence Δn_u is used in the community of VMB experimentalist as:

$$\Delta n = n_\parallel - n_\perp = \Delta n_u \, PB^2 \qquad (22)$$

In the sense of the previous chapter, the normalized Cotton-Mouton birefringence Δn_u is similar as Cotton-Mouton constant k_{CM}, which is also used in the theory of CME.

Gas	Normalized Cotton-Mouton Δn_u birefringence P= 1atm B=1T
O_2	-2.5×10^{-12}
N_2	-2.28×10^{-13}
Ar	5×10^{-15}

| He | 2.4×10^{-16} |

Tab III. Examples of normalized Cotton-Mouton Birefringence in different gases [26]

2.4 Vacuum magnetic birefringence theory

Vacuum magnetic birefringence is a small macroscopic effect based on the framework of Euler - Heisenberg - Weisskopf effective Lagrangian density [3], [4]. For slowly varying electromagnetic fields, to lowest order it is:

$$\mathcal{L}_{EHW} = \frac{1}{2\mu_0}\left(\frac{E^2}{c^2} - B^2\right) + \frac{A_e}{\mu_0}\left[\left(\frac{E^2}{c^2} - B^2\right)^2 + \left(\frac{E}{c} \cdot \boldsymbol{B}\right)\right]. \tag{23}$$

Where

$$A_e = \frac{2\alpha^2 \lambda_e}{45\mu_0 m_e c^2} = 1.32 \times 10^{-24} \ \text{T}^{-2} \tag{24}$$

$\lambda_e = \hbar/m_e c$ is the Compton wavelength of the electron, $\alpha = e^2/4\pi\varepsilon_0\hbar c$ is the fine structure constant, and m_e is the electron mass. The first term in equation (23), is the term coming from classical Lagrangian corresponding to Maxwell's equations in vacuum. In classical theory of electromagnetic fields the light -by-light interaction is not expected. The two other terms tell us that electrodynamics is nonlinear also in vacuum and enable new possible effects to measure.
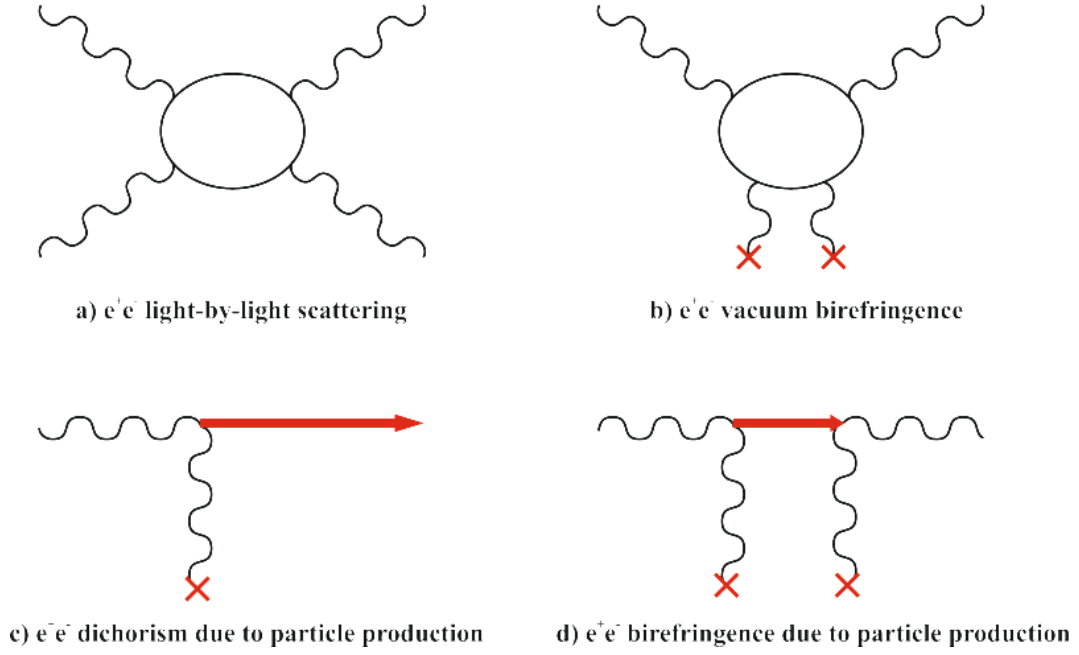
Fig 5. Lowest order Elementary processes leading to the magnetic birefringence and dichroism. [31]

In the frame of the quantum electrodynamics QED our primary interest is in the second Feynman diagram b, where photons interact through a virtual e^+e^- pair. In Fig 5. b diagram, two photons interact with an external magnetic field, and this is the mechanism which is making vacuum a birefringent medium in the presence of an external transversal magnetic field. Considering the complex index of refraction $n + ik$, it can be shown [6], [7], that the magnetic birefringence derived from equation (24) is

$$\Delta n^{(EHW)} = n_\parallel^{(EHW)} - n_\perp^{(EHW)} = 3A_e B_{ext}^{\,2} \tag{25}$$

corresponding to

$$\Delta n^{(EHW)} = 3.24 \times 10^{-22} \quad \text{in} \quad B = 9 \text{ T} \tag{26}$$

The calculations also show that the imaginary part of k is negligible, so no magnetic dichroism is predicted [6] in the framework of QED.

Magnetic birefringence and also dichroism could be introduced in vacuum through the new hypothetical light spin-zero axion-like particles (ALPs) [12], in analogy to

Primakoff effect [50]. Two processes generating dichroism and birefringence are shown in Figures 5c and 5d. Two different Lagrangians describe the pseudoscalar and the scalar cases:

$$\mathcal{L}_a = g_a \emptyset_a \boldsymbol{E} \cdot \boldsymbol{B} \quad \text{and} \quad \mathcal{L}_s = g_s \emptyset_s (E^2 - B^2) \tag{27}$$

Where g_a and g_s are the coupling constants of a pseudoscalar field $\emptyset_a$ and of scalar field $\emptyset_s$. The natural Heaviside-Lorentz units are used, so that $1\,\text{T} = \sqrt{\frac{\hbar^3 c^3}{e^4 \mu_0}} = 195\,\text{eV}^2$ and $1\,\text{m} = \frac{e}{\hbar c} 5.06 \times 10^6\,\text{eV}^{-1}$. For birefringence and dichroism we find [51]:

$$\left|\Delta n^{(ALPs)}\right| = n_\parallel{}^a - 1 = n_\parallel{}^s - 1 = \frac{g_{a,s}^2 B_{ext}^2}{2 m_{a,s}^2} \left(1 - \frac{\sin 2x}{2x}\right) \tag{28a}$$

$$\left|\Delta k^{(ALPs)}\right| = k_\parallel{}^a = k_\parallel{}^s = \frac{2}{\omega L} \left(\frac{g_{a,s} B_{ext} L}{4}\right)^2 \left(\frac{\sin x}{x}\right)^2 \tag{28b}$$

Where $m_{a,s}$ are the masses of the particles, $x = \frac{L m_{a,s}^2}{4\Omega}$, Ω is the photon energy, and L is length of the magnetic field region.

Consider now the vacuum fluctuation of particles with charge $\pm\varepsilon e$ and mass m_ε. The photon propagating trough the homogenic magnetic field may interact with such fluctuation, resulting in a phase delay [52], if the photon energy $\hbar\Omega > 2 m_\varepsilon c^2$, in a pair production.

We will separate the problem for two cases. First for Dirac fermions (Df) and at second to scalar (sc) bosons. The indexes of refraction of photons parallel and perpendicular to the external transverse magnetic field have two different mass regimes defined by a dimensionless parameter χ:

$$\chi \equiv \frac{3}{2} \frac{\hbar\Omega}{m_\varepsilon c^2} \frac{\varepsilon e B_{ext} \hbar}{m_\varepsilon^2 c^2} \tag{29}$$

In the case of fermions, it can be shown that [52]

$$\Delta n^{(Df)} = A_\varepsilon B_{ext}^2 \begin{cases} 3 & \text{for } \chi \ll 1 \\ -\dfrac{9}{7}\dfrac{45}{2}\dfrac{\pi^{\frac{1}{2}}2^{\frac{1}{3}}\left[\Gamma\left(\frac{2}{3}\right)\right]^2}{\Gamma\left(\frac{1}{6}\right)}\chi^{-\frac{4}{3}} & \text{for } \chi \gg 1 \end{cases} \tag{30}$$

where

$$A_\varepsilon = \frac{2}{45\mu_0}\frac{\varepsilon^4\alpha^2\lambda_\varepsilon^3}{m_\varepsilon c^2} \tag{31}$$

similarly to equation (24). In the limit of large masses ($\chi \ll 1$) the expression reduces to equation (25) with the substitution of εe with e and m_ε with m_e. For small masses the birefringence depens on the parameter $\chi^{-\frac{4}{3}}$ resulting in a net dependence of $\Delta n^{(Df)}$ with $B_{ext}^{2/3}$ rather than B_{ext}^2. For dichroism one finds [52]

$$\Delta k^{(Df)} = \frac{1}{8\pi}\frac{\varepsilon^3 e\alpha\lambda B_{ext}}{m_\varepsilon c} \begin{cases} \sqrt{\dfrac{3}{32}}e^{-4/\chi} & \text{for } \chi \ll 1 \\ \dfrac{2\pi}{3\Gamma\left(\frac{1}{6}\right)\Gamma\left(\frac{13}{6}\right)}\chi^{-\frac{1}{3}} & \text{for } \chi \gg 1 \end{cases} \tag{32}$$

The results are very similar to Dirac fermions for the milli-charged scalar particles [52]. There are also two mass regions defined by the same parameter χ. The birefringence is given by

$$\Delta n^{(sc)} = A_\varepsilon B_{ext}^2 \begin{cases} -\dfrac{6}{4} & \text{for } \chi \ll 1 \\ \dfrac{9}{14}\dfrac{45}{2}\dfrac{\pi^{\frac{1}{2}}2^{\frac{1}{3}}\left[\Gamma\left(\frac{2}{3}\right)\right]^2}{\Gamma\left(\frac{1}{6}\right)}\chi^{-\frac{4}{3}} & \text{for } \chi \gg 1 \end{cases} \tag{33}$$

Moreover, dichroism is given by

$$\Delta k^{(sc)} = \frac{1}{8\pi}\frac{\varepsilon^3 e\alpha\lambda B_{ext}}{m_\varepsilon c} \begin{cases} -\sqrt{\dfrac{3}{8}}e^{-4/\chi} & \text{for } \chi \ll 1 \\ -\dfrac{\pi}{3\Gamma\left(\frac{1}{6}\right)\Gamma\left(\frac{13}{6}\right)}\chi^{-\frac{1}{3}} & \text{for } \chi \gg 1 \end{cases} \tag{34}$$

This analysis implies that there is a sign difference in the case of Dirac fermions, both for birefringence and for dichroism.

Contribution from QCD predictions (ALPs, Df, sc) to VMB is about 5% of the Δn_{uv}, therefore in rest of the text, we will focus on the possibility how to measure the QED $\Delta n^{(EHW)}$ part of Δn_{uv}, since no one has reach this level yet.

3   OSQAR experiment

OSQAR (Optical Search for QED Vacuum Birefringence, Axions and Photon Regeneration) experiment at CERN is one of the several running experiments in the field of VMB measurements. Experiment OSQAR was established in 2006, and since then the measurement of VMB is part of its scientific program [53], [54].

First developments of precise ellipsometer for OSQAR experiment were done in 2006 by Miroslav Král. His setup was based on rotating half-wave plate in double pass configuration. Ellipsometer was tested on Cotton-Mouton (Voigt effect) measurement in air and results were published in his Ph.D. thesis in 2007 [33]. In next four years (2007-2011) OSQAR experiment proposed another setup to measure VMB (n-1 experiment) [54], but it has never been used experimentally to measure CME (Cotton-Mouton effect) or VMB in CERN.

In 2011 Dr. Miroslav Šulc got funding from Czech Grant Agency (GAČR) to develop sensitive ellipsometer for VMB measurements and Axion searches through the LSW experiments in project OSQAR. Because I became a Ph.D. student of Dr. Miroslav Šulc and a member of OSQAR experiment in a half of 2011, this new development of sensitive ellipsometer was entrusted to me.

The main idea of GAČR proposal was to use the electro-optic modulator (EOM) instead of rotating half-wave plate to reach higher modulation frequencies for better signal to noise ratio, similar to PVLAS experiment. So this was my part to make a test setup with EOM and implement it with LHC magnets on CME measurement in CERN.

3.1   OSQAR ellipsometer

To calculate the birefringence of anisotropic medium one has to measure the change of ellipticity ψ or change of phase retardation φ induced by difference of refraction indexes Δn, of two orthogonal polarization see Eqs. (19, 20, 21). The simplest *static* ellipsometer is composed by two orthogonally crossed polarizers, the polarizer $\boldsymbol{P}$ and, analyser $\boldsymbol{A}$, with birefringence medium described by $\boldsymbol{T}(\varphi)$ placed between

polarizers with fast axis at $\theta = 45°$ to maximise the ellipticity ψ [43] to be measured.

We use the Jones´ matrices (Table I.) to calculate the light intensity I reaching the detector after the analyser $\boldsymbol{A}$. With intensity I_0 of the light before analyser $\boldsymbol{A}$, we can calculate the light intensity I of this simple ellipsometer as:

$$\boldsymbol{E} = E_0 \cdot \boldsymbol{A} \cdot \boldsymbol{R}(45°) \cdot \boldsymbol{T}(\varphi) \cdot \boldsymbol{R}(-45°) \cdot \boldsymbol{P} \cdot \boldsymbol{J}(\alpha) \tag{35}$$

where $\boldsymbol{A} = \boldsymbol{R}(\theta) \cdot \boldsymbol{P} \cdot \boldsymbol{R}(-\theta)$ for $\theta = 90°$ and $\alpha = 0°$

$$I = \boldsymbol{E} \cdot \boldsymbol{E}^* = I_0 \left(\sin^2 \frac{\varphi}{2} + \sigma^2 \cos^2 \frac{\varphi}{2} \right) \approx I_0(\psi^2 + \sigma^2) \text{ for } \varphi \ll 1 \tag{36}$$

where $\psi = \frac{\varphi}{2}$ is the ellipticity induced by the birefringence medium at $45°$ and σ^2 is the extinction ratio of the crossed polarizers.

For the measurement of tiny ellipticity as in the case of VMB, the ψ^2 ($\psi^2 \approx 10^{-22}$) is very small compared to σ^2 ($\sigma^2 \approx 10^{-8} - 10^{-6}$ for commercially available polarizers). Therefore it is necessary to use the solution of linearizing I with respect to ψ, together with modulation techniques (*homodyne* or *heterodyne*) to get better signal to noise ratio (S/N) in measured signal.

The linearization in low ellipticity measurements is introduced by some other ellipticity, which could be static or dynamic. For VMB modulation techniques in *homodyne* schemes one can use additional statistic ellipticity and modulate the magnetic field, or to use the dynamic spare ellipticity to modulate the birefringence signal directly in the presence of a static external magnetic field.

Modulation of the magnetic field can be realized via modulation of current (continuous or pulsed) in the case of superconducting electromagnets [19], [28]. Modulation of the superconducting electromagnets is possible only in the range from mHz to 1 Hz in a continual regime. In the pulse regime, the frequency is higher (400 Hz), but the repetition rate (duty cycle) is meager [55]. With current modulation one is not able to overcome low-frequency $1/f$ noise very effectively

and with pulse magnets the duty cycle is low so we need very long measurement time t to profit from signal integration.

Another solution of magnetic field modulation is to rotate with magnet itself, to constantly change the angle θ between magnetic and electric field vector. This idea was realized in PVALS (LNL) [21] with enormous effort and cost to rotate with superconducting magnet. Unfortunately this is not possible in OSQAR experiment with LHC spare dipole magnet.

For magnetic field rotation modulation is technically more convenient to use permanent magnets with lower magnetic field and profit from higher modulation frequencies in the range of several Hz (10 Hz). Setup with the rotating permanent magnet was firstly used in Q&A [25] experiment and now in PVLAS (FE) [29]. Usage of two permanent magnets also allows the zero measurements with crossed magnetic fields to check spurious signals coming from the Strait fields acting on the optics [29].

Second modulation possibility in the *homodyne* setups is to use phase modulator to modulate the ellipticity signal. For this purpose, we can use photo-elastic modulator (PEM) or electro-optic modulator (EOM).

In *heterodyne* detection, one has to combine both modulations (magnetic field and ellipticity) to achieve interference between carrier signal PEM/EOM and modulation of the magnetic field. This *heterodyne* detection is used in PVLAS experiment setup, which is most advanced one in the field of VMB searches [31].

Due to lack of possibility to modulate LHC magnet in OSQAR experiment we have started with a *homodyne* technique based on EOM modulation of the birefringent signal.

3.2 Experimental method

In Figure 6. a basic scheme of the OSQAR polarimeter is shown. A linearly polarized light coming from the laser (632 nm) goes first through the Faraday isolator to protect the laser from the back reflection. Then the beam goes through the half waveplate ($\lambda/2$) to set the polarization plane in the zero degree position to avoid any power losses on the polariser P where the beam is highly polarized. The

beam then propagates trough the electro-optic modulator (EOM), which modulates the incoming polarization from the left to right ellipticity with the given frequency f_m and modulation depth T_0. This modulation serves as a career for the measurement signal to optimize signal over noise ratio and to linearize the measurement ellipticity.

The beam then propagates through the birefringence sample, in the measurements presented in this work, it was nitrogen gas in LHC dipole magnet anticryostat with the transversal magnetic field up to $B = 9$ T strength and length of $L = 14.3$ m. In the magnet, light acquires an ellipticity change ψ from the induced linear birefringence. The polarization state of the beam is then analysed by the analyser **A**. The intensity I of the light is detected by the photodiode PD and demodulated by the Lock-in amplifier.
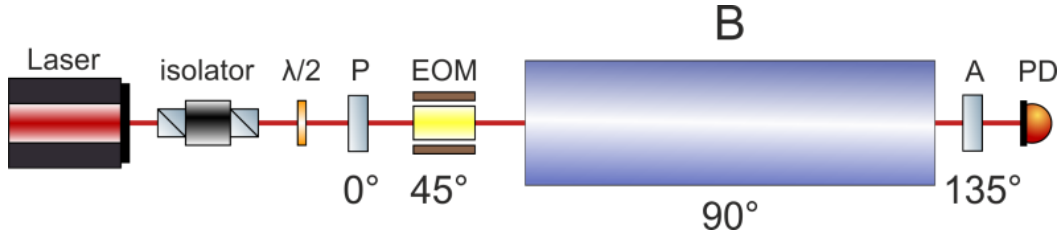
Fig 6. Simplified scheme of OSQAR ellipsometer with the angular orientation of the optical components.

The configuration of each successive component in the setup is at 45 degrees to its previous element [56]. The polarizer **P** and analyser **A** are not crossed, but in 45 degree position.

To calculate the intensity I reaching the detector after the analyser **A** we use Jones´ matrices to describe the effect of the optical elements. The optical element describing linear magnetic birefringence can be written similarly as phase retarder. The direction of the external magnetic field **B** determines the slow axis of the birefringence element.

$$X(\varphi) = \begin{bmatrix} \exp(-i\varphi) & 0 \\ 0 & 1 \end{bmatrix}, \tag{37}$$

where φ is the phase difference between the two polarisation directions added by the linear birefringence according to equation (20). The electric field after the analyser can be calculated as

$$\boldsymbol{E} = E_0 \cdot \boldsymbol{R}(\theta) \cdot \boldsymbol{A} \cdot \boldsymbol{R}(-\theta) \cdot \boldsymbol{R}(\gamma) \cdot \boldsymbol{X}(\varphi) \cdot \boldsymbol{R}(-\gamma) \cdot \boldsymbol{R}(\beta) \cdot \boldsymbol{T}(\xi) \cdot \boldsymbol{R}(-\beta) \cdot \boldsymbol{P} \cdot \boldsymbol{J}(\alpha)$$

$$(38)$$

In this formula, from left to right, one finds the Jones matrices of the analyser $\boldsymbol{A}$ at angle $\theta = 135°$, of the linear birefringence medium $\boldsymbol{X}(\varphi)$ at angle $\gamma = 90°$, of the electro-optic modulator $\boldsymbol{T}(\xi)$ at angle $\beta = 45°$, of the polarizer $\boldsymbol{P}$ determining the zero angle and of the initial polarization $\boldsymbol{J}(\alpha)$ at angle $\alpha = 0°$. The Jones matrix $\boldsymbol{T}(\xi)$ of EOM is same as for phase retarder with slow axis in x direction, where phase change is $\xi = T_0 \sin 2\pi f_m t$. The corresponding intensity I reaching the photodiode from $\boldsymbol{E}$ is

$$I = \boldsymbol{E} \cdot \boldsymbol{E}^* = I_0 \left(\frac{1}{2} + \frac{\sigma^2}{2} + \frac{1}{2}(1 - \sigma^2) \sin \varphi \sin \xi \right) \qquad (39)$$

Because in our case the extension ratio of polarizers is $\sigma^2 \approx 10^{-6}$, we can approximate $1 - \sigma^2 \approx 1$ and also $\frac{1}{2} + \frac{\sigma^2}{2} \approx \frac{1}{2}$, assuming that $\varphi \ll 1$ the $\sin \varphi \approx \varphi$ and substituting $\xi = T_0 \sin 2\pi f_m t$ we get,

$$I = \frac{I_0}{2}(1 + \varphi \sin(T_0 \sin 2\pi f_m t)) \qquad (40)$$

Term of $\sin(T_0 \sin 2\pi f_m t)$ could be transformed using the Bessel function of first kind as,

$$\sin(T_0 \sin 2\pi f_m t) = 2 \sum_{n=odd} J_n(T_0) \sin n 2\pi f_m t \qquad (41)$$

$$I = \frac{I_0}{2}(1 + \varphi(2J_1(T_0) \sin 2\pi f_m t + high\ order\ odd\ terms)) \qquad (42)$$

Where depth of modulation of electro-optic modulator T_0 is given as

$$T_0 = \left(\frac{V_m}{V_\pi}\right)\pi \tag{43}$$

V_m is the amplitude of applied oscillating voltage to EOM and V_π is half wave voltage of EOM.

To measure the phase change φ induced by the birefringence sample, one can use the phase sensitive Lock-in amplifier, locked to the fundamental frequency of EOM f_m and demodulate the signal coming from the photodiode. φ can be calculated as follow:

$$\sqrt{2}V_{1f} = \frac{I_0}{2}\varphi 2J_1(T_0) \tag{44a}$$

$$V_{DC} = \frac{I_0}{2} \tag{44b}$$

$$\varphi = \frac{\sqrt{2}V_{1f}}{V_{DC}2J_1(T_0)} \tag{44c}$$

where V_{1f} is the rms AC output intensity (R value) of DSP Lock – in amplifier for frequency f_m and V_{DC} is DC intensity on photodiode.

3.3   Spurious birefringence

Consider now that in any optical systems, there is always present some artificial birefringence, different from one we want to measure. This spurious birefringence can be significant compared to measured one, especially in the case of VMB measurements. Origin of spurious birefringence is in the imperfection of optical elements, in mechanical stress applied to optical components, vibrations or thermal effects. Spurious birefringence is either static or slowly varying in time.

If the ς is phase change induced by this spurious birefringence, with the fast axis along the x direction and δ is the angle between the fast axis and the initial direction of polarization of the light. This spurious birefringence can be described by the Jones matrix $\boldsymbol{S}$.

$$S(\varsigma, \delta) = R(-\delta) \cdot T(\varsigma) \cdot R(\delta) = \begin{bmatrix} \cos\delta^2 + e^{-i\varsigma}\sin\delta^2 & (1 - e^{-i\varsigma})\cos\delta\sin\delta \\ (1 - e^{-i\varsigma})\cos\delta\sin\delta & e^{-i\varsigma}\cos\delta^2 + \sin\delta^2 \end{bmatrix}$$

$$\text{(45)}$$

moreover, suppose that $\varsigma \ll 1$ we get

$$S(\varsigma, \delta) \approx \begin{bmatrix} 1 - i\,\varsigma\sin\delta^2 & i\,\varsigma\cos\delta\sin\delta \\ i\,\varsigma\cos\delta\sin\delta & 1 - i\,\varsigma\cos\delta^2 \end{bmatrix} \qquad \text{(46)}$$

Implementing now the spurious birefringence into the equation (38), no matter if we place $X(\varphi)$ before or after induced birefringence, since both changes in ellipticity are small.

We suppose that $\sigma^2, \varphi, \varsigma \ll 1$ and therefore we will neglect the terms including $\sigma^2, \varphi^2, \varsigma^2, \varphi\varsigma$. The corresponding intensity I reaching the photodiode from E is:

$$E = E_0 \cdot R(\theta) \cdot A \cdot R(-\theta) \cdot S(\varsigma, \delta) \cdot R(\gamma) \cdot X(\varphi) \cdot R(-\gamma) \cdot R(\beta) \cdot T(\xi) \cdot R(-\beta) \cdot$$
$$P \cdot J(\alpha) \qquad \text{(47)}$$

$$I = E \cdot E^* = \frac{I_0}{2}(1 + (\varphi + \varsigma\cos 2\delta)\sin\xi) \qquad \text{(48)}$$

Equation (48) can be transformed similar to (42) by using the Bessel function of the first kind to express harmonic components of the signal. From (48) we see that maximum change induced by the spurious ellipticity is when the angle $\delta = 0 \; and \; \frac{\pi}{2}$.

If we would like to measure the phase change induced by the birefringence sample φ according to (48), we will finish with the overall value of $\varphi + \varsigma\cos 2\delta$ where the spurious signal is mixed with one to be measured.

A: Static spurious birefringence

The case that the spurious birefringence ς is static. In OSQAR experiment we are not able to modulate birefringence through the magnetic field modulation to get heterodyne signal but we are able to slowly change the magnetic field from 0 to 9T (in 257s) and induce the change to $\varphi(t)$. Then we can calculate the phase change coming from measured birefringence as difference of overall birefringence with magnetic field OFF and ON.

$$(\varphi + \varsigma \cos 2\delta)_{9T} - (\varphi + \varsigma \cos 2\delta)_{0T} = \varphi_{\Delta T} \qquad \varphi_{0T} = 0 \qquad (49)$$

B: Slowly varying spurious birefringence

The case that the spurious birefringence is not static but is slowly varying in time $\varsigma(t)$. In this case one has to introduce modulation of VMB effect (heterodyne detection) to minimize error coming from spurious birefringence. If it is not possible, we should measure the spurious signal in time and then subtract it from birefringence signal as in (49).

After the analysis of spurious birefringence signal $\varsigma(t)$ we have developed the solution of reference branch measurement to measure the spurious birefringence in time and use it for subtraction from birefringence to be measured. Technical solution of reference measurement is discussed in detail in experimental section.

3.4 Intrinsic noise and sensitivity of the ellipsometer

The initial limiting parameter to achieve any measure of a physical quantity is the noise. Especially in the case when we want to measure small effect as VMB the noise and corresponding sensitivity give us an answer if we can succeed or not. The noise in our polarimeter can be caused by several independent sources which are known but there are also some sources which we still need to understand.

There are four known independent noise sources which can be calculated, shot noise, Johnson noise, diode noise (dark current noise), Relative Intensity Noise [31]. The overall noise is an incoherent superposition of each of them

$$i_{tot} = \sqrt{i_{shot}^2 + i_{johnson}^2 + i_{dark}^2 + i_{RIN}^2} \tag{50}$$

The corresponding measurable minimum phase change φ_{min} of our setup can be expressed as follow

$$\varphi_{min} = \frac{i_{tot}}{q\frac{I_0}{2}J_1(T_0)} \tag{51}$$

3.4.1 Shot Noise

The intrinsic r.m.s shot noise is caused by the direct current i_{dc} in the detector. Shot noise was studied by Walter Schottky and has origin in particle behavior of light and electrons. Shot noise has Poisson distribution and is flat (white) in the frequency domain, therefore the shot noise density is constant over $\Delta\nu$. The rms shot noise is expressed by the intensity I_0 as:

$$i_{shot} = \sqrt{2eq\frac{I_0}{2}} \tag{52}$$

The corresponding phase change φ_{shot} of polarimeter is

$$\varphi_{shot} = \frac{\sqrt{2}i_{shot}}{q\frac{I_0}{2}J_1(T_0)} = \frac{\sqrt{2}\sqrt{2eq\frac{I_0}{2}}}{q\frac{I_0}{2}J_1(T_0)} \tag{53}$$

3.4.2 Johnson Noise

Johnson-Nyquist noise or thermal noise has an origin in the thermal motion of the charge carriers in an electrical circuit. It has Poisson distribution and is also flat (white) in the frequency domain. Johnson noise is different from the shot noise and is present when a voltage is applied to, and the macroscopic currents start the flow.

In the photodiode is Johnson noise due to trans-impedance G of the internal amplifier. The Johnson noise rms value

$$i_J = \sqrt{\frac{4k_B T}{G}} \tag{54}$$

The corresponding phase change φ_J of polarimeter is

$$\varphi_J = \frac{\sqrt{2}i_J}{q\frac{I_0}{2}J_1(T_0)} = \frac{\sqrt{2}\sqrt{\frac{4k_B T}{G}}}{q\frac{I_0}{2}J_1(T_0)} \tag{55}$$

3.4.3 Photodiode dark noise

The photodiode dark noise or dark current is a small electric current which is present on the photodiode in the absence of incoming photon signal. Physically, dark current is due to random generation of electron-hole pairs within the depletion region. The formula to calculate the rms value of dark current or diode noise is,

$$i_{dark} = \frac{V_{dark}}{G} \tag{56}$$

The corresponding phase change φ_{dark} of polarimeter is

$$\varphi_{dark} = \frac{\sqrt{2}i_{dark}}{q\frac{I_0}{2}J_1(T_0)} = \frac{\sqrt{2}\frac{V_{dark}}{G}}{q\frac{I_0}{2}J_1(T_0)} \tag{57}$$

3.4.4 Relative intensity noise (RIN)

The relative intensity noise of the laser is caused by laser cavity fluctuation, thermal instability, change in laser gain medium. It is white noise in the range of frequencies up to 100 kHz. It is proportional to laser power and can be calculated as follow,

44

$$i_{RIN}(f_m) = q \frac{I_0}{2} N_{RIN}(f_m) \tag{58}$$

The corresponding phase change φ_{RIN} sensitivity of polarimeter is

$$\varphi_{RIN}(f_m) = \frac{\sqrt{2} i_{RIN}}{q \frac{I_0}{2} J_1(T_0)} = \frac{\sqrt{2} q \frac{I_0}{2} N_{RIN}(f_m)}{q \frac{I_0}{2} J_1(T_0)} \tag{59}$$

Figure 7. shows all the intrinsic noise contributions as function of T_0 in typical operating condition, with $q \approx 0.32$ A/W, $I_0 \approx 0.3$ mW, $G = 2.38$ kΩ, $V_{dark} = 120$ nV/$\sqrt{\text{Hz}}$, $N_{RIN}(f_m) = 4 \times 10^{-6}/\sqrt{\text{Hz}}$, $T \approx 298$ K. The figure shows that the best sensitivity of measurement is archived for modulation depth $T_0 \approx 1.85$ rad, maximum modulation depth of our EOM is $T_0 \approx 1.13$ rad.
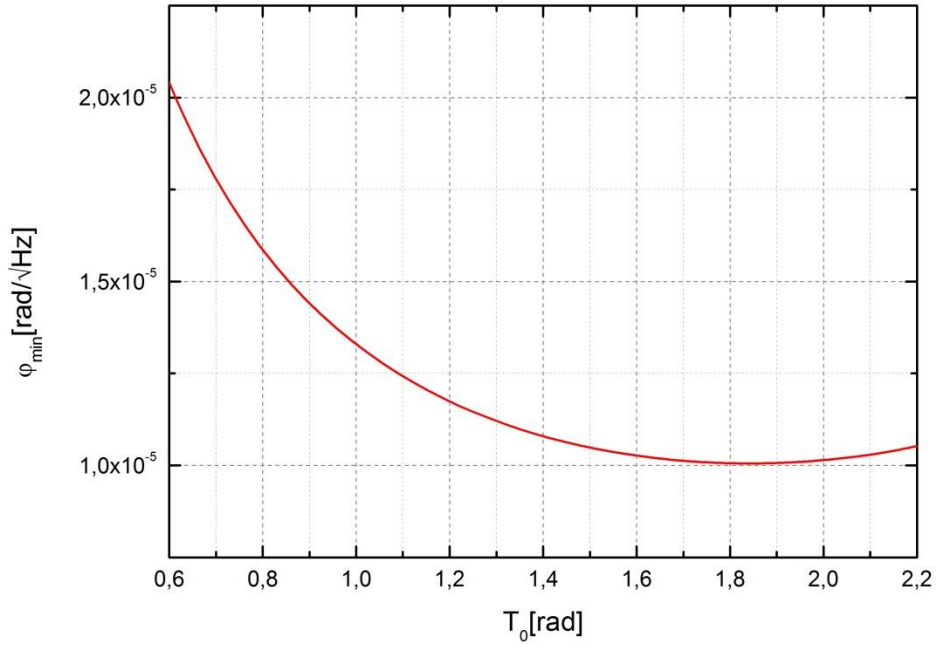
Fig 7. Minimum phase change φ_{min} as a function of the ellipticity modulation depth T_0

3.5 Experimental setup

OSQAR experiment is based in SM 18 hall in CERN (Geneva) see Figure 8. SM 18 hall is the testing hall for all LHC magnets. The whole infrastructure needed for

powering and cooling the LHC dipole magnet is in place, and therefore the experiment is situated in this location. On the other hand, it is the noisy and dusty place, not optimal for sensitive laser experiments. Under the conditions in SM18 and for the testing purpose of modulation techniques, the decision was made to use the different setup from PVLAS ellipsometer, based on EOM and not crossed polarizers as is described in the previous section.

Fig 8. OSQAR experiment in SM18 Hall, CERN

Figure 9. shows a schematic view and a photograph of the apparatus in OSQAR CME (Cotton-Mouton) experiment. The setup is placed on the aluminum table with a rigid frame, and all optics components are screwed to optical breadboards. The light source is 1 mW stabilized HeNe laser from SiOS Company, model SL03. To protect laser from back reflected light from the optical elements, we used the optical isolator from Linos Company with optical isolation typically at the level of 40dB. Glen Tylor type polarizers from Melles Griot Company with extension ratio of $\sigma^2 = 5 \times 10^{-6}$ were used as analyzer and polarizer. Electro-optic modulator is

from Quantum Technology company Model 3050 (DC up to 50MHz). The light was collected by the photodiodes PDA36A from Thorlabs. Modulation signal is provided by the function generator from Agilent model 33120A. Signal is analysed at modulation frequency f_m by Lock-in amplifier from Standford Research model DSP 830. Data are sampled and collected by DAQ system from NI instruments USB 6212 BNC and all data are stored to PC through the LabView interface.

To split the signal for measurement and reference (spurious signals) channels, we have used non-polarizing beam splitter 50/50 from Melles Griot Company (NPBS). For the EOM working point correction in measurement branch, we have used Solei-Babinet compensator from Thorlabs (SBC). Also, other optics to provide the beam through the magnet was used as; mirrors, a beam expander and windows of magnet anticryostat see Figure 9.
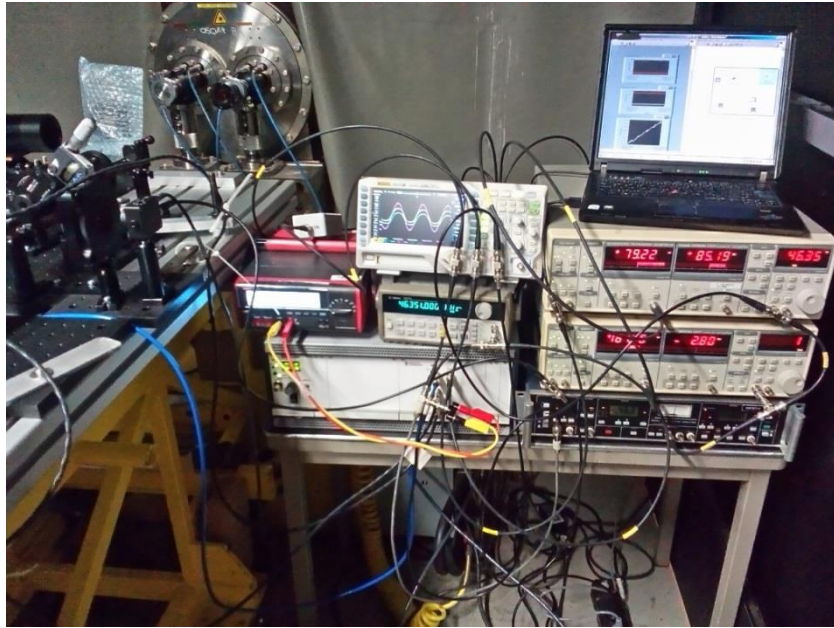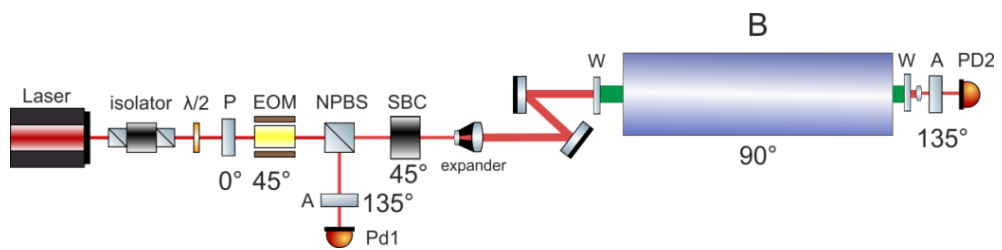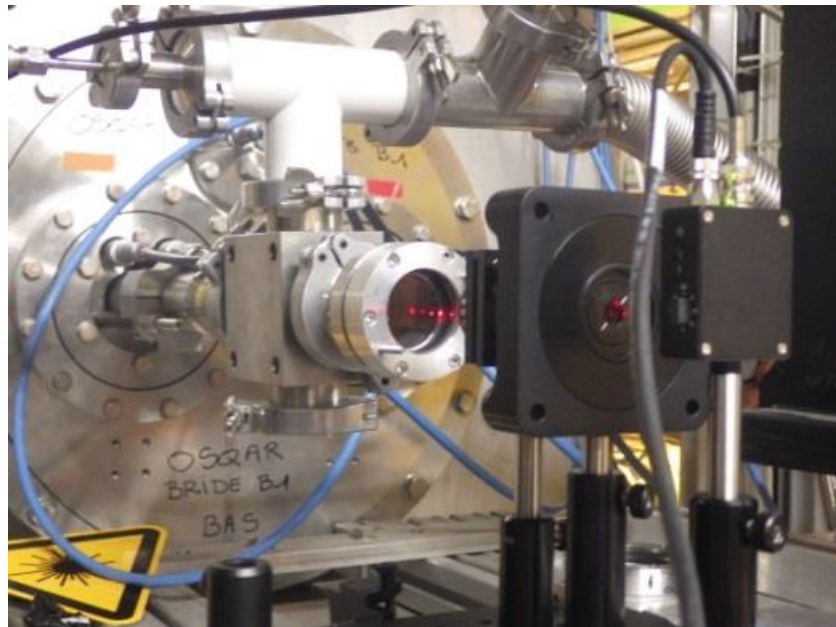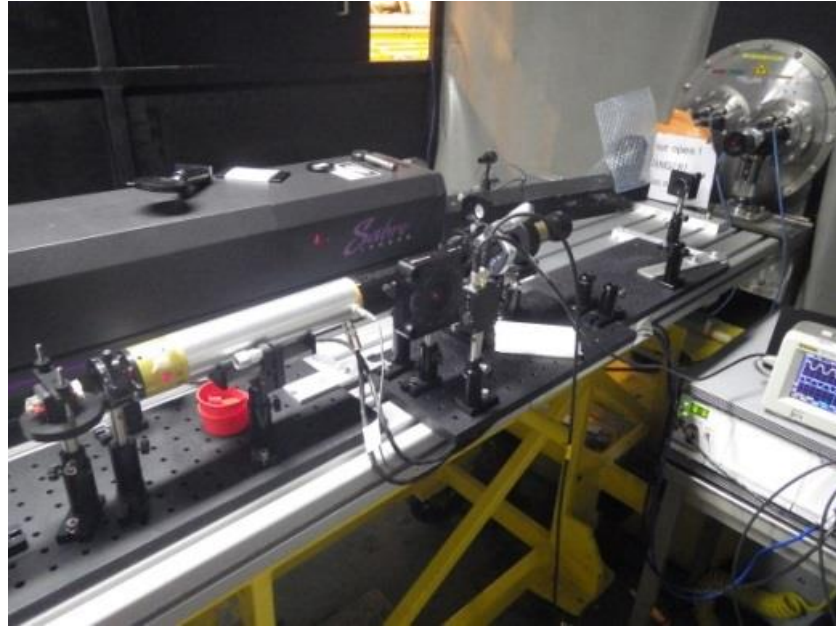
Fig 9. Experimental setup of OSQAR ellipsometer 2014.

3.5.1 Electro-optic modulator tests

All necessary tests of equipment and setup were done in university laboratories at the Technical University of Liberec and then implemented for CME measurement in CERN SM18 hall. Because the ellipsometry technique is based on the modulation of ellipticity by the EOM the first test was made to check the modulating qualities of electro-optic modulator.

According to (44) one has to determine the modulation depth T_0 precisely and corresponding factor $J_1(T_0)$ to calculate correctly the phase change φ. For this purpose we have measured the half wave voltage of EOM V_π and we have also measured the $J_1(T_0)$ as a function of modulation depth $T_0(V_m)$.

Measurement of V_π was realized between crossed polarizers with EOM fast axis at 45 degree. The intensity I on the detector can be calculated as [45]

$$I = I_0 \sin^2 \frac{T}{2} = I_0 \sin^2 \left(\frac{T_{eom}}{2} - \frac{\pi V_{DC}}{2V_\pi} \right), \tag{60}$$

where T is the overall phase change introduced by the EOM, T_{eom} is the phase change introduced by EOM in absence of voltage and V_{DC} represent in this case applied static voltage called BIAS voltage. V_π is measured as applied voltage change between minimum and maximum of detected intensity and corresponds to the phase change of π or $\lambda/2$ see Figure 10.
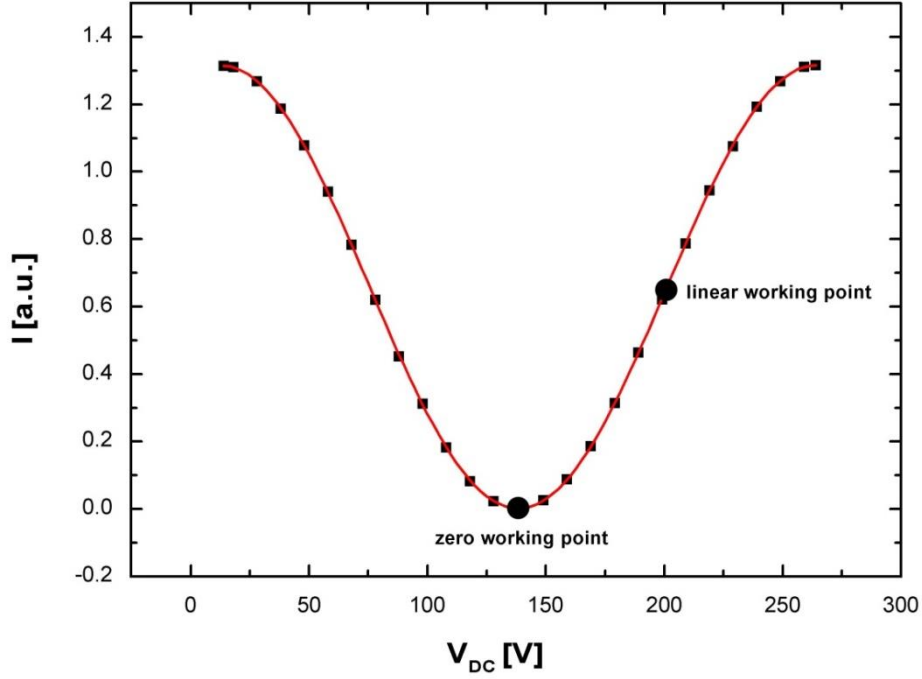
Fig 10. A modulator DC Bias voltage measurement for crossed polarizer and analyzer.

The V_π was measured as 125.8 V.

After determining of V_π we were able to measure calibration plot of modulator for different values of modulation depth T_0, see Figure 11. If we set the EOM via BIAS voltage V_{DC} to the *linear working point* $\frac{T_{eom}}{2} - \frac{\pi V_{DC}}{2V_\pi} = \frac{\pi}{4}$ the corresponding intensity on the photodiode can be seen as follow [57].

$$I = I_0 \sin^2 \frac{T}{2} = I_0 \sin^2 \left(\frac{\pi}{4} - \frac{\pi}{2V_\pi} V_m \sin 2\pi f_m t \right) = \frac{I_0}{2} \left(1 - \sin \left(\frac{V_m}{V_\pi} \pi \sin 2\pi f_m t \right) \right) =$$

$$\frac{I_0}{2} \left(1 - \sin(T_0 \sin 2\pi f_m t) \right) \tag{61}$$

Where $T_0 = \frac{V_m}{V_\pi} \pi$ (43) is representing the depth of modulation

Using the Bessel function of the first kind the (61) can be transformed as

$$I = \frac{I_0}{2} \left(1 - (2J_1(T_0) \sin 2\pi f_m t + high\ order\ odd\ terms) \right) \tag{62}$$

50

$J_1(T_0)$ is measured as

$$J_1(T_0) = \frac{\sqrt{2}V_{1f}}{2V_{DC}} \tag{63}$$

Where V_{1f} is the R value of DSP lock-in amplifier at modulated frequency f_m and V_{DC} is DC voltage on photodiode.
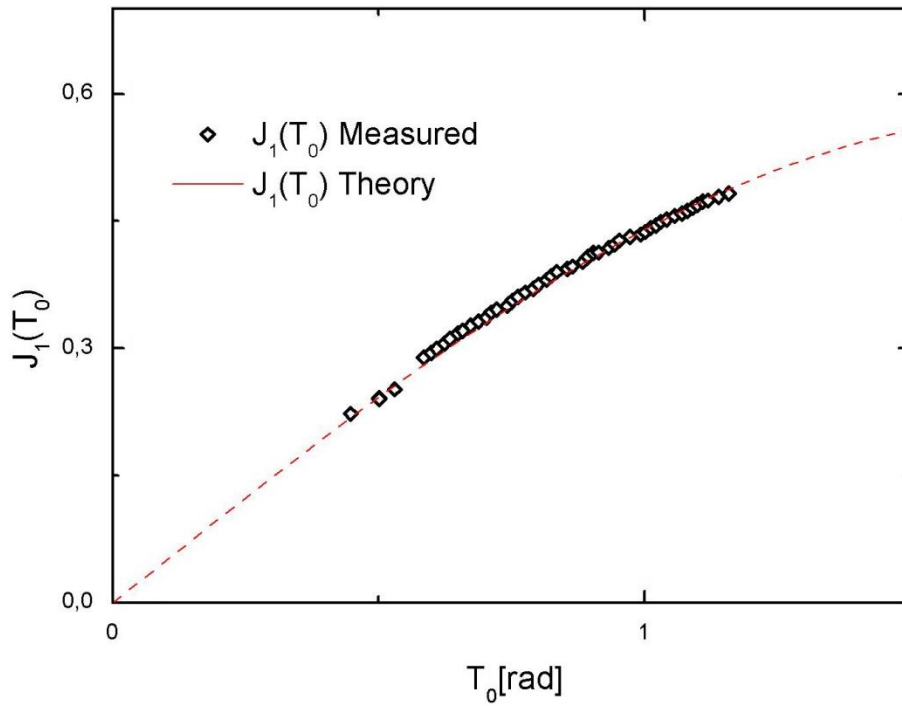
Fig 11. A modulator calibration measurement $J_1(T_0)$

Better agreement of $J_1(T_0)$ has been reached for a greater depth of modulation. If we would be able to achieve a modulation depth across the half-wave voltage $(V_m = V_\pi)$ maximum modulation depth, using the saw-tooth signal would simplify the analysed signal and, Bessel function is no longer needed [58].

3.5.2 Amplitude noise

During the first test of EOM modulator, we have found that the amplitude at measured frequency f_m is not perfectly stable in time, but slowly wary. This could be caused by two phenomena's. At firs by instability of the working point of EOM which drifts slowly in time and second by residual amplitude noise (RAM) [59]. Both phenomena are seen as noise signal in CME measurement similarly to spurious birefringence.

A: EOM working point instability

The volatility of the working point could be solved by control loop acting on the bias voltage [60], using the second harmonic component $2f_m$ as error signal. Because if we get out from *linear working point* the second harmonic component is present.

$$I = I_0 \sin^2 \left(\left(\frac{\pi}{4} + \frac{\Delta}{2} \right) - \frac{\pi}{2V_\pi} V_m \sin 2\pi f_m t \right) = \frac{I_0}{2} \left(1 - \cos \left(\left(\frac{\pi}{2} + \Delta \right) - \right. \right.$$

$$\left. \left. \frac{V_m}{V_\pi} \pi \sin 2\pi f_m t \right) \right) = \frac{I_0}{2} \left(1 - \left(\cos \left(\frac{\pi}{2} + \frac{\Delta V_{Bias}}{V_\pi} \pi \right) \cos(T_0 \sin 2\pi f_m t) + \right. \right.$$

$$\left. \left. \sin \left(\frac{\pi}{2} + \frac{\Delta V_{Bias}}{V_\pi} \pi \right) \sin(T_0 \sin 2\pi f_m t) \right) \right) = \frac{I_0}{2} \left(1 - \right.$$

$$\left(\cos \left(\frac{\pi}{2} + \frac{\Delta V_{Bias}}{V_\pi} \pi \right) (J_0(T_0) + 2J_2(T_0) \sin 2 \times 2\pi f_m t) + \sin \left(\frac{\pi}{2} + \right. \right.$$

$$\left. \left. \frac{\Delta V_{Bias}}{V_\pi} \pi \right) (2J_1(T_0) \sin 2\pi f_m t) \right) \right) \tag{64}$$

Where Δ is the phase difference from working point and ΔV_{Bias} is corresponding bias voltage difference. Minimalizing the ΔV_{Bias} via second harmonic signal holds the working point in right position and (64) became (62).

B: Residual amplitude noise (RAM)

Residual amplitude noise causes other possible amplitude instability of measured signal. Origin of the RAM has many sources and is still under study [59], [60]. RAM rises when the modulation sidebands are not equal in magnitude, not exactly opposite in phase or both. A variety of effects can give rise to RAM.

For example, optical scattering and parasitic interferences between any parallel surfaces, when the polarization of the input beam is misaligned with one of the principal optical axes of the electro-optic crystal. RAM is also sensitive to vibrations and temperature.

RAM is significant for our measurement and presents considerable disturbance into measured signal see Figure 12. RAM in our EOM is caused by scattered light from parallel surfaces of electro-optic crystals and is the strongest source of the spurious signal in measurement.

It is possible to reduce RAM similarly as controlling the working point [59], but we were not able to use this option due to control loop malfunction during the runs. Therefore the reference channel is also introduced to monitor the amount of RAM in the system as well as for spurious birefringence.
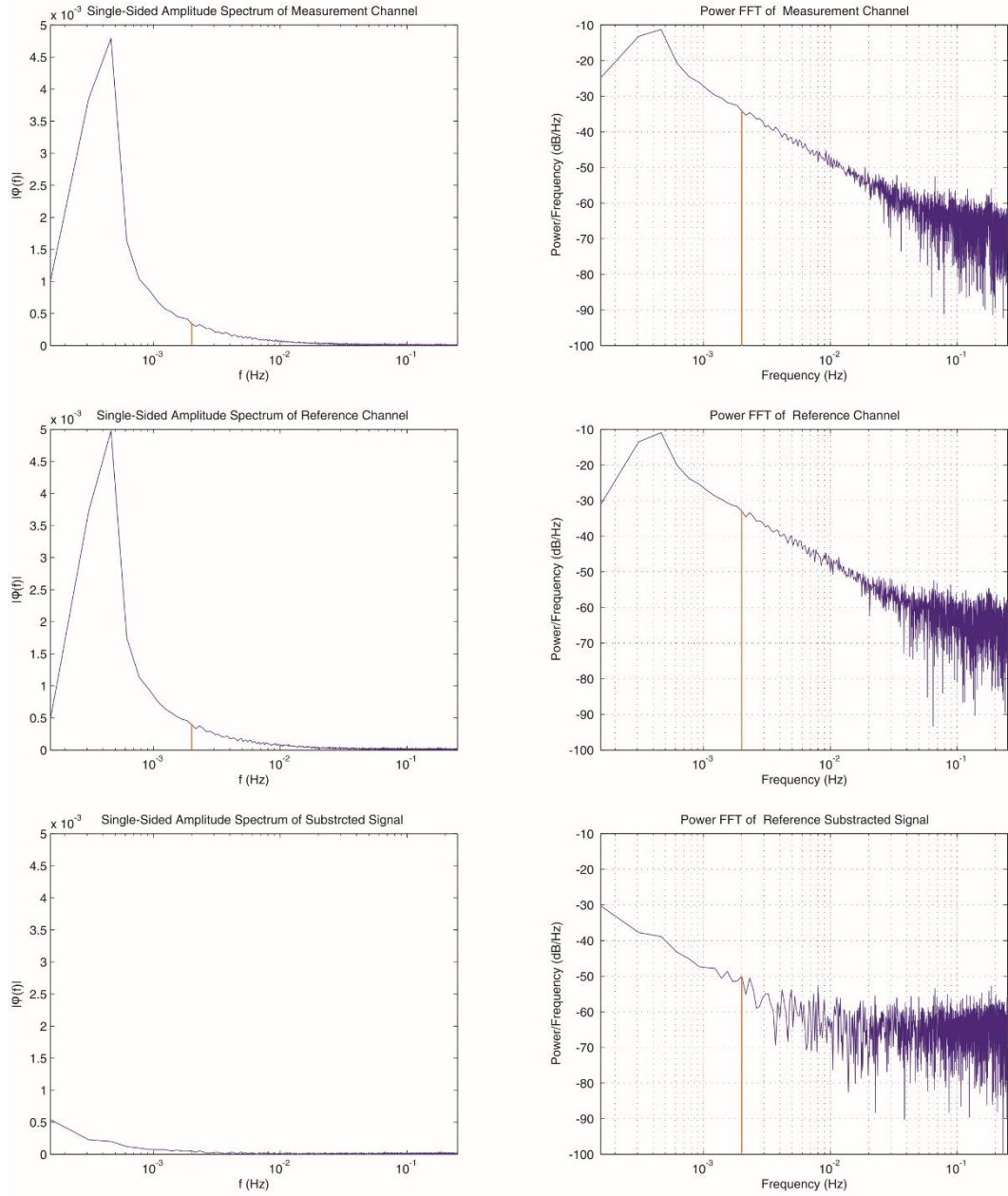
Fig 12. The Spurious signal in Measurement arm (top), in reference branch (middle), and in subtracted signal (bottom). Red line at 2 mHz represents possible LHC magnet modulation frequency

Fig 12. shows FFT and Power spectra of calculated birefringence signal φ in measurement channel, in reference channel and subtracted signal. Data were measured in quiet night condition in SM18 at $B = 0$ T for $t = 6490$ s and sampling frequency was 2 Hz. One can clearly see that spurious signal is centered on 0.5 mHz in both channels and is correlated one to another. Therefore the

spurious signal is highly suppressed after subtraction. Subtracted signal still have some residual peak at 0.5 mHz, because measured and reference channels are not perfectly in phase and equal in amplitude due to different length of the signal paths. Uncorrelated 1/f noise remains present at a frequency of a possible modulation of the LHC dipole magnet $f = 2\,\text{mHz}$ (red line), since spurious (RAM) signal is suppressed by 20 dB.

3.5.2 Setup test with Soleil-Babinet compensator

After testing of EOM parameters and reference channel, we did the test of measuring phase change φ according to (42). We have used Soleil-Babinet (SBC) compensator from Thorlabs Company as phase change φ reference for this testing. Test was done without using of reference channel, since the amplitude and speed of change provided by Soleil-Babinet compensator is far from $0.5\,\text{mHz}$ noise introduced by RAM and other low frequency noises. The procedure of system alignment and measurement is as follow [61].

The electro-optic modulator may be aligned between crossed polarizer and analyzer by maximization of the second harmonic $2f_m$ signal, or by minimization of the first harmonic signal f_m. Proper orientation of the analyser (45°) is then realized by turning it to null second harmonic signal, in the same time we have to check the bias voltage of electro-optic modulator to precisely set the operating point to minimum or zero phase $\frac{T_{eom}}{2} - \frac{\pi V}{2V_\pi} = 0$. Combination of precise orientation and controlling bias voltage V will set the modulator for correct measurement. If the birefringence sample is then inserted, it may be oriented by maximization the fundamental first harmonic f_m signal and again we have to check operation point via bias voltage.

For small retardation, it is best to use the phase sensitive detection provided by dual phase DSP Lock-in amplifier to measure the first harmonic f_m of AC signal, and determine $\sin \varphi$ according to (44)

$$\varphi = \sin^{-1}\left(\frac{\sqrt{2}V_{1f}}{V_{DC}2J_1(T_0)}\right), \tag{65}$$

where, V_{1f} is rms AC output intensity (R value) of DSP Lock-in amplifier for first harmonic component f_m of the signal and V_{DC} is DC voltage on photodiode.

Figure 13. shows the results of the measurement made with Soleil-Babinet compensator as the variable birefringence sample. The Soleil-Babinet compensator can provide full wave retardance adjustment. Digital readout resolution is 0.001 mm, and corresponding repeatability value at 633 nm is 0.001 waves. Because the sine function is symmetric, we can measure only on the interval from zero to ninety degrees, where around maxima gradually loses resolution. The method is used for precise measurement of tiny birefringence, and therefore this problem with lack of resolution or intensity of AC signal can be neglected. Confidence plot Fig 13. represents a good agreement between measured retardation and values, represented by the Soleil-Babinet compensator. Pearson's r value of linearity confidence is 0.9999, slope value of linear fit is (1.0086 ± 0.0027), intercept is (0.0040 ± 0.0026).
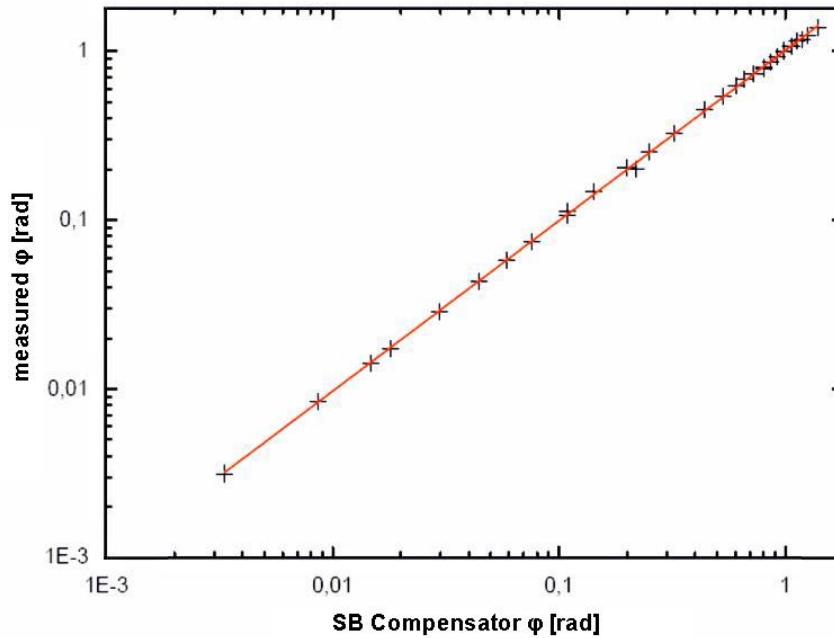
Fig 13. Confidence plot for SB compensator retardation and measured retardation.

3.6   Cotton-Mouton effect measurement

In all VMB experiments the ellipsometer is tested on Cotton-Mouton effect in gases [17], [18], [26], [29], [32]. Because the CME is linearly dependent on pressure, it is ideal effect for the sensitivity testing of the experimental setup. In the final stage of VMB experiment after reaching the ultrahigh-vacuum, we should end up with the contribution from QED and QCD as a main source of birefringence.

In the early developments of VMB ellipsometers, the physical results were mainly corresponding to the CME measurements [8], [17], [18], [26]. Later results were more interested in Axion searches [11], [19], [27], [31] but measurement of VMB (QED) is still challenging.

Following the other experimentalist in the field of VMB, we have tested our ellipsometer on CME measurement in CERN (SM18) with LHC dipole magnet. OSQAR experiment is allowed to use the LHC spare dipole superconducting magnet only for six weeks per year, this every year time frame is split into different experiments as VMB, LSW (Light shining through the wall), CHASE (Chameleon searches studies). In years 2012 – 2015 the main interest was in LSW and only one week per year was dedicated for VMB. Every year plan for VMB was to build ellipsometer after LSW measurements and did the sensitivity tests on CME. Data presented here are from years 2013 and 2014 where the most of the measurement in CME were done. The year 2015 mainly focused on stability analysis for determination of RAM, and in the 2016 year experiment was interrupted due to civil works in SM18.

3.6.1 Magnets

The magnetic field for CME measurement in OSQAR experiment is provided by spare dipole LHC superconducting electromagnets. Figure 14. shows the transverse cross-section. The main parts of LHC dipole are cryostat, with two beam pipes, the collars and the iron yoke see Figure 14.
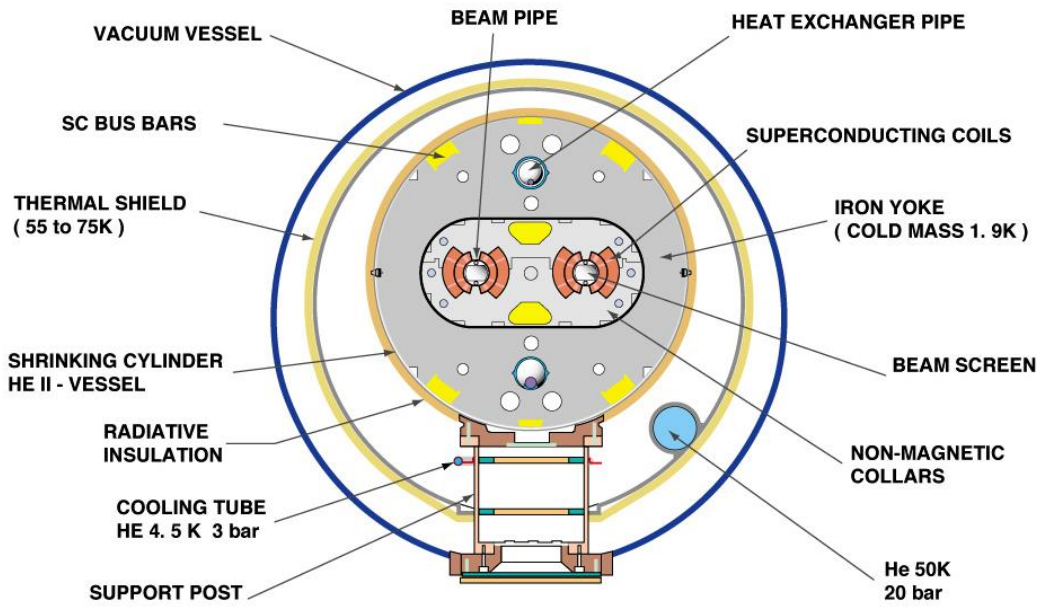
Fig 14. Cross-section of LHC dipole superconducting magnet. [62]

The coils inner diameter is 50 mm, and to deflect the contra rotating protons beams, the field direction in the apertures is opposite see Figure 15. The coil is made of six blocks with a maximum current of about 13 kA. LHC uses the field of about 8.3 T corresponding to 11 850 A. OSQAR magnets are trained to be used at 9 T corresponding to 12 850 A.

The cold mass inside the pressure vessel is filled with liquid He at a pressure more than 1 bar and cooled using a heat exchanger pipe at 1.9 K. A Vacuum vessel, radiative shield and the thermal shield at $55 - 75$ K reduce heat leakages to a minimum. The field inside the tubes is designed not only in the way of the maximum strength but also for perfect uniformity. Magnetic fields errors are at the level of 10^{-4} in 10 mm radius [63].
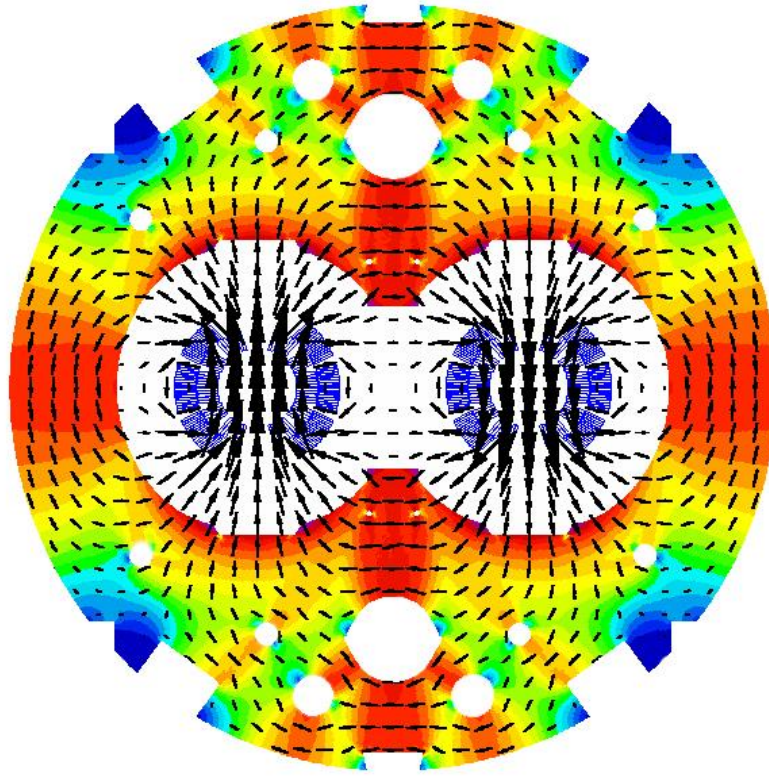
Fig 15. An example of the typical magnetic field emitted by the dipole magnets of the LHC [64]

Because all magnet tests are made in ambient conditions, but the magnets itself must be at 1.9 K one need to use some connection between cold and hot mass at ambient temperature. This connection is called *anti cryostat* and is built as coaxial tube system, with an inner diameter of 40 mm and a wall thickness of 0.7 mm, embedded into magnet coil. The cell is equipped with coaxial heater cables, which keeps the warm bore at ambient temperature. Optical windows closing anti cryostat tube serve as a gas chamber for CME measurements.

3.6.2 Cotton-Mouton effect in Nitrogen

Cotton-Mouton measurements in nitrogen gas as a final test of ellipsometer setup presented and analyzed in previous chapters were realized in years 2013 - 2015. For the testing purpose, the anti cryostat with optical windows was filled with high purity N_2 gas and magnetically induced linear birefringence CME was measured as

a function of pressure. Measurement procedure was the same as with Soleil-Babinet compensator in the previous chapter, but due to RAM and spurious birefringence, the reference channel was necessary to be used [42].

The direction of the magnetic field in the LHC magnet is given as vertical (see Figure 15), all other components must be set under this condition. We started with the precise perpendicular (horizontal) orientation of the polarizer to the magnetic field direction. Then we set into cross-position pair of analyzers for reference and measurement channel. For the proper orientation of the electromagnetic modulator between crossed polarizer and analyzer, we have used the second harmonic component of the detected signal $2f_m$. By the combination of precise orientation of and controlling bias voltage V of EOM, we set the modulator in reference channel to the correct operating point. We did the same for the measurement channel but we have used the Soleil-Babinet compensator as the phase bias control.

The proper orientation of the analyzers is then realized by turning it into the null position of the second harmonic signal. In this case, we, cannot use minimalizing the first harmonic component since some static birefringence is always present in the optics setup.

For the small signal, it is best to use the phase sensitive detection provided by the dual phase DSP Lock-in amplifier. According to (39-44), our signal is analyzed on the first harmonic component of AC signal. All data were stored by DAQ system from National Instruments company via software LabView at sampling frequency typically from 0.1 Hz to 2 Hz. Calculations were done in Matlab and Mathematica software, plots and fitting in Origin software.

After calculation and subtraction of measurement and reference retardation (phase change) $\varphi(B)$ the expected quadratic function were achieved, see Figure 16. Data presented on Figure 16. were made with the nitrogen gas at $P = 1$ bar with $L = 14.31$ m long $B = 9$ T field change in maximum.
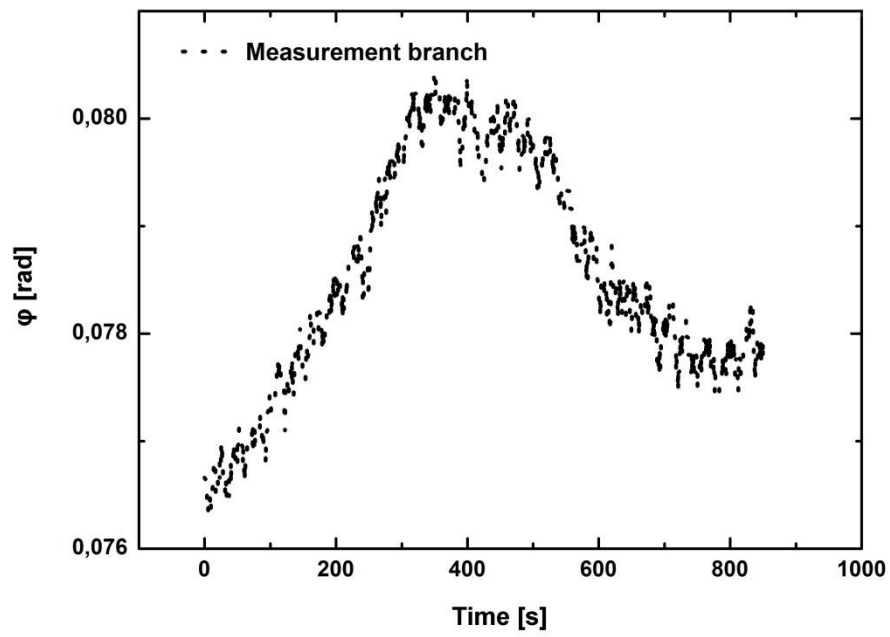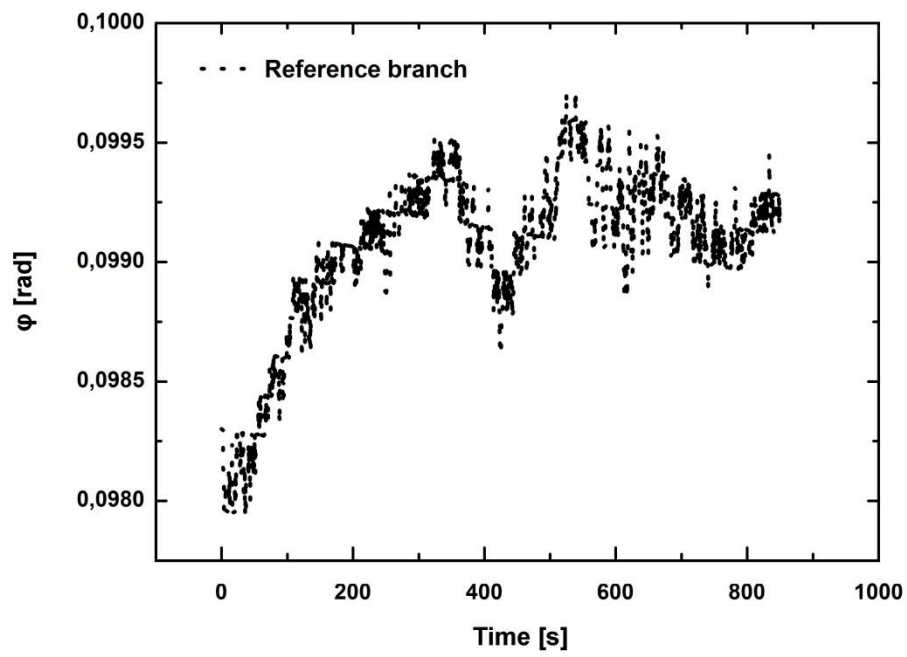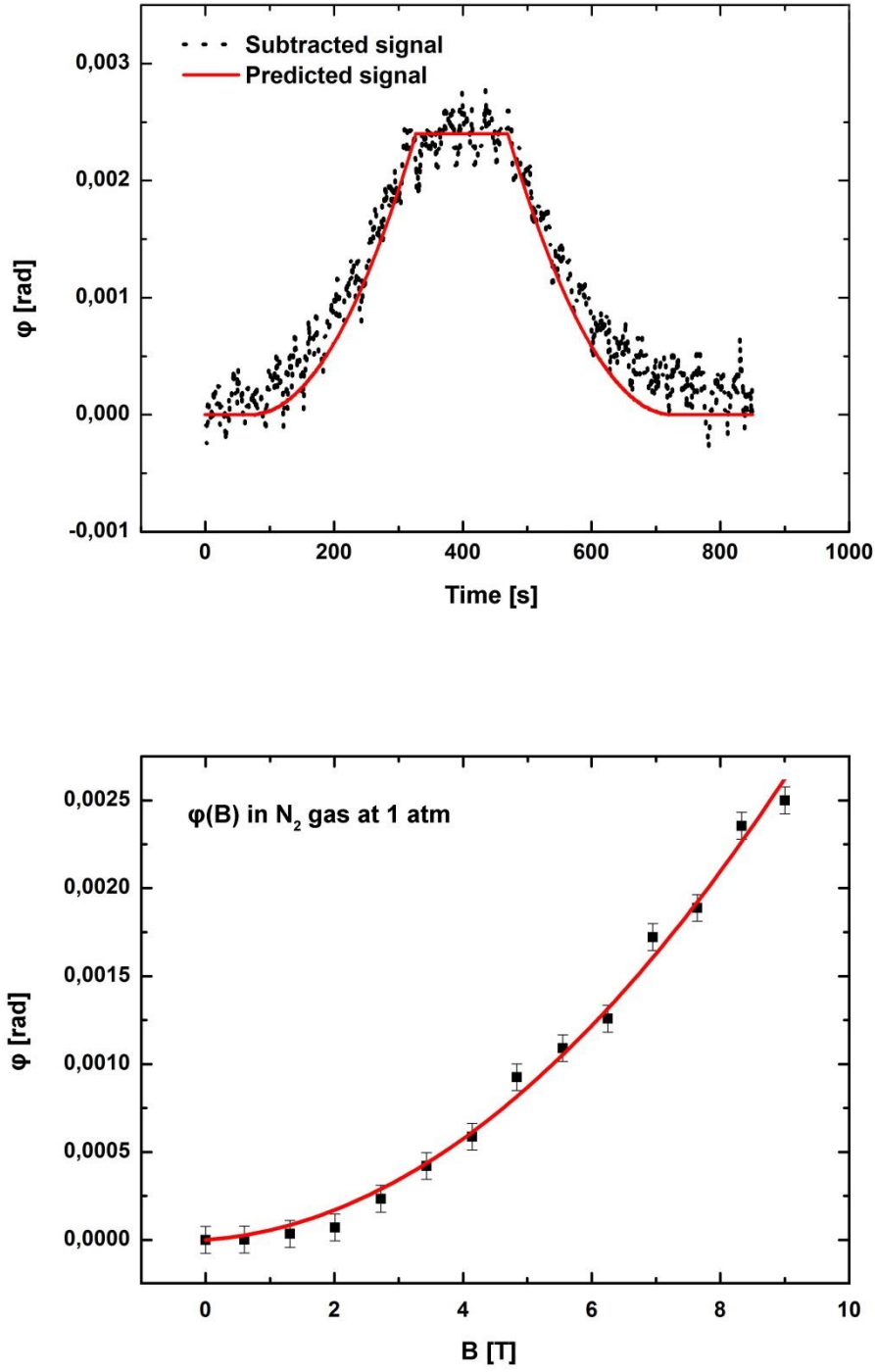
Fig 16. Retardation measured in reference branch. Retardation measured in measurement branch. Subtracted retardation with static offset correction to zero level. Fitted signal is calculated according to the measurement for magnetic field in sequence 0s-70s 0T,70s-327s 0T to 9T with 0.035T/s,327s-470s 9T,470-727s 9T to 0T with -0.035T/s,727s-850s 0T. Retardance as a function of magnetic field.

The fitted signal is calculated to be $\varphi = 0.0024$ rad maximum at $B = 9$ T (12850 A in LHC magnet) with linear ramp of 50 A/s. Figure 16. serves as a demonstration of subtraction technique and represents one of the measurement run. After the proof of repeatability of the measurement, we have measured the Cotton-Mouton effect in nitrogen gas as the function of pressure to put the measurement limit of our ellipsometer. The measurement was in good agreement with other published data, see Figure 17. [26], [65]

The measurements were made as single pass without any path multiplier as a multipath cavity or resonant cavity. The normalized Cotton-Mouton birefringence of N_2 gas was measured and calculated from linear fit as $|\Delta n_u| = (2.26 \mp 0.18) \times 10^{-13} \text{T}^{-2}\text{atm}^{-1}$. Each point in plot for linear fit is a average value of multiple measurements at given pressure from years 2013 and 2014.

The measurement limit of phase change φ for the single pass measurement was set to $2.5x10^{-4}$ rad. For the He-Ne laser and $L = 14.31$ m long $B = 9$ T LHC magnet, it corresponds to the difference in the refractive index $\Delta n_u = 1.8x10^{-14}\text{T}^{-2}\text{atm}^{-1}$. This value is set as half value where the useful signal after the subtraction was no longer significant with B^2 dependency. Minimum value corresponds to sensitivity at level 0.5 mHz determined from long term stability measurements in Figure 12., but is order of magnitude higher then calculated intrinsic noise level (Figure 7.).
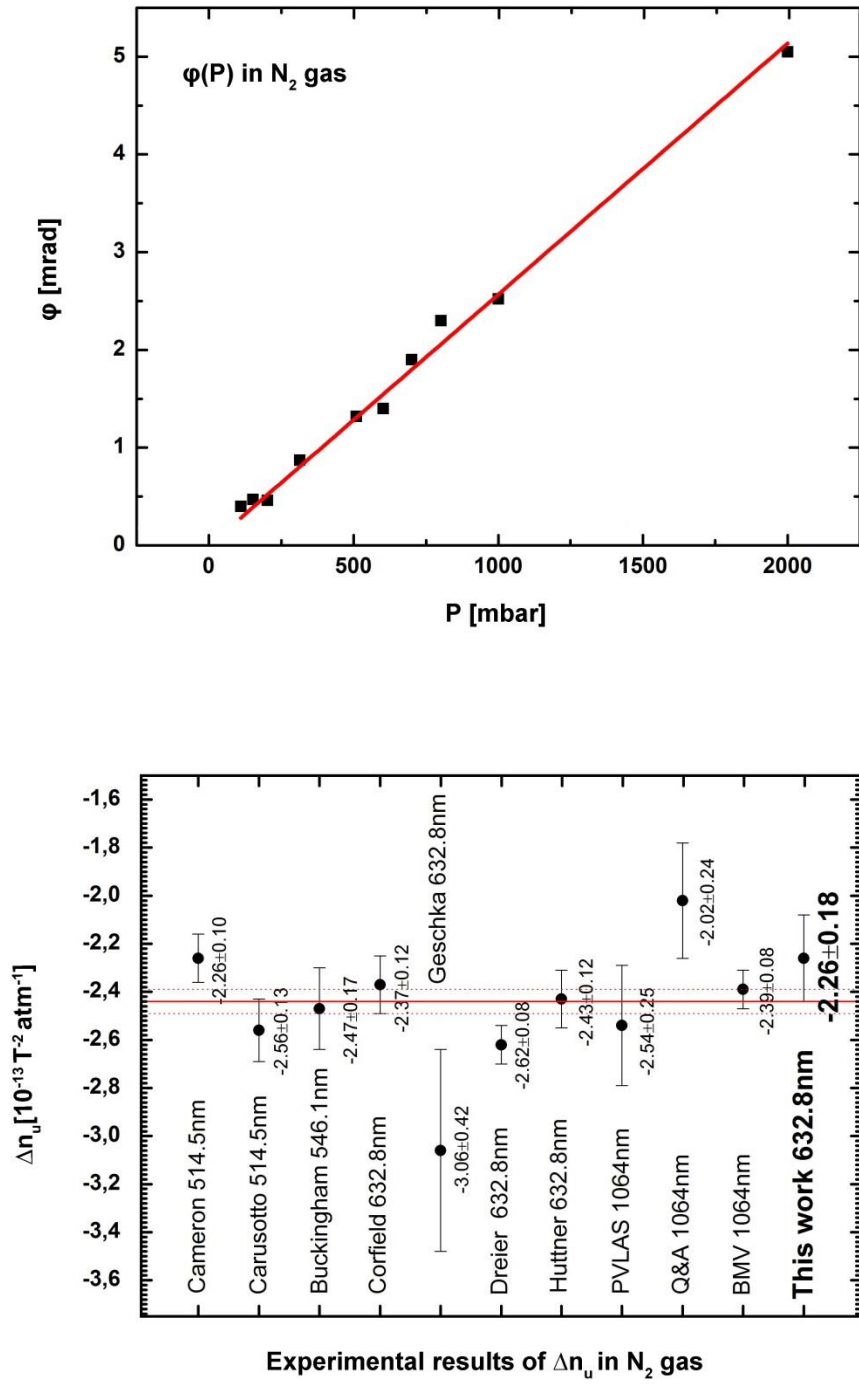
Fig 17. Top: Retardance as a function of .pressure, Bottom, Comparison with other experiments (red line represents the theoretical value of CME in N_2 gas).

4   Improvements

In chapter 3. OSQAR, the setup, and measurements of CME in nitrogen gas in SM18 CERN is presented based on previous analysis of the method. One can see that the measurement limit of $\varphi = 2.5 \times 10^{-4}$ moreover, the even theoretical shot noise level $\varphi_{shot} = 2.4 \times 10^{-7}$ is still far from the predicted value of ellipticity given by QED VMB $\psi_{QED} = 2.3 \times 10^{-14}$ for single pass measurement in $9\,T, 14.31\,m$ long field at a wavelength of $632\,nm$. If we were able to modulate the magnetic field, the integration time to achieve the signal to noise ratio as one would be

$$t = \left(\frac{\psi_{min}}{\psi_{QED}}\right)^2 = \left(\frac{1.25 \times 10^{-4}}{2.3 \times 10^{-14}}\right)^2 \approx 10^{19}\,s \tag{66a}$$

$$t = \left(\frac{\psi_{shot}}{\psi_{QED}}\right)^2 = \left(\frac{1.2 \times 10^{-7}}{2.3 \times 10^{-14}}\right)^2 \approx 10^{13}\,s \tag{66b}$$

where ψ_{min} is current ellipticity measurement limit of our apparatus.

How can we improve our setup to achieve the better or even final results for VMB in reachable integration time? At first, we will analyze the homodyne setup presented for CME measurement of nitrogen gas. In next chapter; we focus on how to realize heterodyne scheme for static magnetic fields, which should be the next step of optical setup in OSQAR VMB experiment.

4.1   Improvements of OSQAR ellipsometer

This chapter is split into two parts. First part: How to improve our present setup sensitivity - RAM suppression, vibration control, vacuum system, electronics, detectors, and optics. Second part: How to increase the signal to be measured - longer optical path in magnetic field, longer and stronger magnetic field, different wavelength.

4.2   Improvement of sensitivity in current setup

To improve sensitivity, we will need to reduce the noise in all four main noise parameters:

$$\varphi_{shot} = \frac{\sqrt{2}\sqrt{2eq\frac{I_0}{2}}}{qI_0 J_1(T_0)}$$ **Shot noise**: increase power, increase detector sensitivity, optimize $J_1(T_0)$

$$\varphi_J = \frac{\sqrt{2}\sqrt{\frac{4k_B T}{G}}}{q\frac{I_0}{2}J_1(T_0)}$$ **Johnson noise**: increase power, increase detector sensitivity, optimize $J_1(T_0)$

$$\varphi_{dark} = \frac{\sqrt{2}\frac{V_{dark}}{G}}{q\frac{I_0}{2}J_1(T_0)}$$ **Dark current noise**: increase power, better detector, optimize $J_1(T_0)$

$$\varphi_{RIN}(f_m) = \frac{\sqrt{2}q\frac{I_0}{2}N_{RIN}(f_m)}{q\frac{I_0}{2}J_1(T_0)}$$ **Relative intensity noise:** optimize $J_1(T_0)$, stabilize power, increase f_m

All other uncontrolled sources of spurious signals as time variable birefringence or RAM contribute mainly to $1/f$ noise: Introduce heterodyne scheme with high modulation of the VMB effect.

If we will be allowed to modulate LHC dipole magnet with 50 A/s, corresponding to the modulation frequency of 2 mHz for a full modulation depth of 9 T magnetic field. The main source of low-frequency noise close to 2 mHz in the present setup is the RAM, centered around 0.5 mHz.

The origin of RAM has many sources, and not all of them are understood. The primary sources of RAM are [59]:

- Instability of ambient temperature
- Imperfect alignment of the electro-optic modulator
- Uncoated layers in optical setup with anti-reflection coatings
- Vibrations

In our setup, we have determined as the primary sources of RAM the EOM crystals itself with uncoated surfaces of the entrance and an exit surface. The best solution would be to change our EOM with another modulator using shorter crystals and antireflection coatings. Alternatively, to use photo-elastic modulator PEM this is based on different physical principle.

Possible solution how to actively compensate the RAM of EOM is based on bias voltage control [59], [60] and we have already successfully tested this solution see Figure 18. Unfortunately, the remote bias control of our EOM during the trial runs of CME was broken. We will implement it in the next term.
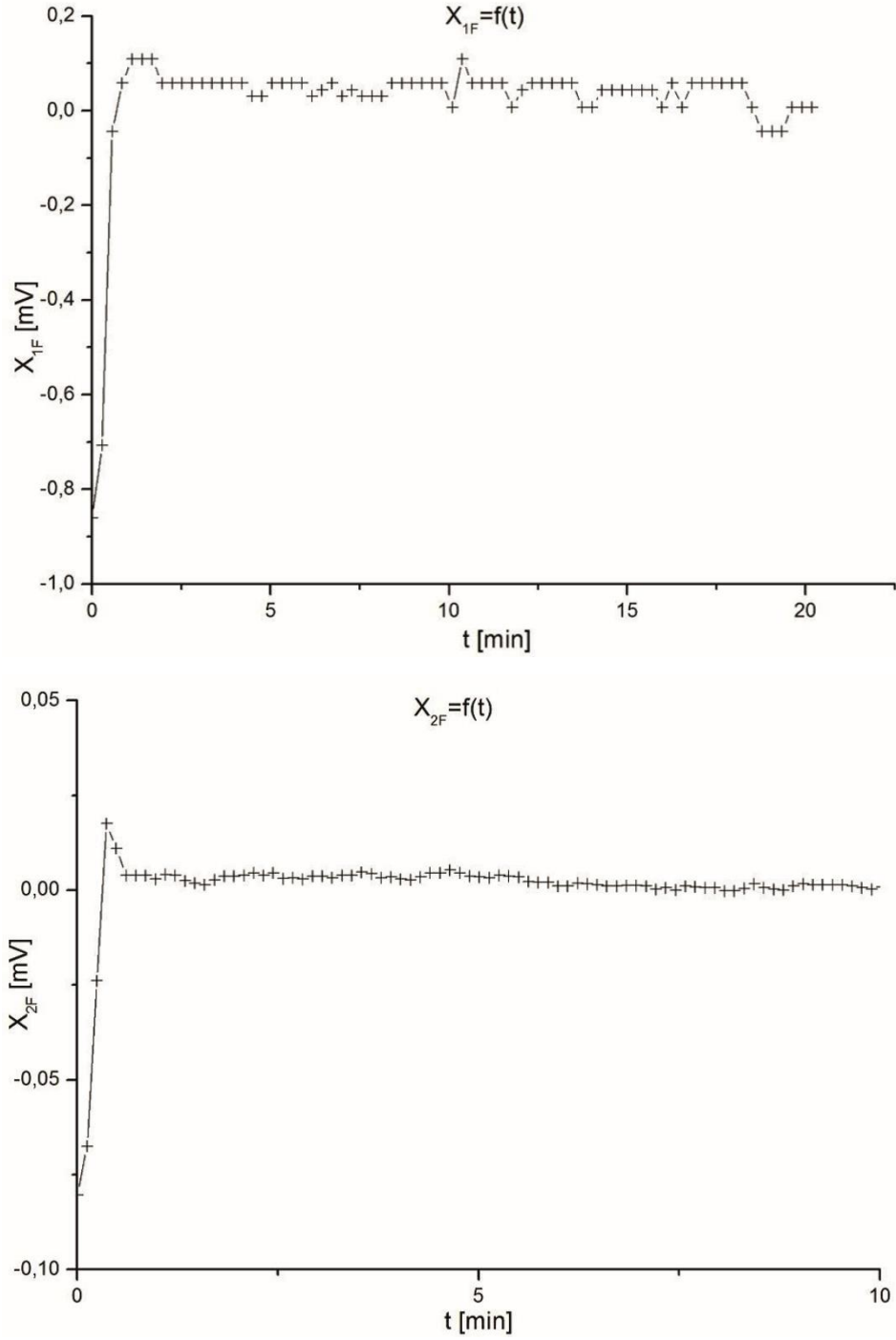
Fig 18. Stabilization of first(top) and second(bottom) harmonic component via control acting on EOM bias voltage to reduce the RAM signal and working point instabilities X_{1f} and X_{2f} represents modulation amplitude of first and second harmonic of the modulated signal

Other sources of noise are coming from the environmental condition of SM18 hall. Vibrations and air motion cause the movement of the beam on the photodiode. This noise is mainly observed in DC term since the modulated signal is well filtered by

68

the Lock –In amplifier. To reduce this noise, we need better vibration isolation of the optical table, based on passive or active vibration suppression. To avoid air motion the whole setup should be put into the vacuum system.

For better measurement sensitivity of the DC term, we can use an optical chopper to modulate the optical power in the range of several tens or hundreds of Hz and then analyze the corresponding DC signal on photodiodes by Lock-in amplifier. Using of the optical chopper and Lock-in amplifier will also reduce $1/f$ noise. Implementation of the optical chopper is easy and we will do it in the next experimental run. Vibration isolation and vacuum system is also easy to implement but it is mainly the matter of funding to buy well isolated optical tables and proper vacuum chambers.

If we take a closer look at the optical elements in the current setup, it is not critical to change any components. From ellipsometry point of view, polarizer and analyzer are the most important parts of the setup, but these become important when we start to use crossed polarizer and analyzer scheme.

Where we have much space for improvement is the detector, electronics and DAQ systems, which are now on a basic level. From the analysis of noise in the system, we see that now the noise is dominated by the thermal noise of the photodiodes and the laser relative intensity noise. Therefore it is necessary to use better detectors with low thermal noise and more stable laser source.

The whole setup from a noise point of view should be optimized to get to the level where we are limited only by the shot noise.

4.3 Increase of measured signal

Analyzing the history of VMB ellipsometers, we find out that principle and sensitivity of the ellipsometers itself are more or less unchanged for several decades. Some of them have reached the shot noise limit [14], [15], [25], [26], [30], [49], [66].

On the other hand, the increase of the measured signal in last 30 years is enormous. The induced ellipticity ψ or phase φ change to be measured is basically dependent on five parameters

$$\psi = \frac{\varphi}{2} \sin 2\theta = \frac{\pi}{\lambda} \Delta n_{uv} B^2 L \sin 2\theta \qquad (67)$$

wavelength λ, normalized birefringence Δn_{uv}, strength of the external magnetic field B^2, optical path length in magnetic field region L and the angle between polarisation direction and direction of magnetic field θ.

From (67) we can see it is best to use $45°$ degree direction between the polarization of the light propagating in a magnetic field and magnetic field direction that for maximizing the ellipticity signal whit respect to θ.

The higher signal is also obtained for shorter wavelengths, but here we are mainly limited to laser technology and quantum efficiency of the detectors. The wavelength used for CME measurements were 1064 nm, 514 nm or 633 nm see Figure 17.

According to (67) we also see that magnet used for CME/VMB measurements has to be as long and strong as possible. The biggest influence has the strength of the magnetic field because it is squared B^2. This is the reason why we use LHC superconducting dipole magnets with state of the art 9 T field over 14.3 m. LHC dipole magnet is the longest and the strongest magnets ever used for CME and VMB measurements. On the other hand if one wants to modulate the magnetic field at higher frequency then several mHz, the LHC magnet is no longer so excellent with its 2 mHz modulation possibility.

Possible optimum between modulation speed, length, duty cycle and strength of the magnetic field is in Halbach configuration [67] of permanent magnets see Figure 19. For CME/VMB experiments Halbach array was used for the first time in Q&A research [25]. Nowadays Halbach magnet configuration is used in PVLAS [31] experiment with 2.3 m long 2.5 T field, which can rotate at 10 Hz.

Another solution is to use pulse electromagnet as in BMV experiment, 14 T, and 500 Hz modulation frequency, but for this option the duty cycle is low, and the effective length of the magnetic field is also limited [11].
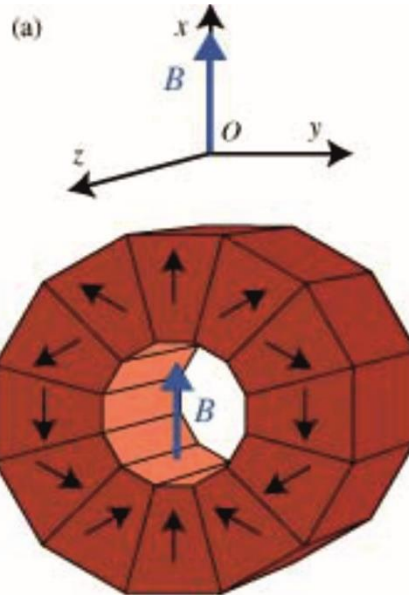
Fig 19. Illustration of Halbach permanent magnet configuration. [68]

If we leave now the possible problems with the modulation of superconducting magnets, how we can increase the ellipticity to be measured when we already have the best magnet to use? The last parameter in (67) which we can enhance is the length of the magnetic field region.

To extend the path of the light propagating in the magnetic field region we have two possible solutions. Firstly, we can use several magnets in line to make the field longer. This solution is possible in practice, but we will be very soon restricted by the space of the experimental hall (SM18) and by the radius of curvature of LHC dipoles. If we would like to put more than two of LHC magnets in line, we will have to straighten them, since LHC dipole magnets are bend to make a circular collider and it is not possible to chain them oppositely to keep a constant diameter of the bore.

A solution of more magnets in line will be used in ALPS IIc experiment, where the HERA dipole magnets will be straightened and installed in HERA tunnel again [37]. ALPS IIc aims to install $2x10$ HERA magnets before 2019 to reach $2x100$ m of magnetic field at 5.3 T. Other possible solution how to increase the optical path in magnetic field is to use the optical path multiplier as delay or resonant optical cavity to let light go back a forth in magnetic field region to amplified the effect to be measured.

4.4   Optical cavities in VMB experiments

Optical cavity was used for the first time in VMB experiment by E. Zavattini in CERN in years 1979 – 1983. Iacopini and Zavattini used what we called optical delay or multipass cavity [14]. In principle, this cavity consists of two mirrors with a hole, which is drilled in entrance mirror see Fig 20. and the light is reflected several times before it escapes out from the cavity. Possible maximum numbers of passes (reflections) through the magnetic field region in the multipass cavity is $N{\sim}1000$ passes.
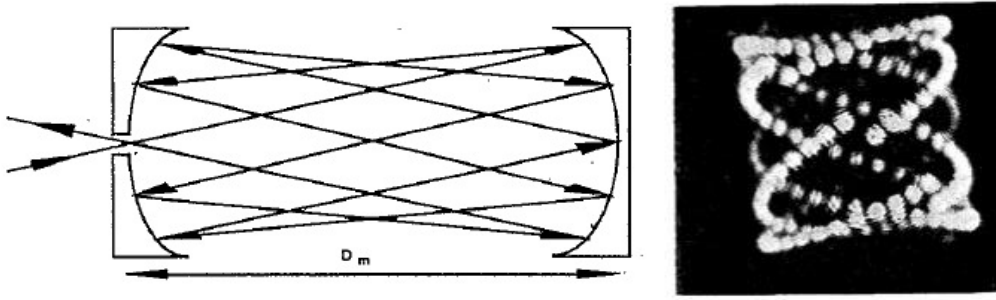
Fig 20. Delay line optical cavity (left), with spot pattern at end mirror (right) [14].

Optical delay cavity was also used in the Brookhaven experiment BRTF [19], where a number of passes were $N{\sim}500$. If we implement the number of passes N in to equation (67) the ellipticity, which we should measure, become

$$\psi = \frac{\varphi}{2} \sin 2\theta = N \frac{\pi}{\lambda} \Delta n_{uv} B^2 L \sin 2\theta \qquad (68)$$

So with the optical delay cavity, we can increase the signal to be measured by factor of 10^3 in maximum.

4.5   Resonant Fabry-Perot cavity

Second possible cavity solution to amplify the signal to be measured is the Resonant Fabry-Perot cavity [45]. The Fabry-Perot cavity is a resonant optical cavity that increases the effective optical path NL. It is made by two mirrors placed at a

separation distance d which is an integer multiple of the light half wavelength. Number of passes or amplification factor in resonant cavity is calculated as

$$N = \frac{2F}{\pi} \qquad (69)$$

Where F is the cavity finesse given as

$$F = \frac{\pi c \tau}{d} \qquad (70)$$

where c is the speed of light in a vacuum and τ is the cavity decay time. Cavity decay time or photon cavity life time can be measured as decay constant after laser locked to cavity is switched off. Intensity of the transmitted beam on the photodiode can be describe as:

$$I(t) = I_0(t_0)e^{-\frac{(t-t_0)}{\tau}}, \qquad (71)$$

where $I_0(t_0)$ is the initial intensity when the laser is switched off. This type of measurement is best to use for high finesse cavity, where the lifetime is long enough to be precisely measured see Figure 21.
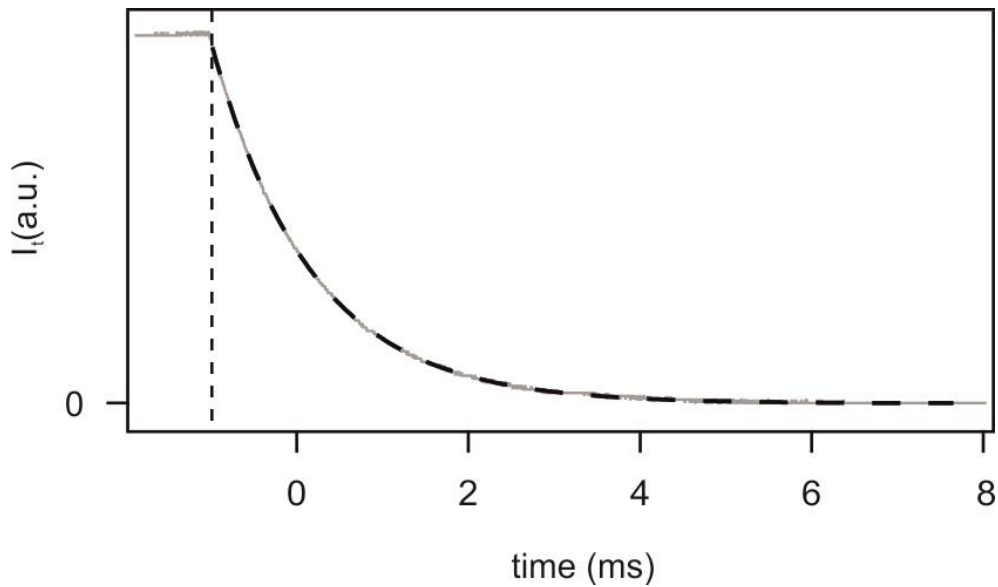
Fig 21. Time evolution of the intensity of the transmitted beam (gray line) in experiment BMV (Toulouse). The laser is switched off at $t = t_0$. Experimental data are fitted by an exponential decay (black dashed line) giving a photon lifetime of $\tau = 1.16$ ms and corresponding finesse of $F = 481\,000$.[69]

Finesse can also be calculated as

$$F = \frac{\Delta v_f}{FSR} \tag{72}$$

where Δv_f is the resonance bandwidth, defined as full width of half maximum (FWHM) of resonant peak and FSR is free spectral range, the optical spacing between fundamental mode (TEM$_{00}$) peaks.

It is easy to measure FSR and FWHM in the case that we have low finesse cavity in the cavity scanning mode (Fabry-Perrot interferometer) see Figure 22.
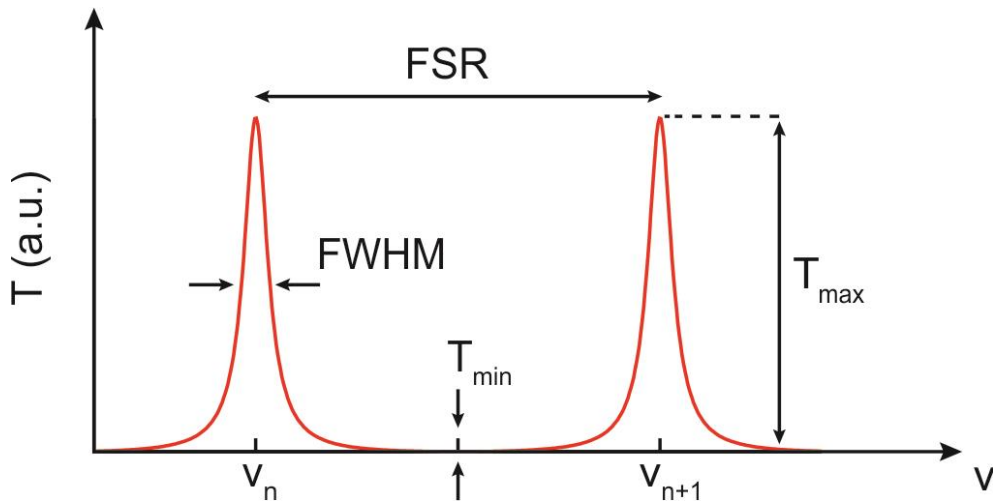

Fig 22. Transmission peaks of a Fabry-Perot interferometer (resonator) in scanning mode

Nowadays the highest finesse cavity ever used in VMB experiments is in PVLAS experiment, with a decay time of $\tau = (2.45 \pm 0.05)$ ms, corresponding to the finesse of $F \approx 700\,000$ and to the amplification factor $N = 445\,000$.[70] To build such a cavity one needs state of the art mirrors with amplitude reflection coefficient of $R = 0.9999955$.

4.6 First tests of cavity for OSQAR experiment

From the previous chapter, we see that amplification factor N provided by the optical resonant cavity is the main reason why the VMB experiments are so close to reach the level of predicted ellipticity from QED [31]. It is also clear that to reach reasonable measurement time to get to S/N as 1, OSQAR need optical cavity or multiple chain of LHC magnets.

Miroslav Král did first studies of an optical cavity for OSQAR experiment in 2007 and results are presented in his Ph.D. thesis [32]. Restart of cavity prototyping begun in the year 2013, when the first tests of CME measurements were done. Cavity development can be split into two parts, first is the optical design of the cavity and all necessary optics in the setup. Second is the locking the optical cavity to keep it at resonance for the desired time of the experiment.

In the beginning, we have started with an optical cavity from an old laser (1970) which was ideal for the testing purpose. It was made of invar body with one of the mirrors glued to the piezo element. It was easy to test cavity scanning mode and define the finesse F, and other necessary parameters see Fig 23.

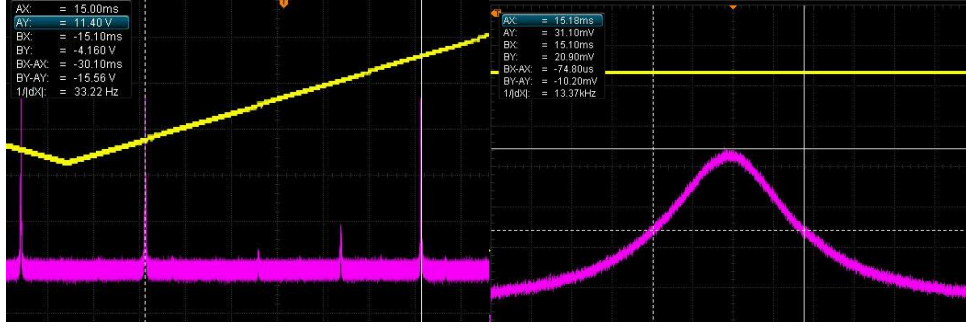As laser source, we used HeNe laser from Sios Company in frequency stability mode same as in CME measurement.
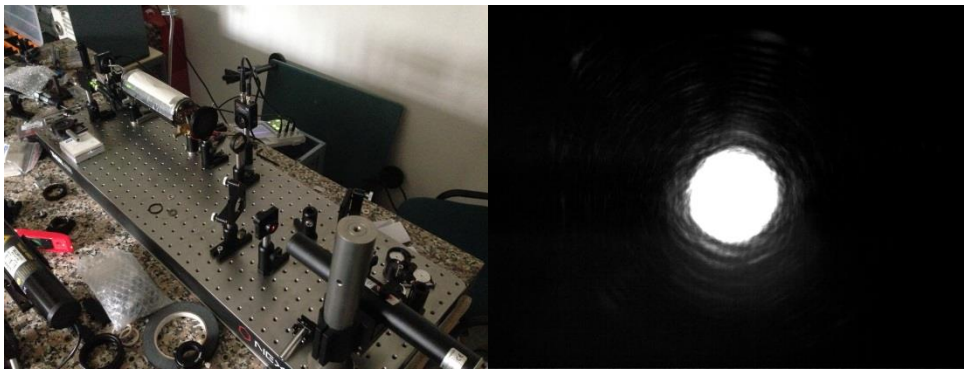
Fig 23. Fabry-Perot resonator test.Top left: optical setup with a cavity from the old laser. Top right: fundamental mode TEM$_{00}$ in resonance check by CCD.

According to (72) we have measured FSR and FWHM and defined the corresponding finesse as $F \approx 400$.

In this particular case of cavity alignment in Fig 23. we see also high order transversal modes of the cavity, corresponding to smaller peaks between TEM$_{00}$ modes. Small peaks indicate that cavity is not perfectly mode matched to the fundamental TEM$_{00}$ mode of the cavity by the incoming laser beam and therefore high order modes can resonate [71]. High order modes raise in the case of cavity misalignment and can be used for the auto-alignment system of the cavity.

After successful mode matching of this short resonator, we have realized the first test of cavity locking. Locking was made as side locking shame [72], with active control of the length of the cavity via piezo element. Control loop was realized as PID regulation by LabView software with cavity output amplitude as an error signal. Since thick Invar body of the optical cavity is very robust and finesse of the cavity is low, it was possible to control the resonator for $2000\ s$ see Figure 24.
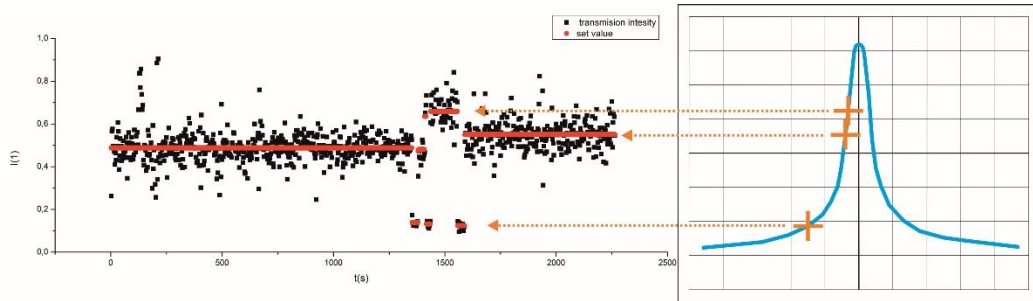

Fig 24. Test of side lock technique in optical lab TUL.

76

Another option how to lock the optical cavity is to control the frequency of the laser light. Control of the light frequency can be realized directly in the laser, acting on laser resonator length, or by using the acoustic-optic modulator in double pass configuration. Also, the combination of both systems is possible and sometimes needed [72].

After tests with short invar resonator, we have started the test of 1 m long prototype in collaboration with Czech Technical University in Prague. The resonator was realized as hemispherical ($ROC = -20$ m). Technical University of Liberec was responsible for optical testing and Czech Technical University in Prague for mechanical solution of cavity design [73].
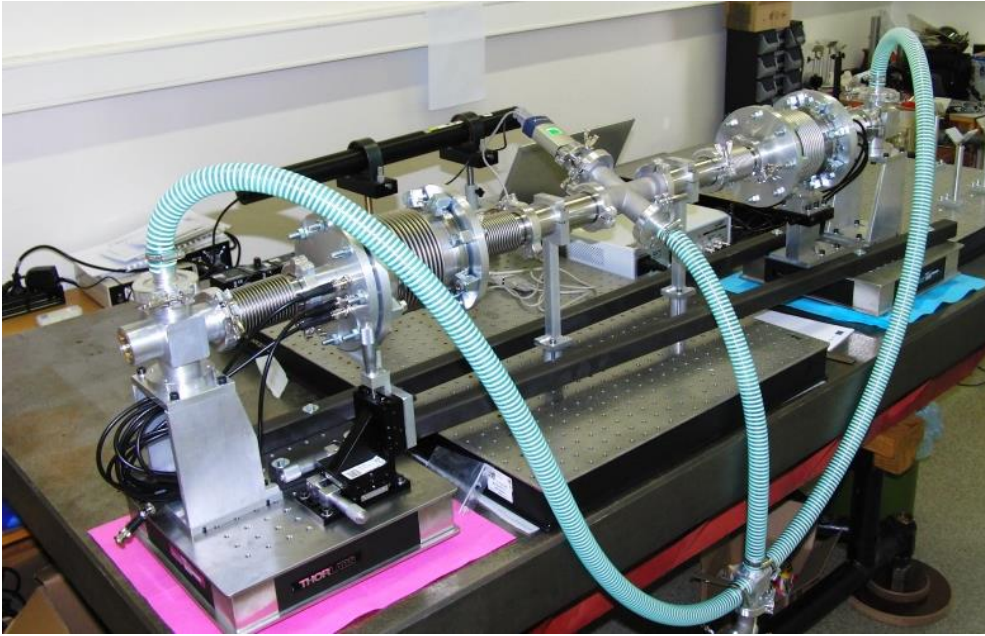

Fig 25. Test cavity at Czech Technical University

Cavity setup was tested at Technical University of Liberec and finesse of the cavity was measured as $F \approx 200$, corresponding to reflectivity coefficients provided by manufacture $R_1 \approx 98\%$, $R_2 \approx 99{,}8\%$ (Toptec, Turnov, Czech).

$$F \approx \frac{\pi(R_1 R_2)^{\frac{1}{4}}}{1-(R_1 R_2)^{\frac{1}{2}}} \approx \frac{\pi(0.98\times 0.998)^{\frac{1}{4}}}{1-(0.98\times 0.998)^{\frac{1}{2}}} \approx 283 \tag{73}$$

Test of locking was also performed, but the stability of the resonator and parameters of the control loop was not good enough to lock the cavity for more than several seconds.

In 2013 we also realized the cavity mounts test in CERN SM18, to see the mechanical quality of the mirrors support and vacuum connections. We have found that vibration noise will be critical for 20 m long cavity in SM18.
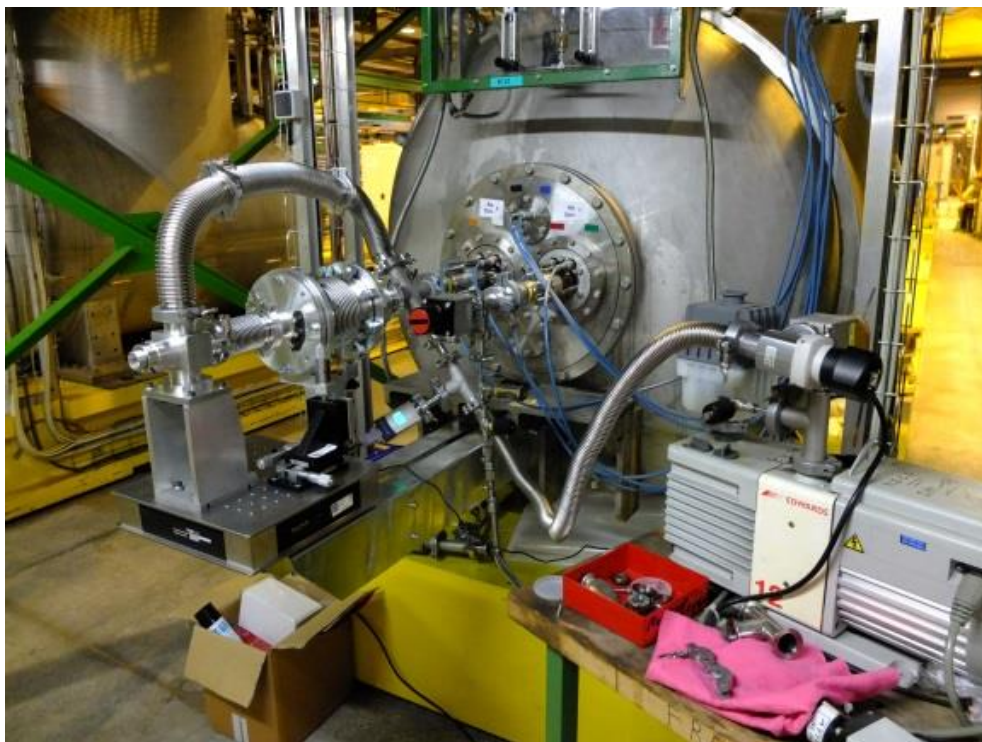
Fig 26. Cavity mounts test in SM18 2013

After the all preliminary tests with an optical resonator, it was clear, that we will need to measure the vibration condition in SM18 precisely and then design the $20\ m$ long optical resonator for experiment OSQAR and suitable locking solution.

4.7 Design and geometry of full-length 20m cavity in SM18 for VMB and LSW experiments

In the first stage of new resonator development, we will focus on the cavity with low finesse about $F = 200$. It is best to use as high as possible finesse from the VMB/LSW experiments point of view, since then we get high amplification length factor N or power build up in the resonator. On the other hand the high finesse in combination with long distance between the mirrors imply narrow resonating peak and require high vibration isolation and laser stability to make resonator stable.

The optical layout and a possible solution for the locking of a laser to a low finesse cavity ($F = 200$) are presented in Fig 27. After the previous tests, a proof of concept will be required in the first stage to demonstrate the possibility of frequency locking a laser to an optical cavity with a sufficiently narrow linewidth. The major point is that lasers used in VMB/LSW experiments in OSQAR have free-running frequency stability in the range of 0.5(Sios) – 5(Verdi) MHz over 20 ms.

The idea is to assemble a prototype test cavity with a finesse of about 200, the length of 1 meter and radius of curvature of the mirrors $ROC = -20$ m, similar to first prototype. The power build-up should be in the range of 70 and linewidth of about 750 kHz. In the first instance a *Tilt locking scheme* [74] will be used for the laser locking and later we will switch to a *Pound-Drever-Hall locking scheme* [75], at this point, it will be possible to implement a *Differential wave front sensing* [76] for cavity auto alignment. Since the lasers that will be used for the tests are not equipped with the piezo tuning option, which is necessary to control the frequency, an external acousto-optic modulator (AOM) in the double pass configuration will be used to shift and stabilize the frequency of the laser to the cavity.
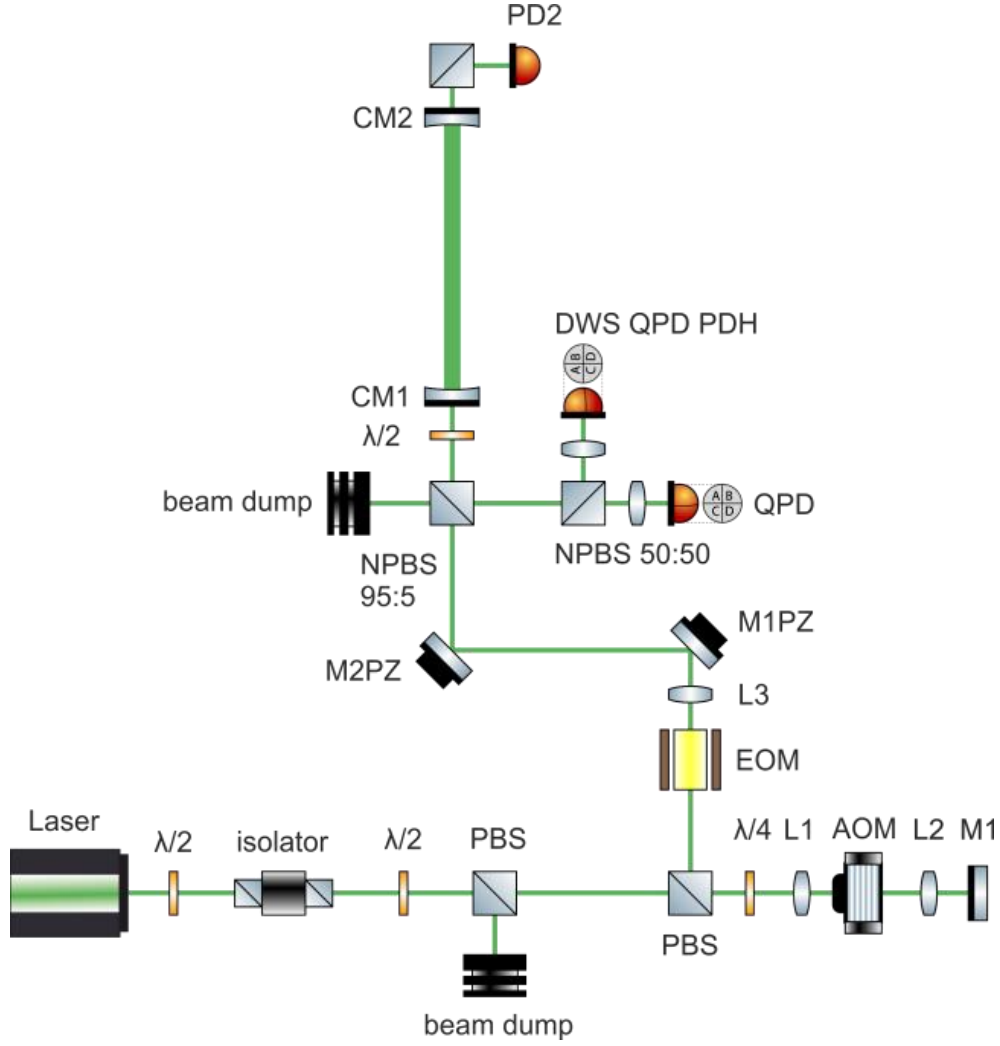
Fig 27. Optical layout scheme. λ/2: half-wave plate; PBS: polarizing beam splitter; L1, L2: lenses; AOM: acoustic-optic modulator; λ/4: quarter-wave plate; L3: coupling lens; M1PZ, M2PZ: piezo controlled beam steering mirrors; EOM: electro-optic modulator; NPBS: non-polarizing beam splitter; QPD: quadrant photodiode; PD: photodiode; CM1, CM2: optical cavity mirrors.

The test optical cavity will use the mirrors which have a radius of curvature $ROC = -20$ m, reflectivity 98.5% and, cavity length will be around 1 m.

For the cavity design in SM18 (CERN), we are mainly limited by the dimension of the free aperture in the anti cryostat and by the bending of the two magnets. From the measurements performed in 2012 with the screening interferometer (Fig 28.), one can see that maximum free aperture for the optical cavity, and the beam passing through the second magnet (LSW option) is about 25 mm.
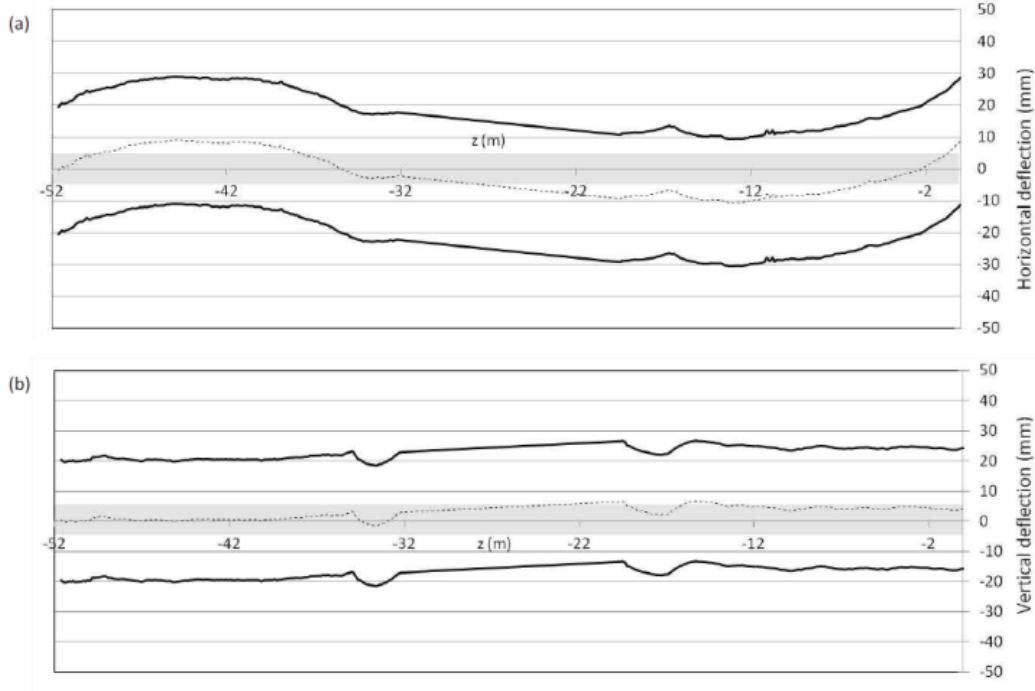
Fig 28. Results of the measurements with a laser tracker system of the alignment at warm conditions of the new spare LHC dipoles dedicated to OSQAR. Dashed lines correspond to a longitudinal scan of the position of the center of the apertures of 40 mm of diameter in the horizontal (a) and vertical directions (b). The gray zone represents the maximum of the laser beam.

In our calculation, we use a value of 22 mm to have at least 1.5 mm on both sides as a safety margin.

As a starting point and for simplicity reasons we restrict our preliminary design to symmetric configurations, so both mirrors have equal ROC. Two possible geometries are initially evaluated, the *confocal* and the *concentric* design. In both cases, due to the symmetric construction, the position of beam waist will be located exactly in the center of the cavity (and of the first magnet). From this information and imposing a maximum beam spot radius of 11 mm (in $1/e^2$) at the end of second magnet, which is located at the measurement side of the experiment (LSW) at about 40 m distance from the optical cavity waist, we calculate the possible values for the radius of curvature of the mirrors. The calculation and values presented here are approximated and are given just as indication of how things could look like at the end. The laser beam will be in the fundamental mode TEM$_{00}$ (Gaussian beam), so we can calculate the cavity waist assuming a spot radius of 11 mm at a distance of 40 m. Under these conditions we get two solutions: $w_0 \approx 0.57$ mm and $w_0 \approx$

82

10.98 mm. The first solution corresponds to a maximally diverging beam and the second solution corresponds to an almost non-diverging beam. All values in-between these two solutions are suitable for the OSQAR experiment. If we calculate the corresponding radius of curvatures we get $R_0 \approx -10.3$ m (almost concentric cavity) and $R_0 \approx -57\,000$ m (quasi-parallel). From the stability point of view of the optical resonator, the best solution is to use the *confocal* geometry which stands in the middle of the line, connecting the extreme solutions in resonator stability plot see Fig 29. If we calculate the cavity waist and the spot radius of the beam detector site for the 20 m confocal resonator we get a waist radius of $w_0 \approx 1.3$ mm and spot radius at 40 m of $w_1 \approx 5.3$ mm. We also have to take in to account the possible damage threshold of the mirrors. From this point one has to calculate the beam size at the mirrors $w_2 \approx 1.8$ mm.
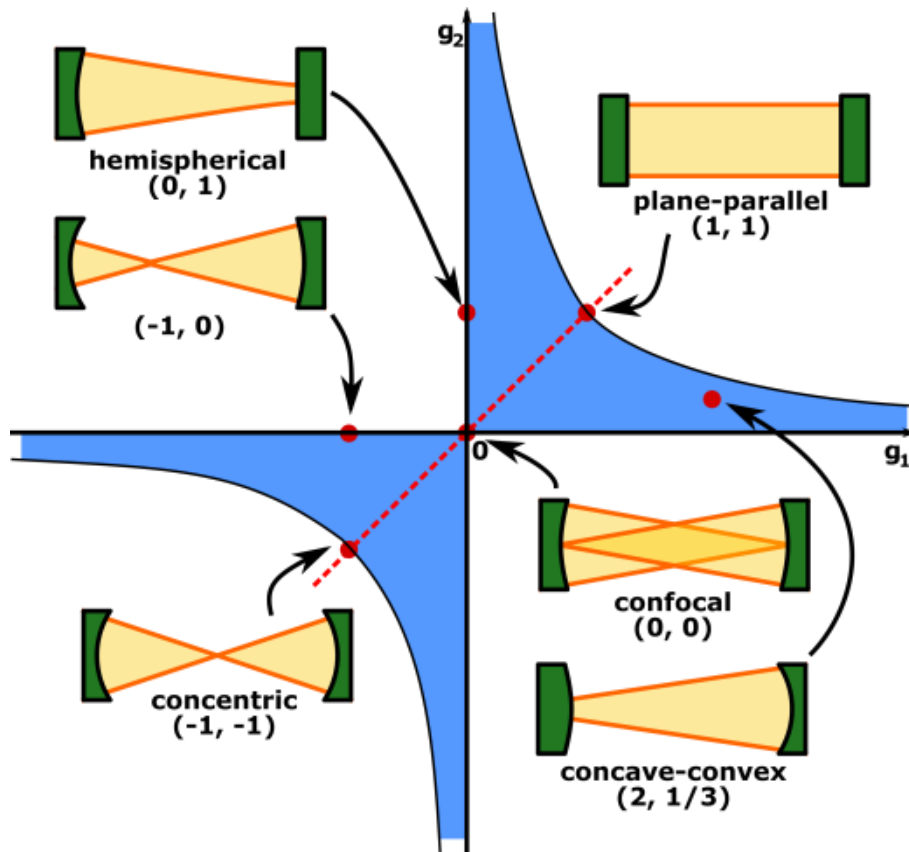

Fig 29. Optical resonant cavity stability plot [77]

For the presented parameters and possible Verdi lasers in LSW experiment power from 5 W to 18 W, in fundamental mode TEM$_{00}$, expected power-build-up 70 and beam radius on the mirrors 1.8 mm, one can calculate the amount power density. For given parameters, we get $7 - 25$ KW/cm^2. For the low finesse cavity, we do not expect any problems with the damaging the mirrors. However, if we will use the cavity build up about 1000 in the later stage, the power density will be $98 - 355$ KW/cm^2 moreover, it can damage the cavity mirrors. In this case, it is possible to use a different design of the cavity to get the larger beam on the mirrors or to use the laser in infrared regime since damage threshold is approximately doubled in infrared. In the case of HeNe laser in VMB the power density is much lower.

The possibility of realizing and operating a 20 m long resonant cavity has been proven already by many groups (see for example preparatory works for the development of LIGO and VIRGO with cavities of several kilometers). The key parameters that have to be controlled are the laser frequency stability and mechanical stability of the optical cavity.

The free-running frequency stability of a Verdi laser is about 5 MHz [79], with slow but significant frequency drifts as high as $30 - 50$ MHz on timescales of 50 s and up to 150 MHz on times of the order of 1000 s. The level of stability depends mostly on the environment in which the laser operates. The acoustic and mechanical noise modulates the laser's resonator length and therefore the emitted wavelength is between a few hundred Hz and a few kHz. Thermal drifts instead are responsible for the drifts over longer timescales. The vibration noise also affects the mechanical stability of the optical cavity. Therefore environmental conditions have to be taken into account and studied.

In Figure 30. is presented a direct comparison of the seismic and mechanical noise level measured in the SM18 experimental hall during regular working hours (11 am) and during nighttime (8 pm). These measurements indicate that the seismic noise condition is within acceptable levels to operate the laser and an optical cavity as the one proposed, with only some sporadic impulses during the day which could unlock the cavity. Several peaks can be observed, and are related to machinery and structural resonances as well as to human activity in the hall.

A feedback system actuating at the laser wavelength with a correction bandwidth of about 10 kHz will be able to sufficiently compensate the frequency fluctuations of the laser and the instabilities induced by mechanical vibrations on the cavity.
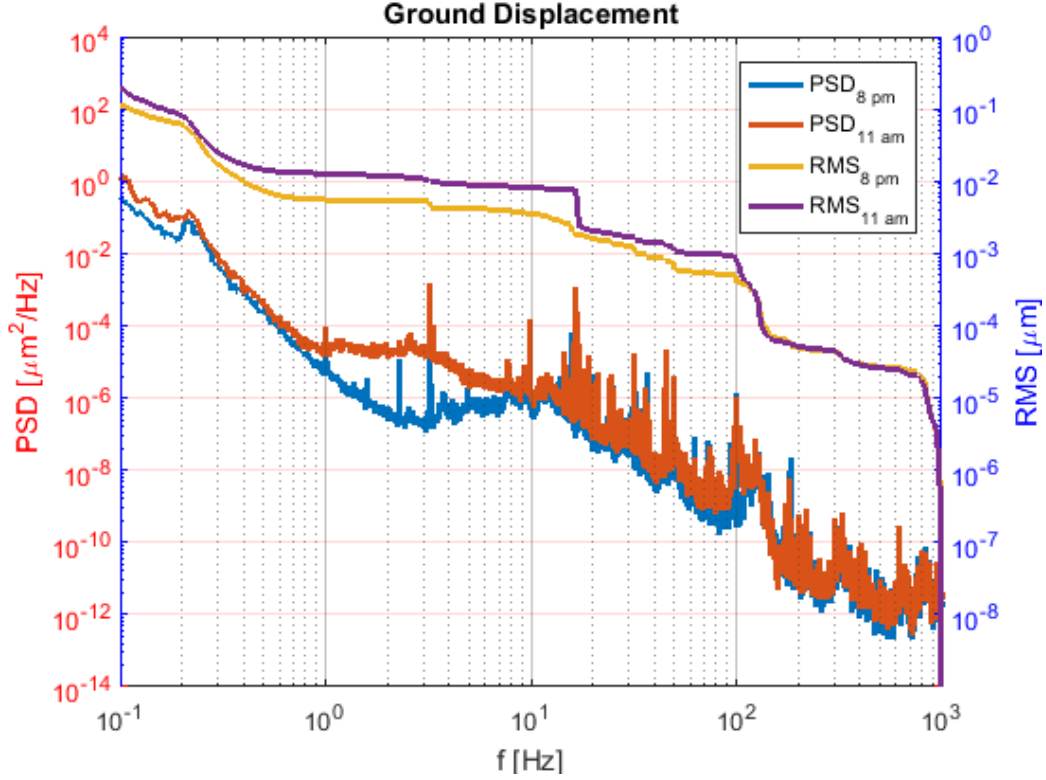

Fig 30. Power Spectral Density (PSD) and RMS displacement measured on the ground in SM18: several peaks related to machinery and structural resonances can be observed, as well as a broadband noise (1-20 Hz) due to human activity in the hall.

In this chapter, we have introduced the possible setup for locking the Verdi or Sios type laser with the free running stability of 5/0.5 MHz over 20 ms to low finesse cavity of $F = 200$ for LSW experiment OSQAR in SM18 hall at CERN. Under the vibration analysis and free running instability of the lasers it will be possible to lock the low finesse cavity for the time required for LSW/VMB measurement.

4.8   Impact of resonator on measurement sensitivity

In last paragraphs, we have shown how important is to implement resonant cavity into VMB experiments to increase the signal to be measured. However, we also

have to point out that high finesse cavities are sources of additional noise and impact the final sensitivity of the ellipsometer. As reported by authors of advanced experiments, this is due to drift of the inherent residual birefringence of high-reflectivity cavity mirrors and also mechanical instability of the resonators [33], [49], [79], [80].

In PVLAS LNL experiment the short term sensitivity for ellipticity was about $2 - 3 \times \frac{10^{-7}}{\sqrt{\text{Hz}}}$ however, long term stability $1 \times \frac{10^{-6}}{\sqrt{\text{Hz}}}$ [24]. In LNL they observed the correlation between seismic noise and ellipticity noise. The PVLAS Legrano apparatus was large and therefore difficult to isolate seismically.

In PVLAS FERRARA for low finesse cavity of 3000, they have reached the shot noise level sensitivity about $1 \times \frac{10^{-8}}{\sqrt{\text{Hz}}}$ however, for high finesse cavity of 400 000, the measured sensitivity was about $3 \times \frac{10^{-7}}{\sqrt{Hz}}$ (6 Hz) and $1.5 \times \frac{10^{-7}}{\sqrt{Hz}}$ (20 Hz), target shot noise sensitivity was about $6 \times \frac{10^{-9}}{\sqrt{\text{Hz}}}$. As PVLAS collaboration pointed out the high finesse cavities are source of $1/f$ birefringence noise [29].

Other problems raised by the fact that static birefringence of the cavity mirrors is acting like wave plate. If one polarization is in resonance the cavity filters the second one, this has to be taken into account in the final ellipticity calculation. Another difficulty with the cavity is the mixing of ellipticity and rotation signal measurement in the situation when the laser is not perfectly locked to the top of the resonant peak [31].

Since the high finesse optical cavity is the source of $1/f$ noise in birefringence signal, it is logical to use heterodyne scheme or homodyne scheme in magnet modulation at as high as possible modulation frequency.

In PVLAS is used the rotating permanent magnet in the heterodyne system at 20 Hz. In BMV is used a pulsed magnet at 500 Hz (pulse time duration meaning) but with slow repetition rate and in homodyne detection.

Other experiments as OSQAR or ALPS IIc (VMB) are going to use superconducting magnets with modulation capability around several mHz and low finesse cavities [37].

5   Heterodyne setup for static magnetic fields

Until now we have said that it is optimal to use the heterodyne scheme as measurement principle in VMB experiments. To be entirely correct about the choice between homodyne and heterodyne measurement we can say, that from the ellipsometer sensitivity point of view both principles are similar [28]. But we speak about the case of homodyne measurement, where we modulate the magnetic field, not the ellipticity as we do currently in the OSQAR experiment. From the sensitivity point of view, PVLAS and BMV are comparable at the level of ellipsometer sensitivity or noise.

We had mentioned before OSQAR experiment had no option to modulate the magnetic field continuously. Until now the only possibility was to ramp up the magnetic field from 0 to 9 T in 257 s manually. However, even if we will be allowed to use modulation of the magnetic field, we get only 2 mHz frequency.

In this last section, we will focus on possibility how to modulate VMB effect in the static magnetic field. This is a solution, which is suitable for superconducting magnets like LHC or Hera dipoles.

5.1   Rotating half wave-plates

A first possible solution of VMB effect modulation in static magnetic fields was published in 2016 by a group of PVLAS, after the vacuum birefringence workshop in DESY Hamburg [81]. In this paper, the simple idea of inserting the two rotating half wave plates into the resonator is presented. The proposed measurement scheme is similar to the one used in PVLAS but the modulation of the VMB effect is not realized via rotating magnetic field, but by the rotating electric field vector see Figure 31.
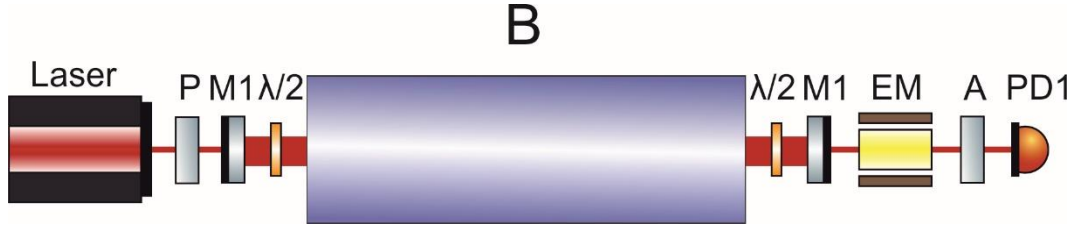
Fig 31. Scheme of proposed experiment to measure VMB with rotating half-wave plates

As we have mentioned before, seeking for highest cavity finesse is not probably the optimal solution for VMB measurement from the noise point of view. It seems to be more efficient to use higher modulation frequencies, as is also written in PVLAS paper see Figure 32.
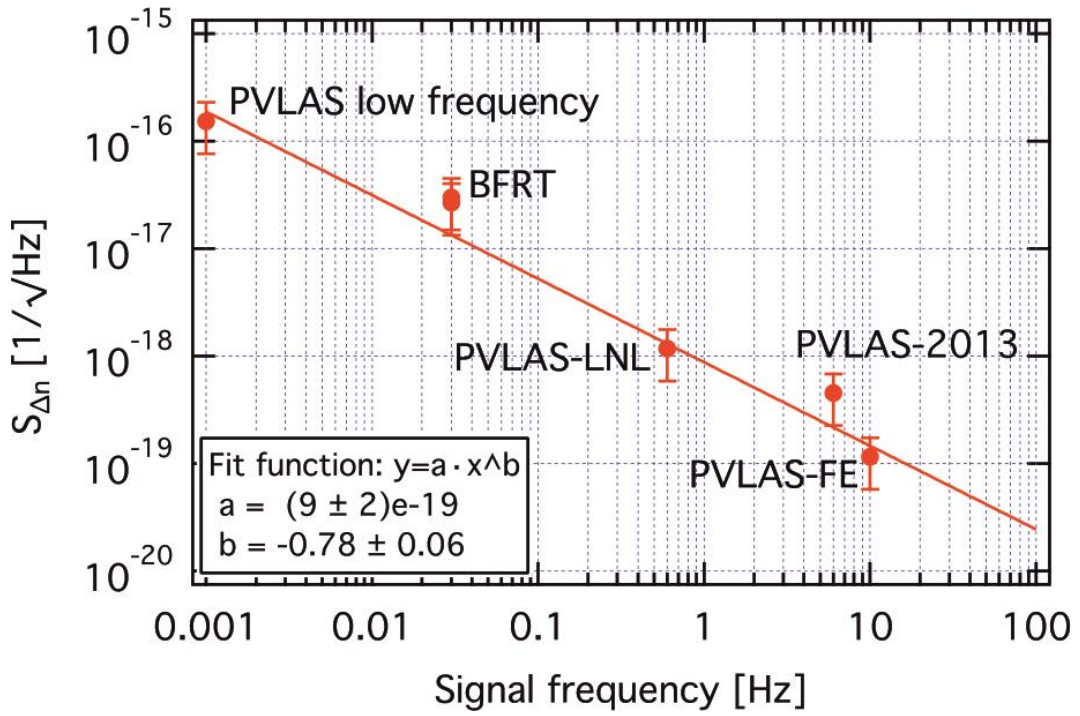

Fig 32. Birefringence noise densities measured in polarimeters setup to measure the magnetic vacuum birefringence plotted as a function of the frequency. Data from the experiments BFRT, PVLAS-LNL, PVLAS-2013, PVLAS-FE are normalized to the length of the optical cavities, to the number of passes and the wavelength. The leftmost point has been measured during the 2015 data taking a campaign of the PVLAS experiment. The two almost equal points from BFRT are measured with two different cavities, one having 34 passes and the other 578 passes. The error bars are an estimated 50% [81].

Using the optical cavity and rotating electric field vector has to reach two conditions. Electric field vector has to rotate in the magnetic field region and has to

be fixed on Fabry-Perot mirrors. If the vector of the electric field were rotating on the mirrors, the mirror birefringence would be modulated together with measured signal.

The advantage of the setup is in its simplicity and possible high modulation frequency of rotating plates. Rotating plates could rotate the electric field vector at frequencies up to several tens of hertz. The signal to be measured is found at the fourth harmonic component.

To the first order in ψ, α_1, α_2, and for the small modulation amplitude T_0 the intensity detected by the photodiode is given as [81]:

$$I(\delta) \approx I_0 \frac{T_r^2}{1-2R\cos\delta+R^2}\left\{\xi^2 + \frac{2\xi(1-R^2)}{1-2R\cos\delta+R^2}\left[\psi\sin(4\phi+4\phi_1)+\alpha_1\sin(2\phi+2\phi_1)+\alpha_2\sin(2\phi+4\phi_1-2\phi_2)\right]\right\} \qquad (74)$$

Where R a T_r are the reflectivity and transmissivity of the cavity mirrors, ϕ_1 a ϕ_2 are the initial angles of rotating half wave plates and we assume that $\phi_2 - \phi_1$ remain constant during rotation. α_1 and α_2 represents small imperfection of the half wave plates. $\phi = v_l t$ is variable angle of the half wave plates and $\xi = T_0 \cos 2\pi f_m t$ is ellipticity modulator term. ψ is the ellipticity to be measured.

This solution is possible to implement in ALPS experiment with Hera magnets or OSQAR experiment with LHC magnets. However, to build and operate such a cavity with rotating plates for the time required to get to S/N as 1, would request a lot of development and funding, with unpredictable results on cavity behavior and ellipsometer sensitivity.

The limitation is also rising from the fact that half wave plates inside the cavity introduce high intracavity losses (0.1% per pass) and therefore the maximum possible finesse would be at the level of 800, which corresponds to amplification factor $N \approx 500$ in maximum.

Of course, cavities in ALPS and OSQAR experiments are also crucial for LSW experiments which are the primary focus of these two collaborations, but the proposed scheme has never been realized experimentally.

Following Figure 31. we can also focus on higher modulation frequencies to overcome the problem with $1/f$ noise and profit from it. One can think to not to use cavity at all, since amplification factor N is low in this particular situation,

5.2 Rotating half wave-plate without optical cavity

The solution with rotating waveplates is, of course, possible to use without the optical cavity see Figure 33 and can be the step before cavity implementation.
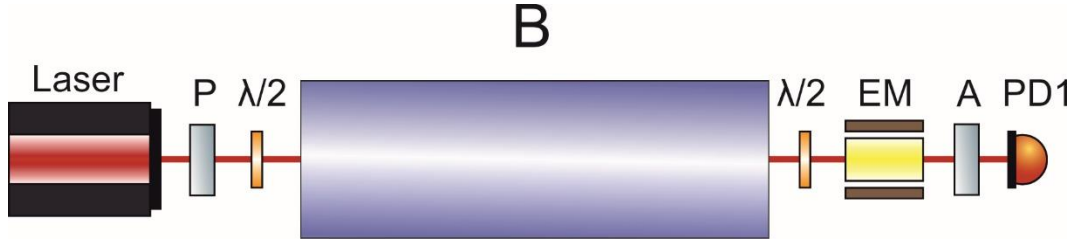

Fig 33. Optical setup scheme of rotating half-wave plates ellipsometer without resonator

The intensity reaching the detector is as follow:

$$I(\delta) \approx I_0\{\xi^2 + 2\xi[\psi \sin(4\phi + 4\phi_1) + \alpha_1 \sin(2\phi + 2\phi_1) + \alpha_2 \sin(2\phi + 4\phi_1 - 2\phi_2)]\} \tag{75}$$

It is an interesting fact on formulas (72, 73), that the ellipticity ψ, which should we measure is connected to the fourth harmonic component of the rotating modulation signal, but the signal proportion to imperfection of the half wave plates α_1, α_2 is on the second harmonic component [81].
This would lead to integration time of

$$t = \left(\frac{\psi_{shot}}{\psi_{QED}}\right)^2 = \left(\frac{7.5\times10^{-9}}{2.3\times10^{-14}}\right)^2 \approx 10^{11} \text{ s} \tag{76}$$

in the case of experiment OSQAR at shot noise limited sensitivity published in PVLAS paper.

So we still need to increase the measured signal or improve the sensitivity of the system.

5.3 Circular polarization rotation

The modulation principles as rotating magnets or rotating half-wave plates can modulate the VMB effect at 20 Hz (40 Hz detected signal), respectively 40 Hz (160 Hz detected signal).

There is also the possibility to produce the effect of rotating vector of the electric field as a net combination of two opposite circular polarization at a different frequency of the light [45], [82]. This net combination is resulting in effect looking like rotating vector of the electric field at a frequency defined by the difference of absolute frequencies of the light in the circularly polarized beams.

In this last paragraph, we would like to introduce this solution, which incorporates two contra-rotating circular polarizations, which is a possibility to modulate the VMB effect measurement up to kHz − MHz range and at the same time to present the heterodyne scheme for a static magnetic field.

One of the possible experimental configuration of measurement is presented in Figure 34.
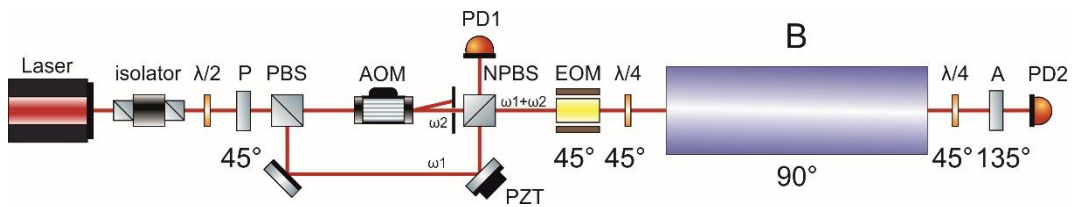
Fig 34. Optical setup scheme of heterodyne ellipsometer with HWP

From left to right we have, laser as source of the light with frequency of ω, optical isolator to protect laser from back reflected and backscattered light, half wave plate to control the polarization plane, polarizer P set to 45 degree to get two components equal in intensity after polarizing beam splitter PBS, polarizing beam splitter to separate two orthogonal polarizations, a acusto-optic modulator (AOM) to increase the frequency of the one polarization component by the factor ϖ, electro-optic

modulator (EOM) to provide modulation in ellipticity at f_m, quarter wave plate to change the orthogonal polarization to two opposite circular polarization, magnetic field region inducing the linear birefringence, second quart wave plate to set back polarization from circular to slightly elliptical and analyser to analyse the final signal before it is detect on photodiode PD2. PZT controlled mirror in combination with photodiode PD1 is there to fix the initial phase between orthogonal polarization components.

The intensity reaching the detector can be calculated by Jones formalism as follows

$$E = R(135) \cdot A_i \cdot R(-135) \cdot S(\varsigma, \delta) \cdot R(45) \cdot QWP_2(\frac{\pi}{2} + \Delta_2) \cdot R(-45) \cdot$$

$$R(90) \cdot X(\varphi) \cdot R(-90) \cdot R(45) \cdot QWP_1(\frac{\pi}{2} + \Delta_1) \cdot T(\xi) \cdot R(-45) \cdot (E_1 + E_2)$$

$$(77)$$

Where $E_1 = \begin{pmatrix} 1 \\ 0 \end{pmatrix} e^{i(2\pi\omega t + o_1)}$ and $E_2 = \begin{pmatrix} 0 \\ 1 \end{pmatrix} e^{i(2\pi(\omega + \varpi)t + o_2)}$ are the two orthogonal components of initial electric field vectors, ω is the fundamental frequency of the laser, Ω frequency shift of the AOM modulator, o_1, o_2 are the phases introduced by the different length of the beam path for both polarizations after PBS.

We start the calculation after the NPBS with two orthogonal polarization components at two different frequencies E_1, E_2. The Δ_1, Δ_2 represents imperfection of the quarter-wave plates and $S(\varsigma, \delta)$ is the spurious birefringence. We are not using $\frac{1}{\sqrt{2}}$ factor in E_1, E_2 for polarization at 45 degree after polarizer P, since at this point we are, not interested in absolute value of I and in particular the final results are divided by the DC component which neglects these term.

We suppose that $\Delta_1, \Delta_2, \varphi, \varsigma \ll 1$ and therefore we will neglect the terms including $\varphi^2, \varsigma^2, \Delta_1{}^2, \Delta_2{}^2$ and their combinations like $\varphi\varsigma, \Delta_1\Delta_2, etc.$ Initial phase difference $o = o_1 - o_2$ in orthogonal polarizations is set to be zero. Therefore we will use the PZT mirror controls to keep $o = 0$. In that case we get on PD2 light intensity as follow,

$$I = \boldsymbol{E} \cdot \boldsymbol{E}^* = I_0(1 - \cos[2\pi\varpi t] + \varsigma\cos[2\delta]\cos[\xi]\sin[2\pi\varpi t] +$$
$$\varphi\sin[\xi]\sin[\varpi t]) \quad (78)$$

Interesting on this solution is the fact that the component of spurious birefringence ς at angle δ is at different frequency, then the component to be measured φ, because $\xi = T_0\sin 2\pi f_m t$

$$\cos[T_0\sin 2\pi f_m t] = J_0(T_0) + 2\sum_{n=1}^{\infty} J_{2n}(T_0)\cos(2n2\pi f_m t)$$
$$\sin[T_0\sin 2\pi f_m t] = 2\sum_{n=1}^{\infty} J_{(2n-1)}(T_0)\sin((2n-1)2\pi f_m t)$$

The phase difference induced by magnetic field φ to be measured corresponds to the odd harmonic components of the signal and spurious birefringence ς to even components. Using the Bessel function of the first kind, up to second harmonics and for maximum spurious signal component at angle $\delta = 0$ we get

$$I = \boldsymbol{E} \cdot \boldsymbol{E}^* = I_0\big(1 - \cos[2\pi\varpi t] + J_0(T_0)\varsigma\sin[2\pi\varpi t] +$$
$$\varsigma J_2(T_0)\sin[2\pi\varpi t]\cos(2\pi 2 f_m t))) + J_{(1)}(T_0)\varphi\sin[2\pi\varpi t]\sin(2\pi f_m t)\big) =$$
$$I_0\Big(1 - \cos[2\pi\varpi t] + J_0(T_0)\varsigma\sin[2\pi\varpi t] + \tfrac{1}{2}J_{(1)}(T_0)\varphi(\cos[2\pi(\varpi - f_m)t] -$$
$$\cos[2\pi(\varpi + f_m)t]) + \tfrac{1}{2}J_2(T_0)\varsigma(\sin[2\pi(\varpi + 2f_m)t] + \sin[2\pi(\varpi - 2f_m)t])\Big)$$
$$(79)$$

From (77) we see that useful signal will correspond to $\varpi \mp f_m$ frequencies and spurious birefringence signal to $\varpi \mp 2f_m$. This heterodyne signal could be then sampled and analysed by FFT spectra to get the value of the φ.

Presented solution can be implemented in future OSQAR II experiment with higher laser power and longer magnetic field. If we assume to use of two LHC magnets with the field of $B = 9$ T with field of $L = 14.3 \times 2 = 28.6$ m and with power laser as $P = 100$ mW at $\lambda = 532$ nm. If we will be able to achieve a shot noise limit, the corresponding time to get signal to noise ratio as $\frac{S}{N} = 1$ for single pass would be

$$t = \left(\frac{\psi_{shot}}{\psi_{QED}}\right)^2 = \left(\frac{6.6\times10^{-9}}{5.5\times10^{-14}}\right)^2 \approx 10^{10} \text{ s} \qquad (80)$$

10^{10} s is still too long integration time, but three orders better from present shot noise sensitivity and ten orders from current noise level measurement see (66 a, b). If we can use such a solution together with an optical cavity, it can lead to lower integration time to reach QED level for Vacuum magnetic birefringence.

6 Conclusion

In the first part of the dissertation, the ellipsometer for OSQAR VMB experiment was presented. The ellipsometer was developed in Technical University of Liberec and tested in the OSQAR experiment at CERN in years 2013 – 2015. Newly developed homodyne ellipsometer suitable for low varying magnetic fields was tested on Cotton-Mouton effect in nitrogen gas, with successful results and expected lower sensitivity. Ellipsometer development and tests were made by the author of the thesis only and represent his original solution solving the slowly varying spurious signals in homodyne ellipsometry in experiment OSQAR.

The second part of the thesis was mainly about the development and testing of resonant optical cavity suitable for VMB and LSW experiments in project OSQAR. Optical cavity was designed and tested in cooperation with OSQAR colleagues resulting in the technical design of 20 m long optical resonator for OSQAR experiments. Author of the thesis was responsible for optical design and cavity prototypes testing.

The last part of the thesis was dedicated to heterodyne ellipsometry measurement suitable for static magnetic fields in VMB experiments. In the last chapter, the author presented the completely new heterodyne ellipsometry solution for VMB experiments. This new solution is the second heterodyne solution ever published for static magnetic fields in VMB experiments.

These new heterodyne ellipsometry technique and homodyne ellipsometry solutions for spurious signals are the main contributions to the VMB ellipsometry experiments and represent new original solution and measurements made by the author of the thesis.

References

[1] J. K. LL.D, 'XL. A new relation between electricity and light: Dielectrified media birefringent', *Philos. Mag. Ser. 4*, vol. 50, no. 332, pp. 337–348, Nov. 1875.

[2] M. H. Cotton A, *Ct R Hebd Séanc Acad Sci*, vol. 141, 1905.

[3] B. K. Hans Euler, 'Über die Streuung von Licht an Licht nach der Diracschen Theorie', *Naturwissenschaften*, vol. 23, no. 246, 1935.

[4] W. H. Hans Euler, 'Folgerungen aus der Diracschen Theorie des Positrons', *Z. Für Phys.*, vol. 98, 1936.

[5] Hans Euler, 'Über die Streuung von Licht an Licht nach der Diracschen Theorie', *Ann. Phys.*, vol. 418, no. 398–448, 1936.

[6] S. L. Adler, 'Photon splitting and photon dispersion in a strong magnetic field', *Ann. Phys.*, vol. 67, no. 2, pp. 599–647, Oct. 1971.

[7] Z. Bialynicka-Birula and I. Bialynicki-Birula, 'Nonlinear Effects in Quantum Electrodynamics. Photon Propagation and Photon Splitting in an External Field', *Phys. Rev. D*, vol. 2, no. 10, pp. 2341–2345, Nov. 1970.

[8] M. Bregant *et al.*, 'New precise measurement of the Cotton-Mouton effect in helium', *Chem. Phys. Lett.*, vol. 471, no. 4–6, pp. 322–325, Mar. 2009.

[9] A. Cadene, D. Sordes, P. Berceau, M. Fouche, R. Battesti, and C. Rizzo, 'Faraday and Cotton-Mouton effects of helium at lambda=1064 nm', *Phys. Rev. A*, vol. 88, no. 4, p. 043815, Oct. 2013.

[10] F. Della Valle *et al.*, 'The PVLAS experiment: measuring vacuum magnetic birefringence and dichroism with a birefringent Fabry-Perot cavity', *Eur. Phys. J. C*, vol. 76, no. 1, p. 24, Jan. 2016.

[11] A. Cadene, P. Berceau, M. Fouche, R. Battesti, and C. Rizzo, 'Vacuum magnetic linear birefringence using pulsed fields: status of the BMV experiment', *Eur. Phys. J. D*, vol. 68, no. 1, p. 16, Jan. 2014.

[12] L. Maiani, R. Petronzio, and E. Zavattini, 'Effects of nearly massless, spin-zero particles on light propagation in a magnetic field', *Phys. Lett. B*, vol. 175, no. 3, pp. 359–363, Aug. 1986.

[13] R. D. Peccei and H. R. Quinn, 'CP Conservation in the Presence of Pseudoparticles', *Phys. Rev. Lett.*, vol. 38, no. 25, pp. 1440–1443, Jun. 1977.

[14] E. Iacopini and E. Zavattini, 'Experimental method to detect the vacuum birefringence induced by a magnetic field', *Phys. Lett. B*, vol. 85, no. 1, pp. 151–154, Jul. 1979.

[15] E. Iacopini, B. Smith, G. Stefanini, and E. Zavattini, 'On a sensitive ellipsometer to detect the vacuum polarization induced by a magnetic field', *Il Nuovo Cimento B 1971-1996*, vol. 61, no. 1, pp. 21–37, Jan. 1981.

[16] E. Iacopini and E. Zavattini, 'Vacuum Polarization Effects in the (mu-He-4)+ Atom and the Born-Infeld Electromagnetic Theory', *Nuovo Cimento Della Soc. Ital. Fis. B-Gen. Phys. Relativ. Astron. Math. Phys. Methods*, vol. 78, no. 1, pp. 38–52, 1983.

[17] S. Carusotto, E. Polacco, E. Iacopini, G. Stefanini, and E. Zavattini, 'Measurement of the Magnetic Birefringence in Oxygen and Nitrogen Gases', *Opt. Commun.*, vol. 42, no. 2, pp. 104–108, 1982.

[18]   R. Cameron *et al.*, '1st Measurement of the Magnetic Birefringence of Helium Gas', *Phys. Lett. A*, vol. 157, no. 2–3, pp. 125–128, Jul. 1991.

[19]   R. Cameron *et al.*, 'Search for Nearly Massless, Weakly Coupled Particles by Optical Techniques', *Phys. Rev. D*, vol. 47, no. 9, pp. 3707–3725, May 1993.

[20]   D. Bakalov *et al.*, 'The measurement of vacuum polarization: The PVLAS experiment', *Hyperfine Interact.*, vol. 114, no. 1–4, pp. 103–113, 1998.

[21]   D. Bakalov *et al.*, 'Experimental method to detect the magnetic birefringence of vacuum', *Quantum Semiclassical Opt.*, vol. 10, no. 1, pp. 239–250, Feb. 1998.

[22]   D. Bakalov *et al.*, 'Pvlas - Vacuum Birefringence and Production and Detection of Nearly Massless, Weakly Coupled Particles by Optical Techniques', *Nucl. Phys. B*, pp. 180–182, May 1994.

[23]   E. Zavattini *et al.*, 'Experimental observation of optical rotation generated in vacuum by a magnetic field', *Phys. Rev. Lett.*, vol. 96, no. 11, p. 110406, Mar. 2006.

[24]   E. Zavattini *et al.*, 'New PVLAS results and limits on magnetically induced optical rotation and ellipticity in vacuum', *Phys. Rev. D*, vol. 77, no. 3, p. 032006, Feb. 2008.

[25]   S.-J. Chen, H.-H. Mei, and W.-T. Ni, 'Q & A experiment to search for vacuum dichroism, pseudoscalar-photon interaction and millicharged fermions', *Mod. Phys. Lett. A*, vol. 22, no. 37, pp. 2815–2831, Dec. 2007.

[26]   H.-H. Mei, W.-T. Ni, S.-J. Chen, and S.-S. Pan, 'Measurement of the Cotton-Mouton effect in nitrogen, oxygen, carbon dioxide, argon, and krypton with the Q & A apparatus', *Chem. Phys. Lett.*, vol. 471, no. 4–6, pp. 216–221, Mar. 2009.

[27]   H.-H. Mei, W.-T. Ni, S.-J. Chen, and S.-S. Pan, 'Axion Search with Q & a Experiment', *Mod. Phys. Lett. A*, vol. 25, no. 11–12, pp. 983–993, Apr. 2010.

[28]   R. Battesti *et al.*, 'The BMV experiment: a novel apparatus to study the propagation of light in a transverse magnetic field', *Eur. Phys. J. D*, vol. 46, no. 2, pp. 323–333, Feb. 2008.

[29]   F. Della Valle *et al.*, 'Measurements of vacuum magnetic birefringence using permanent dipole magnets: the PVLAS experiment', *New J. Phys.*, vol. 15, p. 053026, May 2013.

[30]   F. Della Valle *et al.*, 'First results from the new PVLAS apparatus: A new limit on vacuum magnetic birefringence', *Phys. Rev. D*, vol. 90, no. 9, p. 092003, Nov. 2014.

[31]   F. Della Valle *et al.*, 'The PVLAS experiment: measuring vacuum magnetic birefringence and dichroism with a birefringent Fabry-Perot cavity', *Eur. Phys. J. C*, vol. 76, no. 1, p. 24, Jan. 2016.

[32]   M. Král, 'Feasibility Study of an Experiment to Measure Vacuum Magnetic Birefringence', Dissertation, Czech Technical University in Prague, Prague, 2007

[33]   J. L. Hall, J. Ye, and L. S. Ma, 'Measurement of mirror birefringence at the sub-ppm level: Proposed application to a test of QED', *Phys. Rev. A*, vol. 62, no. 1, p. art. no.-013815, Jul. 2000.

[34]   S. A. Lee *et al.*, 'Measurement of the Magnetically-Induced QED Birefringence of the Vacuum and Improved Laboratory Search for Axions',

Proposal submitted to Fermi National Accelerator Laboratory, Illinois, Mar. *1995*.

[35]   T. Dafni *et al.*, 'An update on the Axion Helioscopes front: current activities at CAST and the IAXO project.', *Nucl. Part. Phys. Proc.*, vol. 273, pp. 244–249, Jun. 2016.

[36]   S. Andriamonje *et al.*, 'An improved limit on the axion-photon coupling from the CAST experiment', *J. Cosmol. Astropart. Phys.*, no. 4, p. 010, Apr. 2007.

[37]   R. Baehre *et al.*, 'Any light particle search II - Technical Design Report', *J. Instrum.*, vol. 8, p. T09001, Sep. 2013.

[38]   K. Ehret *et al.*, 'New ALPS results on hidden-sector lightweights', *Phys. Lett. B*, vol. 689, no. 4–5, pp. 149–155, May 2010.

[39]   M. Sulc *et al.*, 'Axion search by laser-based experiment OSQAR', *Nucl. Instrum. Methods Phys. Res. Sect. -Accel. Spectrometers Detect. Assoc. Equip.*, vol. 718, pp. 530–532, Aug. 2013.

[40]   R. Ballou *et al.*, 'New exclusion limits on scalar and pseudoscalar axionlike particles from light shining through a wall', *Phys. Rev. D*, vol. 92, no. 9, p. 092002, Nov. 2015.

[41]   P. Pugnat *et al.*, 'Search for weakly interacting sub-eV particles with the OSQAR laser-based experiment: results and perspectives', *Eur. Phys. J. C*, vol. 74, no. 8, p. 3027, Aug. 2014.

[42]   S. Kunc and M. Sulc, 'High sensitive method for optical birefringence measurement', in *Optics and Measurement Conference 2014*, vol. 9442, J. Kovacicinova and T. Vit, Eds. Bellingham: Spie-Int Soc Optical Engineering, 2015, p. 94420O.

[43]   'Handbook of Ellipsometry - 1st Edition'. [Online]. Available: https://www.elsevier.com/books/handbook-of-ellipsometry/tompkins/978-0-8155-1499-2. [Accessed: 28-Mar-2017].

[44]   R. C. Jones, 'A New Calculus for the Treatment of Optical SystemsI. Description and Discussion of the Calculus', *JOSA*, vol. 31, no. 7, pp. 488–493, Jul. 1941.

[45]   'Wiley: Fundamentals of Photonics, 2nd Edition - Bahaa E. A. Saleh, Malvin Carl Teich'. [Online]. Available: http://www.wiley.com/WileyCDA/WileyTitle/productCd-0471358320.html. [Accessed: 28-Mar-2017].

[46]   G. G. G. Ropars, 'A depolarizer as a possible precise sunstone for Viking navigation by polarized skylight', *R. Soc. Lond. Proc. Ser. A*, vol. 468, no. 2139, pp. 671–684, 2012.

[47]   J. C. Maxwell, 'A Dynamical Theory of the Electromagnetic Field', *Philos. Trans. R. Soc. Lond.*, vol. 155, pp. 459–512, Jan. 1865.

[48]   Kerr John, 'The Effects of a Magnetic Field on Radiation', *Am. Book Co.*, 1900.

[49]   M. Durand, J. Morville, and D. Romanini, 'Shot-noise-limited measurement of sub-parts-per-trillion birefringence phase shift in a high-finesse cavity', *Phys. Rev. A*, vol. 82, no. 3, p. 031803, Sep. 2010.

[50]   H. Primakoff, 'Photo-Production of Neutral Mesons in Nuclear Electric Fields and the Mean Life of the Neutral Meson', *Phys. Rev.*, vol. 81, no. 5, pp. 899–899, Mar. 1951.

[51]   G. Raffelt and L. Stodolsky, 'Mixing of the photon with low-mass particles', *Phys. Rev. D*, vol. 37, no. 5, pp. 1237–1249, Mar. 1988.

[52]   H. Gies, J. Jaeckel, and A. Ringwald, 'Polarized Light Propagating in a Magnetic Field as a Probe for Millicharged Fermions', *Phys. Rev. Lett.*, vol. 97, no. 14, p. 140402, Oct. 2006.

[53]   P. Pugnat *et al.*, 'QED Test and Axion Search by means of Optical Techniques', Letter of Intent to the CERN SPSC, Geneva, Oct. 2005.

[54]   P. Pugnat *et al.*, 'Optical Search for QED vacuum magnetic birefringence, Axions and photon Regeneration (OSQAR)', Proposal submitted to the CERN SPSC, Geneva, Nov. 2006.

[55]   S. Askenazy *et al.*, 'A 25T dipole pulsed magnet to study the magnetic birefringence of vacuum: the BMV project', presented at the QED 2000, 2000.

[56]   F. A. Modine, R. W. Major, and E. Sonder, 'High Frequency Polarization Modulation Method for Measuring Birefringence', *Appl. Opt.*, vol. 14, no. 3, pp. 757–760, Mar. 1975.

[57]   M. Bass *et al.*, *Handbook of Optics, Third Edition Volume I: Geometrical and Physical Optics, Polarized Light, Components and Instruments(set)*, 3 edition. New York: McGraw-Hill Education, 2009.

[58]   S. Y. Lee, J. F. Lin, and Y. L. Lo, 'Measurements of phase retardation and principal axis angle using an electro-optic modulated Mach–Zehnder interferometer', *Opt. Lasers Eng.*, vol. 43, no. 6, pp. 704–720, Jun. 2005.

[59]   W. Zhang *et al.*, 'Reduction of residual amplitude modulation to 1×10^{-6} for frequency modulation and laser stabilization', *Opt. Lett.*, vol. 39, no. 7, pp. 1980–1983, Apr. 2014.

[60]   J. Snoddy, Y. Li, F. Ravet, and X. Bao, 'Stabilization of electro-optic modulator bias voltage drift using a lock-in amplifier and a proportional-integral-derivative controller in a distributed Brillouin sensor system', *Appl. Opt.*, vol. 46, no. 9, pp. 1482–1485, Mar. 2007.

[61]   S. Kunc and M. Sulc, 'High Frequency Modulation Method for Measuring of Birefringence', in *Oam 2012 - Optics and Measurement International Conference*, vol. 48, M. Sulc, V. Kopecky, V. Ledl, R. Melich, and M. Skeren, Eds. Cedex A: E D P Sciences, 2013, p. 00012.

[62]   'Cross section of LHC dipole. - CERN Document Server'. [Online]. Available: https://cds.cern.ch/record/841539?ln=sk. [Accessed: 04-Aug-2017].

[63]   'LHC Magnets'. [Online]. Available: http://lhc-machine-outreach.web.cern.ch/lhc-machine-outreach/introduction.htm. [Accessed: 30-Sep-2016].

[64]   'Quantum Diaries'. [Online]. Available: http://www.quantumdiaries.org/2011/04/24/the-cern-accelerator-complex/. [Accessed: 04-Aug-2017].

[65]   C. Rizzo, A. Rizzo, and D. M. Bishop, 'The Cotton-Mouton effect in gases: Experiment and theory', *Int. Rev. Phys. Chem.*, vol. 16, no. 1, pp. 81–111, Jan. 1997.

[66]   G. Zavattini, U. Gastaldi, R. Pengo, G. Ruoso, F. Della Valle, and E. Milotti, 'Measuring the Magnetic Birefringence of Vacuum: The Pvlas Experiment', *Int. J. Mod. Phys. A*, vol. 27, no. 15, p. 1260017, Jun. 2012.

[67]   K. Halbach, 'Design of permanent multipole magnets with oriented rare earth cobalt material', *Nucl. Instrum. Methods*, vol. 169, no. 1, pp. 1–10, Feb. 1980.

[68]   'Permanent magnet assembly producing a strong tilted homogeneous magnetic field: Towards magic angle field spinning NMR and MRI', *ResearchGate*. [Online]. Available: https://www.researchgate.net/publication/47301501_Permanent_magnet_asse mbly_producing_a_strong_tilted_homogeneous_magnetic_field_Towards_ma gic_angle_field_spinning_NMR_and_MRI. [Accessed: 31-Jul-2017].

[69]   P. Berceau, M. Fouché, R. Battesti, and C. Rizzo, 'Magnetic linear birefringence measurements using pulsed fields', *Phys. Rev. A*, vol. 85, no. 1, p. 013837, Jan. 2012.

[70]   F. D. Valle *et al.*, 'Extremely long decay time optical cavity', *Opt. Express*, vol. 22, no. 10, pp. 11570–11577, May 2014.

[71]   D. Z. Anderson, 'Alignment of resonant optical cavities', *Appl. Opt.*, vol. 23, no. 17, p. 2944, Sep. 1984.

[72]   'Wiley: Frequency Standards: Basics and Applications - Fritz Riehle'. [Online]. Available: http://www.wiley.com/WileyCDA/WileyTitle/productCd-3527605959.html. [Accessed: 25-Apr-2017].

[73]   J. Hosek, K. Macuchova, S. Nemcova, S. Kunc, and M. Sulc, 'Opto-mechanical design of vacuum laser resonator for the OSQAR experiment', in *Photonics, Devices, and Systems Vi*, vol. 9450, P. Tomanek, D. Senderakova, and P. Pata, Eds. Bellingham: Spie-Int Soc Optical Engineering, 2015, p. 945003.

[74]   D. A. Shaddock, M. B. Gray, and D. E. McClelland, 'Frequency locking a laser to an optical cavity by use of spatial mode interference', *Opt. Lett.*, vol. 24, no. 21, p. 1499, Nov. 1999.

[75]   R. W. P. Drever *et al.*, 'Laser phase and frequency stabilization using an optical resonator', *Appl. Phys. B*, vol. 31, no. 2, pp. 97–105, Jun. 1983.

[76]   E. Morrison, B. J. Meers, D. I. Robertson, and H. Ward, 'Automatic alignment of optical interferometers', *Appl. Opt.*, vol. 33, no. 22, pp. 5041–5049, Aug. 1994.

[77]   'Optical cavity', *Wikipedia*. 15-May-2017.

[78]   'Coherent Inc. Verdi V Series DPSS Laser for Ti:Sapphire Pumping'. [Online]. Available: http://www.coherent.com/products/?1852/Verdi-V-Series. [Accessed: 30-Sep-2016].

[79]   PVLAS Collaboration *et al.*, 'Limits on low energy photon-photon scattering from an experiment on magnetic vacuum birefringence', *Phys. Rev. D*, vol. 78, no. 3, p. 032006, Aug. 2008.

[80]   F. Bielsa, A. Dupays, M. Fouché, R. Battesti, C. Robilliard, and C. Rizzo, 'Birefringence of interferential mirrors at normal incidence', *Appl. Phys. B*, vol. 97, no. 2, p. 457, Oct. 2009.

[81]   G. Zavattini, F. Della Valle, A. Ejlli, and G. Ruoso, 'A polarisation modulation scheme for measuring vacuum magnetic birefringence with static fields', *ArXiv160103986 Phys.*, Jan. 2016.

[82]   C. Pawong, R. Chitaree, and C. Soankwan, 'The rotating linearly polarized light from a polarizing Mach-Zehnder interferometer: Production and applications', *Opt. Laser Technol.*, vol. 43, pp. 461–468, Apr. 2011.

Publications and Presentations

Publications (Web of Science):

OSQAR VMB

S. Kunc, G. Messineo, M. Schott, and M. Sulc, 'Passive optical resonator for OSQAR LSW experiment', in *Optics and Measurement International Conference 2016*, vol. 10151, J. Kovacicinova, Ed. Bellingham: Spie-Int Soc Optical Engineering, 2016, p. 1015104.

S. Kunc and M. Sulc, 'High sensitive method for optical birefringence measurement', in *Optics and Measurement Conference 2014*, vol. 9442, J. Kovacicinova and T. Vit, Eds. Bellingham: Spie-Int Soc Optical Engineering, 2015, p. 94420O.

J. Hosek, K. Macuchova, S. Nemcova, S. Kunc, and M. Sulc, 'Opto-mechanical design of vacuum laser resonator for the OSQAR experiment', in *Photonics, Devices, and Systems Vi*, vol. 9450, P. Tomanek, D. Senderakova, and P. Pata, Eds. Bellingham: Spie-Int Soc Optical Engineering, 2015, p. 945003.

S. Kunc and M. Sulc, 'High Frequency Modulation Method for Measuring of Birefringence', in *Oam 2012 - Optics and Measurement International Conference*, vol. 48, M. Sulc, V. Kopecky, V. Ledl, R. Melich, and M. Skeren, Eds. Cedex A: E D P Sciences, 2013, p. 00012.

OSQAR LSW

R. Ballou *et al.*, 'New exclusion limits on scalar and pseudoscalar axionlike particles from light shining through a wall', *Phys. Rev. D*, vol. 92, no. 9, p. 092002, Nov. 2015.

P. Pugnat *et al.*, 'Search for weakly interacting sub-eV particles with the OSQAR laser-based experiment: results and perspectives', *Eur. Phys. J. C*, vol. 74, no. 8, p. 3027, Aug. 2014.

M. Sulc *et al.*, 'Axion search by laser-based experiment OSQAR', *Nucl. Instrum. Methods Phys. Res. Sect. -Accel. Spectrometers Detect. Assoc. Equip.*, vol. 718, pp. 530–532, Aug. 2013.

Presentations:

13th PATRAS Workshop on Axions, WIMPs and WISPs, Thessaloniki 2017, Poster

SPSC Committee Meeting, CERN, Geneva, 2016, Oral speech

Optics and Measurement International Conference 2016, Liberec, 2016, Oral speech

QED vacuum birefringence workshop, 2015, DESY, Hamburg, Invited speech

The XXII International Workshop High Energy Physics and Quantum Field Theory, Samara, 2015, Invited speech

Optics and Measurement International Conference 2014, Liberec, 2014, Oral speech

10th PATRAS Workshop on Axions, WIMPs and WISPs, CERN, Geneva, 2014, Poster

Optics and Measurement International Conference 2012, Liberec, 2012, Poster

Curriculum Vitae

Name:	Štěpán Kunc
Address:	Senovážná 84/2 460 01 Liberec 1 Česká Republika
E-mail:	stepan.kunc@email.cz
Date of birth:	16.8.1984
Place of birth:	Jablonec nad Nisou, Česká Republika

Education and skills:

From 9/2011
Ph.D. study
Study program: Applied sciences in engineering
Specialization Area: Physical engineering
Department of Physics, Faculty of Sciences,
Humanities and Education, Technical University of
Liberec, Czech Republic

02/2011
Master's study
Study program: Electronics and informatics
Specialization Area: Science engineering
Department of Mechatronics and interdisciplinary
studies, Technical University of Liberec, Czech
Republic

From 5/2011
Member of experiment OSQAR

From 1/2014
Technical coordinator of experiment OSQAR

Investigator and co-investigator of 15 grants of the Technical University of
Liberec, The Grant agency of the Czech Republic, Grants of Ministry of
education, Structural funds of the European Union and others.